

AD-A188 792

SELF-BORING PRESSUREMETER IN PLUVIALLY DEPOSITED SANDS
(U) CENTRO DI RICERCA IDRAULICA E STRUTTURALE MILAN
(ITALY) R BELLOTTI ET AL. JUN 87 DAJA45-84-C-0034

1/2

UNCLASSIFIED

F/C 14/2

NL

1.0
1.1
1.25
1.4
1.6
1.8
2.0
2.2
2.5
2.8
3.2
3.6
4.0
4.5
5.0
5.6
6.3
7.1
8.0
9.0
10.0
11.2
12.5
14.0
16.0
18.0
20.0
22.4
25.0
28.0
31.5
36.0
40.0
45.0
50.0
56.0
63.0
71.0
80.0
90.0
100.0

DTIC FILE COPY

②

AD-A188 792

AD

SELF-BORING PRESSUREMETER IN PLUVIALLY DEPOSITED SANDS

Final Technical Report

by

R. Bellotti, V. Crippa, V.N. Ghionna, M. Janiolkowski
and P.K. Robertson

June 1987

United States Army

EUROPEAN RESEARCH OFFICE OF THE U.S. ARMY

London England

CONTRACT NUMBER DAJA45-84-C-0034

ENEL CRIS - MILAN (ITALY)

DTIC
ELECTE
DEC 02 1987
S D
DH

Approved for Public Release, distribution unlimited

97 11 006

UNCLASSIFIED

SECURITY CLASSIFICATION OF THIS PAGE (When Data Entered)

REPORT DOCUMENTATION PAGE		READ INSTRUCTIONS BEFORE COMPLETING FORM
1. REPORT NUMBER	2. GOVT ACCESSION NO.	3. RECIPIENT'S CATALOG NUMBER
4. TITLE (and Subtitle) SELF-BORING PRESSUREMETER IN PLUVIALLY DEPOSITED SANDS		5. TYPE OF REPORT & PERIOD COVERED FINAL TECHNICAL REPORT Aug '84 - Aug '87
7. AUTHOR(s) R. Bellotti, V. Crippa, V.N. Ghionna, M. Jamiolkowski, and P.K. Robertson		6. PERFORMING ORG. REPORT NUMBER BELLOTTI
9. PERFORMING ORGANIZATION NAME AND ADDRESS ENEL-CRIS Via Ornato, 90/14 20162 - MILANO (ITALY)		8. CONTRACT OR GRANT NUMBER(s) DATA 45-84-C-0034 BELLOTTI
11. CONTROLLING OFFICE NAME AND ADDRESS USAR DSG (UK) Box 65, FPO NY 09510 1500		10. PROGRAM ELEMENT, PROJECT, TASK AREA & WORK UNIT NUMBERS 61102A 1L161102BH57EN-CI
14. MONITORING AGENCY NAME & ADDRESS (if different from Controlling Office)		12. REPORT DATE June 1987
		13. NUMBER OF PAGES 33
		15. SECURITY CLASS. (of this report) UNCLASSIFIED
		15a. DECLASSIFICATION/DOWNGRADING SCHEDULE
16. DISTRIBUTION STATEMENT (of this Report) Approved for Public Release Distribution Unlimited		
17. DISTRIBUTION STATEMENT (of the abstract entered in Block 20, if different from Report)		
18. SUPPLEMENTARY NOTES		
19. KEY WORDS (Continue on reverse side if necessary and identify by block number) Self-boring pressuremeter, Sands, Initial in-situ horizontal stress, Shear modulus, Shear Strength, Limit Pressure, Calibration Chamber		
20. ABSTRACT (Continue on reverse side if necessary and identify by block number) This report presents the results of 47 self-boring pressuremeter (SBP) tests performed under strictly controlled boundary conditions on pluvially deposited Ticino and Høksund sand samples in the Calibration Chamber existing at ENEL-CRIS (Milan-Italy): N°25 tests were performed with the probe in place during sample preparation and N°22 with the probe self-bored into saturated sand.		

SECURITY CLASSIFICATION OF THIS PAGE(When Data Entered)

20. The purpose of the testing was to evaluate the performance of the self-boring pressuremeter and to critically review existing interpretation methods of SBPT in sand.

Accession For	
NTIS GRA&I	<input checked="checked" type="checkbox"/>
DTIC TAB	<input type="checkbox"/>
Unannounced	<input type="checkbox"/>
Justification	
By	
Distribution/	
Availability Codes	
D,at	Avail and/or Special
A-1	

SECURITY CLASSIFICATION OF THIS PAGE(When Data Entered)

TABLE OF CONTENTS

1.	INTRODUCTION	page	5
2.	TEST EQUIPMENT	page	5
	2.1. Calibration Chamber (CC)	page	5
	2.2. Self-boring Pressuremeter	page	6
3.	TEST SAND	page	7
4.	TEST PROCEDURES	page	7
	4.1. Sample Formation	page	7
	4.2. Probe Installation	page	7
	4.2.1. Ideal	page	7
	4.2.2. Self-bored	page	8
	4.3. Sample Stresses	page	8
	4.4. Pressuremeter Expansion	page	9
5.	TEST RESULTS	page	10
	5.1. Initial Horizontal Stress	page	10
	5.1.1. Initial Horizontal Stress:		
	Ideal Installation	page	10
	5.1.2. Evaluation of Stress Concentration	page	11
	5.1.3. Mechanical Compliance of Strain Arms	page	11
	5.1.4. Evaluation of Arching Effects	page	13
	5.1.5. Initial Horizontal Stress:		
	Self-Bored Installation	page	13
	5.2. Shear Modulus	page	14
	5.3. Shear Strength	page	21
	5.4. Limit Pressure	page	25
	5.5. Boundary Conditions	page	25
6.	SUMMARY AND CONCLUSIONS	page	26
	LITERATURE CITED	page	29
	NOTATIONS	page	32
	TABLES		
	FIGURES		
	APPENDIXES		

LIST OF TABLES

- TABLE 1: SUMMARY OF INSTALLATION CONDITIONS DURING SELF-BORING
- TABLE 2: SUMMARY OF GENERAL CALIBRATION CHAMBER CONDITIONS AFTER SAMPLE CONSOLIDATION
- TABLE 3: SUMMARY OF PROBE AND CC CONDITIONS DURING SELF-BORED TESTS
- TABLE 4: SUMMARY OF LITF-OFF PRESSURES OF INDIVIDUAL ARMS
- TABLE 5: SUMMARY OF LIMIT PRESSURE AND SECANT SHEAR MODULUS
- TABLE 6: SUMMARY OF 1ST UNLOADING-RELOADING CYCLE
- TABLE 7: SUMMARY OF 2ND UNLOADING-RELOADING CYCLE
- TABLE 8: SUMMARY OF 3RD UNLOADING-RELOADING CYCLE
- TABLE 9: SUMMARY OF 4TH UNLOADING-RELOADING CYCLE
- TABLE 10: SUMMARY OF 1ST RELOADING-UNLOADING CYCLE
- TABLE 11: SUMMARY OF CALCULATED ANGLES OF FRICTION AND DILATANCY [$\phi'_{cv} = 34^\circ$]

LIST OF FIGURES

- FIG. 1: SCHEMATIC CROSS-SECTION OF ENEL-CRIS CALIBRATION CHAMBER
- FIG. 2: SCHEMATIC OUTLINE OF CC LOADING AND DATA ACQUISITION SYSTEM FOR SBPT IN SAND
- FIG. 3: SCHEMATIC OUTLINE OF SELF-BORING PRESSUREMETER PROBE CAMKOMETER MARK VIII
- FIG. 4: GENERAL CHARACTERISTICS OF TICINO AND HOKKSUND SAND
- FIG. 5: SCHEMATIC OUTLINE OF SAND SPREADER
- FIG. 6: SCHEMATIC OUTLINE OF IDEAL INSTALLATION PROCEDURE IN CC
- FIG. 7: SCHEMATIC OUTLINE OF SELF-BORING INSTALLATION PROCEDURE IN CC

- FIG. 8: EXAMPLE OF TYPICAL SAMPLE CONSOLIDATION
- FIG. 9: AVAILABLE BOUNDARY CONDITIONS IN CC
- FIG. 10: TYPICAL TEST RESULT FROM SBPT IN CC
- FIG. 11: COMPARISON BETWEEN MEASURED AVERAGE LIFT-OFF STRESSES (p_o) AND APPLIED BOUNDARY STRESSES (σ_{ho}): IDEAL INSTALLATION
- FIG. 12: 1-D STRESSING OF CAMBRIDGE K_o - CELL IN CC
- FIG. 13: EXAMPLE OF STRAIN ARM COMPLIANCE DURING SAMPLE CONSOLIDATION STAGE
- FIG. 14: EXAMPLE OF PRONOUNCED MECHANICAL COMPLIANCE OF STRAIN ARMS DURING PRESSUREMETER EXPANSION
- FIG. 15: DETAILS OF ORIGINAL AND MODIFIED SBP STRAIN ARMS
- FIG. 16: COMPARISON BETWEEN MEASURED AVERAGE LIFT-OFF STRESSES (p_o) AND APPLIED BOUNDARY STRESS (σ_{ho}): SELF-BORED INSTALLATION
- FIG. 17: SCHEMATIC OF SHEAR MODULI FROM SBP TEST
- FIG. 18: SCHEMATIC OF EFFECTIVE STRESS PATH OF SOIL ELEMENT ADJACENT TO AN EXPANDING PRESSUREMETER
- FIG. 19: SCHEMATIC OF UNLOADING-RELOADING CYCLE DURING SBPT IN SAND
- FIG. 20: TYPICAL RESULTS OF SIMPLE SHEAR TESTS ON SAND (AFTER STROUD) AND THE IDEAL SOIL MODEL ASSUMED BY HUGHES ET al. (1977).
- FIG. 21: CALCULATED STRESS STRAIN RELATIONSHIPS FROM TEST No.222 ($D_R = 46.2\%$) USING METHOD BY MANASSERO (1987)
- FIG. 22: CALCULATED STRESS STRAIN RELATIONSHIPS FROM TEST No.228 ($D_R = 77\%$) USING METHOD BY MANASSERO (1987)
- FIG. 23: ANGLE β ; DEVIATION OF ESP FROM ISOTROPIC ELASTIC BEHAVIOUR (FOR WHICH $\beta = 90^\circ$)
- FIG. 24: DETERMINATION OF ϕ_{cv} FROM RING SHEAR TESTS
- FIG. 25: COMPARISON OF CALCULATED ϕ_P^{PS} FROM SBPT AND EQUIVALENT ϕ_P^{PS} FROM TRIAXIAL TESTS

LIST OF APPENDIXES

- APP. I : EXAMPLE OF COMPUTER GENERATED PLOTS FOR TYPICAL TEST
RESULT
- APP. II : COMPLETE LISTING FOR EACH SBPT RESULTS
- APP. III: CALCULATION OF AVERAGE STRESS ON HORIZONTAL PLANE
AROUND EXPANDING CAVITY
- APP. IV : DETAILS ON MANASSERO (1987) METHOD FOR DETERMINATION
OF ϕ FROM SBPT IN SAND

1. INTRODUCTION

This report presents the results of 47 self-boring pressuremeter tests (SBPT's) performed in the ENEL-CRIS(*) calibration chamber (CC). The tests were performed in dry and saturated Ticino and Hokksund sand. Pressuremeter tests were performed with the probe in-place during sample preparation ("ideal installation") and with the probe self-bored into the saturated sand.

The purpose of the testing was to evaluate the performance of the self-boring pressuremeter (SBP) probe under strictly controlled laboratory conditions and to critically review existing interpretation methods of the SBPT in sands. The SBP probe used in the study was the Camkometer Mark VIII manufactured by Cambridge In-situ Ltd., England.

2. TEST EQUIPMENT

2.1. Calibration Chamber (CC)

The ENEL-CRIS calibration chamber was designed to calibrate and evaluate different in-situ testing devices in sands under strictly controlled boundary conditions.

A complete description of the chamber is given by Bellotti et al. (1982). The equipment consists of a double wall chamber, a loading frame, a mass sand spreader for sand deposition and a saturation system. The chamber can test a cylindrical sample of sand 1.2 m (3.9 feet) in diameter and 1.5 m (4.9 feet) in height.

A schematic cross-section of the ENEL-CRIS calibration chamber is shown in Figure 1.

The sample is confined laterally with a flexible rubber membrane surrounded by water through which the horizontal stresses are applied. The bottom of the sample is supported on a water filled cushion resting on a rigid steel piston.

The vertical confining stress is applied through the water filled base cushion and vertical deflection of the sample is controlled by the movement of the base steel piston. The top of the sample is confined by a rigid top plate and fixed beam.

The double-walled chamber allows the application of a zero average lateral strain boundary condition to the test sample by maintaining the pressure in the double-wall cavity equal to the lateral pressure acting on the sample membrane.

(*) ENEL - CRIS: Italian National Electricity Board - Hydraulic and Structural Research Center.

The axial and lateral confining pressures can be varied independently so that the ratio of the applied horizontal stress (σ_h) to the vertical stress (σ_v) can be maintained at any desired value.

A schematic cross-section of the CC loading system is shown in Figure 2.

2.2. Self-boring Pressuremeter

The SBP probe used in the study was the Camkometer Mark VIII manufactured by Cambridge In-Situ Ltd., England. A schematic outline of the SBP probe is given in Figure 3.

The SBP probe is essentially a thick walled steel cylinder with a flexible membrane attached to the outside. The instrument is advanced into the ground as the soil displaced by a sharp cutting shoe is removed up the center of the probe by the action of a rotating cutter inside the shoe. The cuttings are flushed to the surface by water or drilling mud which is pumped down to the cutting head.

The cylindrical adiprene membrane used in this study was 82 mm in diameter and 490 mm in length, corresponding to a length to diameter ratio (L/D) of approximately 6. The adiprene membrane was designed to be flush with the body of the probe. An outer flexible protective membrane with stainless steel strips ("chinese lantern") can be placed over the adiprene membrane during penetration and testing in dense or abrasive soils.

Once the instrument is at the desired test depth, the membrane is expanded against the soil using pressurized N_2 gas. The radial expansion of the membrane is measured at the mid-height of the membrane by three pivoted levers, called strain arms. The strain arms are located at 120 degrees around the circumference. The strain arms are kept in light contact with the inside of the membrane by strain gauged cantilever springs (Figure 3). Individual and average readings were taken of the three strain arms. The sensitivity of the strain arms was approximately 0.02 mm/mV.

A strain gauged total pressure cell (TPC) is located inside the probe to measure the inflation gas pressure. Two strain gauged pore pressure cells (PPC) are also incorporated into the membrane. The sensitivity of the PPC and TPC was approximately 8 kPa/mV.

The data from all six transducers (3 strain, 1 total pressure, 2 pore pressure) was collected by the original data acquisition system consisting of a data capture unit, and a thermal paper printer with the addition of a cartridge equipped HP 9825 computer and a wider paper tape printer. The output was also recorded on a four channel Y-T chart recorder and an X-Y plotter for simultaneous plotting of raw data (Fig.2).

3. TEST SAND

Two natural sands have been tested; Ticino sand from Italy and Hokksund sand from Norway. Both sands have a uniform gradation and are medium to coarse grained with a mean grain size, $D_{50}=0.53$ mm, and 0.39 mm for Ticino and Hokksund sand, respectively.

General characteristics of the sands and grain size distributions are given in Fig.4.

A detailed description of the physical properties of the two sands is given by Baldi et al. (1985).

During the course of the testing different batches of Ticino sand were used. However, each batch was tested to ensure consistent grain size characteristics.

4. TEST PROCEDURES

4.1. Sample Formation

All test samples were prepared by pluvial deposition of dry sand in air using a gravity mass sand spreader (Jacobsen, 1976). A schematic representation of the mass sand spreader is shown in Figure 5.

The pluvial deposition method has the following advantages;

- good repeatability
- wide range of obtainable relative densities
($20\% \leq D_R \leq 98\%$)
- good homogeneity of sample
- cost effectiveness.

The homogeneity of the samples is generally good although somewhat erratic for medium dense specimens ($40\% \leq D_R \leq 60\%$). Full details concerning sample homogeneity is given by Baldi et al. (1985).

Sample formation is performed in one operation and the sand container holds enough sand necessary for specimen preparation.

4.2. Probe Installation

4.2.1. Ideal

To evaluate and avoid the influence of the self-boring installation on the pressuremeter results a series of tests were performed with "ideal installation".

For ideal installation the probe was placed in the CC before sample formation. A schematic outline of the ideal installation procedure is shown in Figure 6.

The SBP probe was placed in the center of the CC with the mid-height of the membrane approximately 65 cm (25 inches) from the sample base. A protective cylinder was placed above the probe and extended up to the base of the sand container (see Fig.6). This was done to avoid sand falling onto the top of the probe during sample formation.

4.2.2. Self-bored

To simulate field self-boring conditions a series of tests were performed with the probe self-bored into the CC. A schematic outline of the self-bored installation procedure is given in Figure 7.

The sand samples were first formed using pluvial deposition and then saturated with de-aired water. Full details of the saturation procedures are given by Bellotti et al. (1982). The probe was self-bored into the CC using water as the flushing fluid. Drainage was generally allowed at the base of the sample. A summary of the installation conditions during self-boring is given in Table 1.

Installation was performed with various boundary conditions in order to evaluate their influence on the test results (see Table 1).

A small vacuum (5 t/m^2) was applied to the inside of the SBP probe to maintain the adiprene membrane in close contact with the body of the probe.

The cutter speed was generally maintained at a rate of about 60 revolutions per minute. The distance of the cutter from the leading edge of the cutting shoe was varied from about 1.9 cm (0.75 inch) to 5.4 cm (2.13 inches). For the tests in dense sand the adiprene membrane was generally protected by using the chinese lantern. The size of the cutting shoe was adjusted to be the same diameter as the membranes.

The probe was advanced into the CC at a rate of about 3 cm/min. (1.18 inches/min).

A flowmeter was used to monitor the flow rate of the flushing water sent to the cutter. The flow rate was generally about 9 to 12 lt/min. The flow rates from the probe and calibration drainage lines were also monitored. During the installation, the CC pore pressures and boundary stresses and strains were monitored. All the sand flushed out from the CC during installation was carefully collected and weighted (oven-dry).

4.3. Sample Stresses

Following sample formation and probe installation, the sample was subjected to one-dimensional consolidation under conditions of no average lateral strain (i.e. $\Delta\epsilon_h = 0$). Normally

consolidated (NC) and mechanically overconsolidated (OC) specimens were reproduced.

During the loading and unloading consolidation phases, changes in vertical effective stress (σ'_v) and the corresponding vertical strain (ϵ_v) were recorded. This allowed the calculation of the constrained modulus (M_o) and the coefficient of earth pressure at rest (K_o).

A summary of the general CC conditions at the end of consolidation is given in Table 2.

An example of data collected during a typical sample stressing is given in Figure 8.

During the SBPT the sample boundary conditions could be controlled.

A summary of the possible boundary conditions is given in Figure 9.

The boundary conditions applied during each pressuremeter test are given in Table 2.

The most common boundary condition applied was constant vertical ($\sigma_v = \text{constant}$) and horizontal ($\sigma_h = \text{constant}$) stresses (BC1).

4.4. Pressuremeter Expansion

After sample stressing and the self-boring insertion when appropriate, the pressuremeter test was performed by expanding the membrane to a maximum cavity strain (ϵ_o) of about 10%. Cavity strain is defined in terms of circumferential strain;

$$\epsilon_o = \frac{\Delta R}{R_o} \quad \dots (1)$$

where:

R_o = initial cavity radius

ΔR = increment of cavity radius.

Generally, before the beginning of the expansion phase, a relaxation time ranging between:

- 30' to 60' in tests with ideal installation
- 60' to 180' in tests with self-boring installation

was allowed.

Only strain controlled tests were performed using an electronic Strain Control Unit (SCU) supplied by Cambridge In-Situ Ltd.

The SCU automatically adjusts the expansion pressure as a function of the output from the strain arms.

Constant strain rates of 0.1%/hour up to 2% per minute can be achieved. Generally, tests were performed at a strain rate of about 1%/minute.

Generally, during each expansion phase, two or three unloading-reloading (UR) loops and, during the contraction phase, one or two reloading-unloading (RU) loops were performed. The strain

amplitude for each UR or RU loop was maintained constant and in the order of 0.1 to 0.2%.

An example of a typical pressuremeter test result is shown in Figure 10.

Typical pressuremeter tests show the average strain for the three strain arms. The average strain is calculated at any instant in time as the numerical average of each strain arm measurement.

A summary of the probe and chamber conditions for the tests using self-bored installation is given in Table 1.

Data from all transducers in the SBP probe were stored on computer cassettes and printed in digital form on a paper tape printer. After each test the basic data was processed and corrected for membrane stiffness. Examples of the computer generated plots are given in Appendix I.

5. TEST RESULTS

A complete listing of all the test results is given in Appendix II.

5.1. Initial Horizontal Stress

It is generally postulated that, if the SBP probe is inserted into the ground with minimum disturbance to the surrounding soil, the total horizontal stress (σ_{ho}) existing in the soil prior to insertion can be measured. The σ_{ho} is measured by recording the corrected SBP cavity pressure (p_o) causing "lift-off" of the pressuremeter membrane. This postulation should be especially valid in the case of the "ideal-installation" used in the CC for test No.201 to 236, inclusive and No.262 and 263. Table 4 presents a summary of lift-off stresses for each strain arm. The lift-off stress was determined from a visual inspection of the early part of the expansion curve.

5.1.1. Initial Horizontal Stress: Ideal Installation

Examination of the results in Table 4, for ideal installation, shows that the measured average lift-off stress (p_o) is often significantly different than the applied boundary stress (σ_{ho}). Figure 11(a) presents a comparison of the measured average lift-off stress and the applied boundary stress for the tests with ideal-installation.

The average lift-off stress is defined as the observed "lift-off" from the cavity expansion versus average strain plot, as shown in Fig.10. This lift-off is generally very close to the first lift-off of one of the arms.

The reasons for the differences are not clear but may be caused by one or more of the following:

- a. stress concentration around the rigid SBP probe during one-dimensional stressing,
- b. mechanical compliance of the strain arms,
- c. arching effects caused by the presence of an annulus of looser sand around the SBP probe.

In the field, the possible existence of anisotropic stress fields [Dalton and Hawkins (1982)] should also be considered, but this possibility does not exist in the triaxial CC tests.

5.1.2. Evaluation of Stress Concentration

The possibility of stress concentrations around the probe in the CC during the consolidation stage was investigated using a rigid self-boring K_0 -cell manufactured by Cambridge In-Situ Ltd. The K_0 -cell has the same diameter as the SBP probe and consists of a rigid steel cylinder with a K_0 -cell mounted flush on one side. The K_0 -cell is strain-gauged and operated on a null-indicator principle. Gas pressure on the inside of the cylinder is constantly adjusted to ensure no lateral strain of the K_0 -cell.

One test was performed (Test N°226) using the K_0 -cell with ideal-installation in the CC. The test was carried out using Ticino sand at a $D_r = 60\%$. The sample was stressed under boundary conditions BC 1 up to a stress of $\sigma_{ho} = 10 \text{ kg/cm}^2$ and $\sigma_{vo} = 6.2 \text{ kg/cm}^2$. A comparison between the applied horizontal stress (σ_{ho}) and the measured stress (P_h) recorded with the K_0 -cell is shown in Figure 12.

The results from this special test indicate that there is little or no stress concentration around the SBP probe after ideal-installation in sand in the CC. A comparison between the K_0 -cell results and the SBP probe results is also included in Figure 11.

5.1.3. Mechanical Compliance of Strain Arms

The problem of mechanical compliance of the strain arms has been investigated in detail. The first indications of this phenomena emerged during SBP tests performed at several Italian clay and sand sites using the same SBP equipment used in this study [Ghionna et al. (1983), Jamiolkowski et al. (1985), Bruzzi et al. (1986)].

The following observations emerged from the field tests:

- a. the "lift-off" pressures from each strain arm were almost always different. This occurred even in soil deposits for which it was difficult to justify, based on geologic history, the presence of anisotropic horizontal in-situ stresses,

- b. the differences between the three measured "lift-off" pressures tended to increase with increasing soil stiffness and ambient in-situ soil stress.

These observations indicated a possible problem due to mechanical compliance of the strain arms. These problems were further confirmed during the CC testing when the following observations were made:

- despite the "ideal installation" of the SBP probe and the simple stress history of the CC specimens, different "lift-off" pressures were recorded for each of the three strain arms. The difference was more pronounced in the stiffer samples,
- during the sample stressing with the probe installed, apparent inward movement of the strain arms was recorded when the radial chamber stress was increased and apparent outward movement when the chamber stress was decreased. An example of this phenomenon is shown in Figure 13.

Figure 14 presents the results of the initial portion of expansion curves recorded with each strain arm and with the averaged strain for a test with pronounced mechanical compliance.

The mechanical compliance of the strain arms tends to confuse the initial part of the expansion curves and makes the detection of the lift-off pressure uncertain.

The detection of the lift-off pressure becomes more difficult with increasing stiffness of the surrounding soil because the slope of the initial portion of the expansion curve becomes very steep.

In an effort to eliminate or at least reduce the mechanical compliance the three strain arms were modified.

A comparison between the original and modified strain arm designs is shown in Figure 15. The modified arms had the following major changes:

- the body of the arms were made thicker and stiffer and were machined from stainless steel instead of the original brass,
- the alignment of the pivots and arms with respect to their seats on the probe body were improved,
- the pivots were modified by using precision miniature bearings.

All the tests from N°225 onwards used a SBP probe with the modified strain arms.

Figure 11(b) shows a comparison between the measured average lift-off stress (with modified arms) and the applied chamber stress for the remaining CC tests with ideal installation. The results indicate that the modifications to the strain arms have minimized to some extent the mechanical compliance but have not completely removed the problem.

At present, based on the CC results using ideal installation it appears that the strain measuring system in the existing version of the Cambridge In-Situ Ltd., Camkometer (Mark VIII) requires radical changes in order to improve the precision of the measured lift-off pressures, especially in stiffer soils.

5.1.4. Evaluation of Arching Effects

The possible problem of arching around the SBP probe has not been directly investigated. The experience gained in the evaluation of sample homogeneity of pluvially deposited CC samples [Baldi et al., (1985)] indicates that D_R tends to increase slightly towards the center of the sample. However, this experience refers to samples formed without the SBP probe installed inside the CC.

5.1.5. Initial Horizontal Stress: Self-Bored Installation

Figure 16 compares the measured average lift-off pressures against the applied boundary stress (σ_{ho}) for the CC tests with self-boring installation. In almost all cases the measured average lift-off stress is less than the applied stress and often close to the water pressure in the CC. This indicates significant sample disturbance during the installation, especially in loose and medium dense samples.

The ratio between the average lift-off stress (p_o (AV)) and the applied boundary stress (σ_{ho}) for the self-bored installation is:

$$\frac{p_o \text{ (AV)}}{\sigma_{ho}} = 0.47 \pm 0.28 \quad \dots (2)$$

Table 4 presents a summary of the individual lift-off pressures for each strain arm. Examination of Table 4 shows that, for the self-bored installation, the variation between lift-off pressures from the individual arms is extremely large.

Because sands are generally stiff in comparison to soft clays, the measurement of in-situ stress in sands is extremely difficult.

A slight outward disturbance during self-boring will tend to produce an overestimate of σ_{ho} . A slight inward disturbance during self-boring can cause the sand around the probe to arch and produce a significant underestimate of σ_{ho} .

Based on the CC results, it appears that the measurement of in-situ stresses in sands using the self-boring pressuremeter is extremely sensitive to disturbance.

5.2. Shear Modulus

The evaluation of deformation characteristics of soils from the results of a SBPT is usually linked to the assumption that the probe is expanded in a linear, isotropic, elastic, perfectly plastic soil. With this assumption the soil surrounding the probe is subjected to pure shear only. This holds true provided the applied pressuremeter cavity effective stress (p') stays below the yield stress (p'_y) of the soil element adjacent to the cavity wall. The values of p'_y in a purely frictional Coulomb material is given by the formula [Baguelin et al. (1978)]:

$$p'_y = p'_o (1 + \sin \phi) \quad \dots (3)$$

For the range of effective cavity stress $p'_o < p' \leq p'_y$, the expansion curve should have a constant slope $d_p/d\epsilon_o = 2 G_i$ [Baguelin et al. (1972, 1978)] where:

G_i = initial shear modulus of tested soil, see Fig.17

The above is true for SBPT's performed in an infinite medium (i.e. in-situ). However Fahey (1980) demonstrated that because of the limited dimensions of a CC the initial slope of expansion curves obtained in the CC tend to be slightly too small. In this study, the effect of the limited dimensions of the ENEL CRIS CC has only a minor effect, resulting in a reduction of less than 3% on the measured values of G . The definition of G_i given above implicitly incorporates the following simplified assumptions:

- a. The length (L) to diameter (D) ratio of the probe is sufficiently large to ensure deformations of the surrounding soil occur in plane strain conditions ($\epsilon_z = 0$).
- b. The expansion proceeds with no volume change in the surrounding soil mass (i.e. linear, isotropic elastic material).
- c. All soil elements surrounding the expanding cavity have the same stress strain characteristics.

The first assumption (a) appears reasonable for the Camkometer probe used in this research, where the $L/D=6$. The other assumptions (b) and (c) are both strictly linked to the hypothesis made about the stress-strain relationship of soil. Both assumptions require that the effective stress path (ESP) projected on the horizontal plane should have a shape as shown schematically in Fig.18. In reality because of, the strain non-linearity, elastic anisotropy, and work hardening plasticity, etc., the behaviour of sands deviates from that of the isotropic-elastic perfectly plastic material so that volume

changes occur even during the early stage of the expansion. A more realistic ESP, as obtained by Manassero (1987), is qualitatively also shown in Fig.18. Comparison of the two stress paths shown in Fig.18 clearly indicates that beyond the initial elastic stage (point 1') the mean effective stress (σ'_0) in the soil surrounding the expanding pressuremeter probe is not constant and consequently the volumetric strain cannot be equal to zero.

Since the modulus (G_i) can only be determined with validity from the very early part of the expansion curve the value is very sensitive to disturbance.

An alternative to the assessment of G_i from the initial part of the expansion curve is to evaluate G from correctly performed unloading-reloading (G_{UR}) and reloading-unloading (G_{RU}) loops as illustrated in Fig.17. According to Wroth (1982) the amplitude of the unloading should be performed in such a manner as to avoid the failure of the soil at the cavity wall in extension. For an isotropic-elastic, perfectly plastic material the magnitude of the effective cavity stress change ($\Delta p'$) during an elastic unloading should therefore not exceed the following:

$$\Delta p' = \frac{2 \sin \phi_{PS}}{1 + \sin \phi_{PS}} p'_c \quad \dots (4)$$

where:

ϕ_{PS} = friction angle under conditions of plain strain
 p'_c = effective cavity stress at which unloading loop starts.

The slope of the secant within the loop, (see Fig.17) is again equal to $2 G_{UR}$ or $2 G_{RU}$. Both G_{UR} and G_{RU} represent an "elastic" shear stiffness of the tested sand. Within the framework of elasto-plasticity it can be demonstrated that during a drained test any unloading of the expanding cavity wall will bring the surrounding soil below the current yield surface. Inside this yield surface, (see Fig.19) the strains are small and to a large extent recoverable.

In addition to the above mentioned moduli (G_i , G_{UR} , G_{RU}) it is also possible to evaluate directly from the expansion curve the secant pressuremeter modulus G_s , as shown in Figure 17. The assessment of G_s is also based on the assumption of an elastic soil behaviour which, except for the very early part of the expansion curve where $G_s = G_i$, and during unloading-reloading cycles, is conceptually not true.

Despite the lack of a clear physical meaning, G_s is frequently incorporated in the empirical design rules for shallow and deep foundations in France [Baguelin et al. (1978)].

Table 5 reports the values of G_s computed at cavity strains equal to 0.5%, 1.0% and 1.5%.

Values of G_{UR} for the different unloading-reloading cycles are given in Tables 6 to 9. Values of G_{RU} for the reloading-unloading cycle are given in Table 10.

In all soils, and especially in sands, the early part of the self-bored pressuremeter curve is strongly influenced by disturbance due to the installation. Therefore, G_i and G_s are also strongly influenced by disturbance. On the other hand, G_{UR} and G_{RU} are almost completely independent from the initial shape of the expansion curve and hence, independent from disturbance.

Despite this advantage, there is still the problem of how to apply the measured G_{UR} and G_{RU} values in engineering design. This requires some assessment of the average stress and shear strain levels relevant to the measured moduli [Robertson (1982)]. As with all boundary value problems this is difficult to assess and requires a number of simplifying assumptions.

Concerning the relevant stress level, existing practice has been to refer G_{UR} to the average stress existing around the expanding pressuremeter probe. This average stress may be either the mean octahedral effective stress [Robertson (1982)] or the mean value of the plane strain effective stress [Fahey and Randolph (1984)].

In this study the latter stress will be adopted.

When a value of the reference stress has been selected, the following tentative procedure can be used to relate the measured G_{UR} and G_{RU} values to any level of effective stress:

- Consider the value of G_{UR} corresponding to a given value of the double shear strain amplitude of the cycle ($\Delta\gamma = \gamma_B - \gamma_A$) and to the effective cavity stress from which the cycle starts (p'_C), see Fig.19 and Tables 6 through 10.
- Compute the weighted average of the current effective stress (p'_{AV}) existing around the SBP probe at p'_C , adopting an appropriate constitutive equation:

$$p'_{AV} = \chi p'_C \quad \dots (5)$$

For elastic perfectly plastic material, referring to the average stress on the horizontal plane existing in the plastic zone ($r_C \leq r \leq R_p$), the parameter χ can be computed from the following equation, see also Appendix III:

$$\chi = \frac{1}{(1 - \sin \phi^{PS})} \cdot \frac{\left[\frac{p'_C}{\sigma'_{ho} (1 + \sin \phi^{PS})} \right]^{\omega_1} - 1}{\left[\frac{p'_C}{\sigma'_{ho} (1 + \sin \phi^{PS})} \right]^{\omega_2} - 1} \quad \dots (6)$$

where:

σ'_{ho} = initial effective horizontal stress. In a high quality SBPT σ'_{ho} should be closed to the measured effective lift-off pressure p'_0

$$\omega_1 = \frac{1 - \sin \phi^{PS}}{2 \sin \phi^{PS}} \quad \dots (7)$$

$$\omega_2 = \frac{2 \sin \phi^{PS}}{1 + \sin \phi^{PS}} \quad \dots (8)$$

r = radial distance from center of cavity

R_p = radius of plastic zone

r'_C = radius of cavity when cavity pressure = p'_C

In practice the true value of σ'_{ho} is generally unknown, therefore, the assessment of χ is made by introducing into the above formula the measured value of p'_0 .

The values of χ computed for each SBPT performed in the CC are given in Tables 6 through 10 together with the corresponding values of p'_{AV} .

The use of the relationship, $p'_{AV} = \chi p'_C$, is correct provided the following condition is satisfied:

$$p'_C > \sigma'_{ho} (1 + \sin \phi^{PS}) \quad \dots (9)$$

If this condition is not fulfilled the p'_{AV} should be assumed equal to $\sigma'_{ho} = p'_0$.

- Once the p'_{AV} is assessed it is possible to compute the modulus number K_G from the following empirical formula proposed by Janbu (1963):

$$G_{UR} = K_G p_a \left[\frac{p'_{AV}}{p_a} \right]^n \quad \dots (10)$$

where:

K_G = modulus number

n = modulus exponent

p_a = reference stress, usually $p_a = 98.1$ kPa

p'_{AV} = average effective stress around the probe

For sand, the modulus exponent is generally within the range of 0.4 to 0.5, with a slight tendency to increase with increasing level of strain [Wroth et al. (1979)]. Knowing the value of K_G it is possible to compute the shear modulus G for any desired stress level.

Following the procedure outlined above, the measured G_{UR} and G_{RU} values for each cycle have been referred to the effective horizontal stress σ'_{ho} applied to the boundary of the CC specimen, assuming $n=0.43$ as obtained by Lo Presti (1987). The corresponding values of G_{URO} and G_{RUO} are given in Tables 6 through 10.

The same tables also show the values of maximum dynamic shear modulus (G_o) obtained from resonant column tests performed by Lo Presti (1987) on pluvially deposited Ticino sand. The value of G_o corresponding to each SBPT has been computed using the following empirical equation based on the experimental data obtained by Lo Presti (1987):

$$G_o = 647.0 \cdot p_a \left(\frac{\sigma'_{ho}}{p_a} \right)^{0.43} \frac{(2.27 - e)^2}{1+e} \quad \dots(11)$$

where:

e = void ratio of the sand in the CC (*)

p_a = reference stress = 98.1 kPa

In order to make a meaningful comparison between the G_{URO} and G_o values it is necessary to consider other factors influencing the deformation characteristics of sand. Among them, the most relevant is the strain level. Each cycle is characterized by the double shear strain amplitude ($\Delta\gamma$) at the cavity wall where:

$$\Delta\gamma = \gamma_B - \gamma_A = 2 (\epsilon_{OB} - \epsilon_{OA}) \quad \dots(12)$$

Values of $\Delta\gamma$ are reported in Tables 6 through 10.

The maximum shear modulus G_o corresponds to a shear strain level less than $10^{-4}\%$, which is two orders of magnitude smaller than the strains at which G_{UR} and G_{RU} have been measured. In order to be able to compare G_o against G_{UR} , at the same strain level, it is necessary to use a relationship which can match the decay of G with increasing γ . The simplest solution is offered by the well known hyperbolic stress-strain relation in the form proposed by Hardin and Drnevich (1972):

(*) Computed assuming the specific weight of the tested sands 26.35 kN/m³ and 26.72 kN/m³ for Ticino and Høksund sands, respectively.

$$\frac{G}{G_0} = \frac{1}{1 + \frac{\gamma}{\gamma_r}} = \frac{1}{1 + \frac{G_0 \gamma}{\tau_{\max}}} \quad \dots(13)$$

where:

G = shear modulus

γ = shear strain

τ_{\max} = maximum shear stress

γ_r = reference strain = $\frac{G_0}{\tau_{\max}}$

Referring to the SBP unloading-reloading cycle and relating the above given hyperbolic formula directly to the modulus number (K_G), one gets:

$$\frac{G_{UR}}{G_0} = \frac{1}{1 + \frac{G_0 \Delta \gamma_{AV}}{2 \sigma'_{ho} \sin \phi^{PS}}} \quad \dots(14)$$

and therefore:

$$K_{G_0} = K_{G_{UR}} (\sigma'_{ho})^{n_{UR} - n_0} \cdot \left[1 + \frac{K_{G_0} (\sigma'_{ho})^{n_0} \cdot \Delta \gamma_{AV}}{2 \sigma'_{ho} \sin \phi^{PS}} \right] \quad \dots(15)$$

where:

K_{G_0} = modulus number related to the maximum dynamic shear modulus

$K_{G_{UR}}$ = modulus number as computed from G_{UR} , see equation ... (10)

$\Delta \gamma_{AV}$ = average strain in the plastic zone around the expanding probe

n_0 = modulus exponent related to the maximum dynamic shear modulus, G_0

n_{UR} = modulus exponent related to G_{UR} , see equation ... (10)

Referring to the data given in Tables 6 through 10 and assuming:

• $\Delta \gamma_{AV} \approx 0.45 \Delta \gamma$, see Robertson (1982)

• $n_0 = n_{UR} = 0.43$

• σ'_{ho} = boundary stress applied to the CC specimen,

one can assess, extrapolating using the hyperbolic stress strain relation, the value of K_{G_0} and hence compute;

$$G_0^{SBP} = f(G_{UR}, \Delta \gamma, \sigma'_{ho}) \quad \dots(16)$$

For the available tests in this study this approach gives, for the 1st and 2nd unloading-reloading cycles, the following:

$$1.3 \leq \frac{G_o}{G_o^{SBP}} \leq 1.8 \quad \dots (17)$$

where:

G_o = maximum dynamic shear modulus as measured in the resonant column tests

G_o^{SBP} = maximum dynamic shear modulus assessed from G_{UR} .

The lack of coincidence between G_o and G_o^{SBP} may be due to the following:

- The oversimplified and approximate nature of the procedure used to obtain G_o^{SBP} from G_{UR} .
- The influence of the number of unload-reload cycles on the shear stiffness of sands. Values of G_{UR} have been measured during a single unloading-reloading cycle. Therefore the extrapolated G_o^{SBP} values should be referred to the 1st unload-reload cycle while the resonant column G_o has been measured after thousands of unload-reload cycles. For the given level of shear strain amplitude this factor can be expected to be responsible for differences between G_o and G_o^{SBP} of up to about 10 to 20 percent.
- The pluvially deposited sand tends to exhibit an anisotropic behaviour. Within the framework of the theory of elasticity for transversally isotropic soils, the available shear moduli can be defined as follows:

$G_{UR} = G_{HH}$ = shear modulus for shearing in horizontal direction

$G_o = G_{VH}$ = shear modulus for shearing in vertical direction

However this factor does little to justify the observed differences between G_o and G_o^{SBP} . The results of large scale tests performed by Stokoe and co-workers [Knox (1982, Stokoe and Ni (1985), Lee (1986)] indicate that, in sand the velocity of the horizontally polarized shear wave (v_s^{HH}) is 1.1 to 1.15 higher than the vertically polarized shear wave velocity (v_s^{VH}). This data indicates a G_{HH}/G_{VH} ratio ranging between 1.2 and 1.3, therefore suggesting $G_o^{SBP} > G_o$.

5.3. Shear Strength

Theoretical methods for the determination of the peak friction angle (ϕ) of sands from pressuremeter test data have been proposed by several authors; i.e. Gibson and Anderson (1961), Ladanyi (1963), Vésic (1972), Hughes et al. (1977), Robertson (1982) and Manassero (1987). Each method relies on a model for the sand behaviour. Most of the above methods consider that sand has a constant friction angle at failure. However, not all methods allow for the fact that sand changes in volume during shearing.

In Ladanyi's method the volume change is considered to be constant at the point the failure stress ratio is reached. This volume change is introduced into the assessment of the friction angle by a trial and error method.

Vésic's solution uses the results of laboratory tests directly to determine volume change. However, the problem of determining the appropriate laboratory density to perform the tests, is not easy to resolve. Also, the laboratory tests may not produce reliable volume change behaviour because the in-situ structure and fabric cannot be reproduced in the laboratory.

The solution developed by Hughes et al. (1977) relies on the fact that the volume changes are occurring during the expansion of the cavity and the amount of volume change (dilation) is closely related to the current friction angle developed. This approach brings together the stress dilatancy concept of Rowe (1962) and the observed behaviour of sand in simple shear, as for example, observed by Stroud (1971).

Figure 20 shows typical results of simple shear tests on sand conducted by Stroud (1971) and the ideal soil model assumed in the method by Hughes et al. (1977).

In the method proposed by Hughes et al. (1977), it was shown that:

$$\log \left(\frac{\Delta R}{R_0} + \frac{c}{2} \right) = \frac{n+1}{1-N} \cdot \log (p-u_0) + \text{constant} \quad \dots (18)$$

where:

- R_0 = initial radius of pressuremeter
- ΔR = change in radius of pressuremeter
- $\Delta R/R_0$ = cavity strain, ϵ_0
- c = intercept shown on Fig.20 (c) and (d)
- p = total pressuremeter cavity stress
- u_0 = pore water pressure
- $\frac{1-N}{n+1}$ = $\frac{(1+\sin \nu)}{(1+\sin \phi)} \cdot \sin \phi$ = slope S
- $\sin \nu$ = maximum dilation rate

In the above method the intercept "c" is assumed zero and a plot of the pressuremeter data in terms of $\log (p-u_0)$ (effective cavity stress) against $\log (\Delta R/R_0)$ will tend towards a straight line with a slope S. This slope is related to the in-situ friction angle (ϕ) and the maximum dilation rate ($\sin \nu$).

For very dense sands the intercept "c" is essentially negligible and for all practical purposes can be ignored. The results of the laboratory studies conducted by Jewel et al. (1980) in very dense sands ($D_R = 90\%$) using the self-boring pressuremeter probe show that the above technique appears to work very successfully. In loose materials the method is not so convenient as the pressuremeter does not expand sufficiently for the sand around the probe to reach the linear portion of its volumetric strain/shear strain curve.

The method by Robertson (1982) expands on the method by Hughes et al. (1977) but incorporates an empirical correction to account for the non-linear nature of the volume change - shear strain relationship (see Figure 20).

The method developed by Manassero (1987) is also a further development of the Hughes et al. (1977) method but incorporates the full non-linear nature of the stress-strain curves. The method assumes that Rowe's stress dilatancy concept is valid and solves the shear-volume coupling in a unique manner by using a finite difference numerical solution.

The method by Manassero (1987) allows the complete stress strain and stress path to be calculated for each pressuremeter test. Figures 21 and 22 show typical examples of the calculated stress strain and stress paths for pressuremeter tests with ideal installation. From the stress path plots (d) in Figures 21 and 22 it is clear that the soil surrounding the probe is initially strain hardening up to the point of peak strength $(\sigma'_x/\sigma'_y)_{\max}$, and then strain softening.

The deviation of the soil behaviour from the simple isotropic elastic behaviour can be represented by the angle β (see Fig. 23), which is the angle between the point of peak strength $(\sigma'_x/\sigma'_y)_{\max}$ and the initial mean normal stress, p_0 . Values of β are given in Table 11 for each pressuremeter test analysed using the method by Manassero (1987). In order to avoid numerical instability in the calculation of the stress strain curves and stress paths using the method by Manassero (1987) a 7th order polynomial function was made to fit the measured curve.

Full details of the method by Manassero (1987) is given in Appendix IV.

The methods by Hughes et al. (1977), Robertson (1982) and Manassero (1987) have been evaluated using the results from the SBPT's performed in the CC, and results are presented in Table 11.

All three methods require a knowledge of the friction angle at constant volume (ϕ_{cv}). Values of ϕ_{cv} were determined for Ticino and Hokksund sand using a ring shear apparatus. A summary of the ring shear results are shown in Figure 24. An average value of $\phi_{cv} = 34^\circ$ was used in the analyses.

A summary of the calculated angles of friction and dilatancy obtained from the pressuremeter tests performed in the CC are presented in Table 11.

Peak friction angles have also been determined from triaxial tests on Ticino sand at various stress levels and densities. Triaxial specimens were formed using the same pluvial deposition technique as used to form the CC specimens.

The peak friction angles (ϕ_p^{PS}) and dilation angles (ν^{PS}) determined from the pressuremeter are obtained under approximately plain strain conditions and are related to the average effective stress around the probe during the test. Therefore, to compare the calculated peak friction angles from the pressuremeter (ϕ_p^{PS}) with those obtained from triaxial tests (ϕ_p^{TX}) requires some corrections to account for stress level at failure (σ_{ff}) and boundary conditions (plain strain-triaxial).

The peak friction angles obtained from the laboratory triaxial compression tests (ϕ_p^{TX}) were corrected to the equivalent stress level at failure (σ_{ff}) occurring in each pressuremeter test and then corrected to an equivalent plain strain value (ϕ_p^{PS}).

The stress level at failure (σ_{ff}) for each pressuremeter test was calculated assuming a linear elastic isotropic soil behaviour, where:

$$\sigma_{ff} = \sigma'_{ho} [1 - \sin^2 \phi_p^{PS}] \quad \dots(19)$$

The values of ϕ_p^{TX} were then determined at the σ_{ff} stress level using the curved strength envelope equation developed by Baligh (1975), where:

$$\tan \phi_p^{TX} = \tan \phi_o^{TX} + \tan \alpha \left[\frac{1}{2.3} - \log \cdot \frac{\sigma_{ff}}{p_a} \right] \quad \dots(20)$$

where:

ϕ^{TX} = secant friction angle from triaxial compression test at $\sigma_{ff} = 2.72 p_a$

p_a = reference stress = 98.1 kPa

α = angle which describes the curvature of the failure envelope

Values for ϕ_O^{TX} and α for Ticino sand are given by Baldi et al. (1986).

The triaxial friction angle values were then converted to equivalent ϕ_p^{PS} using the following equation by Lade and Lee (1976);

$$\phi_p^{PS} = \phi_p^{TX} \cdot 1.5 - 17^\circ$$

The calculated equivalent ϕ_p^{PS} values determined from the laboratory triaxial results are also shown in Table 11.

Comparisons between the calculated ϕ_p^{PS} from the SBPT results using the methods by Hughes et al. (1977), Robertson (1982) and Manassero (1987) and the equivalent ϕ_p^{PS} obtained from triaxial results are shown in Figure 25. The following comments can be made about the results presented in Figure 25.

1. No method provides a reliable estimate of ϕ_p^{PS} for sands from the SBPT.
2. The method by Robertson (1982) appears to produce less scatter.
3. Generally the scatter in calculated ϕ_p^{PS} is slightly larger for the test results where the probe was self-bored into the CC.

It is interesting to note that, although most of the self-bored results gave very poor values of ϕ_{ho} due to disturbance, the self-bored data gave reasonable values of ϕ_p^{PS} . This is consistent with observations made in the field (Ghionna et al., 1983; Jamiolkowski et al., 1985; Bruzzi et al., 1986).

Based on the CC results, it appears that the determination of peak friction angle (ϕ_p^{PS}) in sands using the self-boring pressuremeter is not very reliable and depends on the method of analyses.

Table 11 also provides the values of the state parameter (ϕ), as defined by Been and Jefferies (1985). The ϕ combines the influence of both mean effective stress level and void ratio on the dilatancy of sand and may correlate to the parameters reflecting the behaviour at failure, i.e. ϕ , ν .

5.4. Limit Pressure

Table 5 presents the calculated limit pressures (P_{lim}) from each SBPT using two existing methods. The two methods evaluated were:

WW
 P_{lim} : Method by Windle and Wroth (1977)

AA
 P_{lim} : Method by Al Awkati (1985)

Examples of the plots to calculate P_{lim} are shown in Appendix I.

Unfortunately, the concept of a limit pressure is not applicable to pressuremeter tests in sand, especially with a maximum cavity strain of only 10%. Because there is no fundamental concept to support the values of P_{lim} , their application to design is related to empirical correlations. This is further complicated by the fact that different values of P_{lim} are obtained from the different methods (see Table 5).

5.5. Boundary Conditions

The laboratory studies by Fahey (1980) showed that the condition of a constant horizontal stress boundary at some finite distance from the expanding pressuremeter had the effect of producing an apparent strain softening in the pressure expansion curve. This situation was not observed in any of the pressuremeter tests performed for this study. The reasons for this apparent lack of boundary effect could be the following:

- The ENEL-CRIS CC is 1.2 m in diameter, compared to the 0.9 m diameter CC used by Fahey (1980).
- Fahey studied only very dense sand ($D_r = 92\%$) in which the plastic zone expands rapidly during the pressuremeter test. For the tests in this study where $D_r = 90\%$ there was no strain softening observed.

No influence of boundary effects could be observed for the interpreted values of σ_{ho} , G and ϕ .

6. SUMMARY AND CONCLUSIONS

A series of 47 self-boring pressuremeter tests have been performed in the ENEL-CRIS calibration chamber. 25 tests were performed with the probe in-place during sample preparation (i.e. ideal installation) and 22 tests were performed with the probe self-bored into saturated sand. 1 test was not completed due to a ruptured membrane during probe installation (Test No. 34).

The purpose of the testing was to evaluate the performance of the self-boring pressuremeter probe under strictly controlled laboratory conditions and to critically review existing interpretation methods of SBPT in sands. The SBP probe used in the study was the Camkometer Mark VIII manufactured by Cambridge In-Situ Ltd., England. The results of the testing can be summarized as follows:

1. Assessment of in-situ stress (σ_{ho})

- Ideal installation:
Large scatter exists in the experimental data because of mechanical compliance of the strain measurement system. The precision required (approximately 0.005 mm) is probably beyond the limits of a mechanical system. There is, therefore, a need for improvement in the measurement system of lift-off pressure, possibly by adding non-contact precision transducers. The existing strain arm design is sufficiently reliable to measure radial displacement during the main expansion phase.
- Self-bored installation:
The disturbance caused by the self-boring process generally rendered the measured lift-off pressure too low, highly scattered and generally unreliable. However, the soil tested in this study (i.e. freshly deposited, unaged, uncemented, clean sand) creates particularly unfavourable conditions with respect to the reliable assessment of in-situ stress. More reliable assessment of σ_{ho} may be possible in natural sand deposits.

2. Assessment of Shear Modulus, G

- Even for the same sand (grain size, fabric, stress history, etc.) the shear stiffness is a complex function of; void ratio (e), effective stress (p'), shear strain (γ), number of cycles (N_c) and anisotropy and plasticity.
- There is a need to improve the link between the measured G and the stiffness required for specific design problems.
- The initial shear moduli (G_i) and the secant shear moduli (G_s) are both sensitive to disturbance and are very complex to locate within the framework of elasto-plastic theory.
Therefore, G_i and G_s are almost impossible to link to other laboratory and in-situ tests and to design problems.
- The shear moduli determined from unload-reload cycles (G_{UR} or G_{RU}) are "elastic" but non-linear and are much less sensitive to disturbance due to installation. G_{UR} or G_{RU} should be linked to the relevant design problems via appropriate corrections accounting for stress (p') and strain (γ) level. Soil anisotropy should also be considered, since SBPT $G_{UR} = G_{HH}$, while in many practical problems the value G_{VH} is appropriate.
- Because G_{UR} and G_{RU} reflects the shear stiffness of sands inside the current yield surface they implicitly refer only to overconsolidated (OC) materials.
- When relating G_{UR} to the dynamic shear modulus (G_o) the influence of number of cycles (N_c) should also be considered.
- Further theoretical work is required concerning the application of G_{UR} to engineering design practice.
- At present G_{UR} represents a rather unique method to assess directly some kind of shear stiffness for natural sands in-situ, with the exception of the dynamic shear moduli from in-situ shear wave velocity measurements.

3. Assessment of peak friction angle ϕ_p^{PS}

- A large scatter exists between the calculated ϕ_p^{PS} from the SBPT results and the equivalent values of ϕ_p^{PS} obtained from triaxial compression tests.
- None of the existing methods evaluated (Hughes et al., 1977; Robertson, 1982; Manassero, 1987) provided consistently reliable values of the peak friction angle under plane strain conditions (ϕ_p^{PS}).
- Evaluation of the reference friction angle from laboratory triaxial testing is complicated by the curvature of the failure envelope, the variation in stress level at failure (σ_{ff}) in the pressuremeter test and the strain conditions (plain strain-triaxial).
- The calculation of ϕ_p^{PS} from the self-bored pressuremeter tests appear to be less sensitive to initial disturbance than the measurement of in-situ stress (σ_{ho}).
- The method by Robertson (1982) appears to produce less scatter.
- Because of the relatively high densities ($D_R > 40\%$) and low stresses (max 500 kPa) the sand tested had $\phi_p^{PS} \geq 41^\circ$. Therefore, the high friction angles creates particularly unfavourable conditions for the ϕ methods evaluated.

The objective of this study has been to verify the performance of the SBPT in sand and to critically review existing approaches to interpretation of the data for geotechnical design.

The objectives of this study have been reached. However, the study has produced extensive data concerning the SBPT in sand and not all the information has been fully studied and discussed in this report. Further research can be performed to fully evaluate all the available data resulting from this study.

LITERATURE CITED

- AL AWKATI A., (1975). "On Problems of Soil Bearing Capacity at Depth". Ph. D. Thesis, Duke Univ., Durham, N.C.
- BAGUELIN F., JEZEQUEL J.F., LE MEE H. and LE MEHAUTE A., (1972). "Expansion of Cylindrical Probes in Cohesive Soils". JSMFD, ASCE, SM11.
- BAGUELIN F., JEZEQUEL J.F. and SHIELDS D.H., (1978). "The Pressuremeter and Foundation Engineering". Trans. Tech. Publications, Clausthall.
- BALDI G. et al. (1985). "Laboratory Validation of In-Situ Tests". AGI, Jubilee Volume, XI ICSMFE, San Francisco.
- BALDI G. et al., (1986). "Interpretation of CPT's and CPTU's. II Part: Drained Penetration on Sands". Proc. IV Int. Geotech. Seminar NTI on Field Instrumentation and in Situ Measurements, Singapore.
- BALIGH M.M., (1975). "Theory of Deep Site Static Cone Penetration Resistance". Res. Rep. R75-56, N.517, MIT Cambridge Mass.
- BELLOTTI R., BIZZI G., GHIONNA V.N., (1982). "Design Construction and Use of a Calibration Chamber". Proc. ESOP II, Amsterdam, V.2.
- BEEN K. and JEFFERIES M.G., (1985). "A State Parameter for Sand". Geotechnique, N.2.
- BRUZZI D. et al. (1986). "Self-Boring Pressuremeter in Po River Sand". Proc. II Int. Symp. on the Pressuremeter and Its Marine Applications. Texas A&M Univ., ASTM STP 950.
- DALTON J.P.C., HAWKINS P.G., (1982). "Some Measurements of the In-Situ Stress in a Meadow in Cambridge Shire Country Side". Gr. Engng. N.5.
- FAHEY M., (1980). "A Study of the Pressuremeter Test in Dense Sand". Ph. D. Thesis, Cambridge Univ., U.K.
- FAHEY M., RANDOLPH M.F., (1984). "Effect of Disturbance on Parameters Derived from Self-Boring Pressuremeter Tests in Sand", Geotechnique, N.1

- GHIONNA V.N., JAMIOLKOWSKI M., LACASSE S., LADD C.C., LANCELLOTTA R. and LUNNE T., (1983). "Evaluation of Self-Boring Pressuremeter". Proc. Int. Symp. on Soil and Rock Investigation by In-Situ Testing, Paris, V.2
- GIBSON R.E. and ANDERSON W.F., (1961). "In-Situ Measurement of Soil Properties with the Pressuremeter". Civ. Eng. & Publ. Works, Rev., May.
- HARDIN B.O. and DRNEVICH V.P., (1972). "Shear Modulus and Damping in Soils: Design Equations and Curves", JSMFED, ASCE SM7.
- HUGHES J.M.O., WROTH C.P. & WINDLE D., (1977). "Pressuremeter Tests in Sands". Geotechnique, N.4.
- JACOBSEN M., (1976). "On Pluvial Compaction of Sand". Rep. N.9. Laboratoiert for fundering. Aalborg Univ., Denmark.
- JAMIOLKOWSKI M., LADD C.C., GERMAINE J.T., LANCELLOTTA R., (1985). "New Developments in Field and Laboratory Testing of Soils". Proc. XI ICSMFE, San Francisco, Theme Lectures, V.1.
- JANBU N., (1963). "Soil Compressibility as Determined by Oedometer and Triaxial Tests". Proc. III ECSMFE, S.1, Wiesbaden.
- KNOX D.P., (1982). "Effect of State of Stress on Velocity of Low Amplitude Shear Wave Propagating Along Principal Stress Direction in Dry Sand". Ph. D. Thesis Texas Univ., Austin.
- LADANYI B., (1963). "Evaluation of Pressuremeter Tests in Granular Soils". Proc. of the II Pan American Conf. SMFE São Paulo, V.1.
- LADÉ P.V. & LEE K.L., (1976). "Engineering properties of Soil", Report UCLA-ENG-7652, California Univ., Los Angeles.
- LEE S.H.H., (1986). "Investigation on Low Amplitude Shear Wave Velocity in Anisotropic Material". Ph. D. Thesis, Texas Univ., Austin.
- LO PRESTI D., (1987). "Mechanical Behaviour of Ticino Sand from Resonant Column Test". Ph. D. Thesis, Politecnico di Torino, Torino.
- MANASSERO M., (1987). "Stress-Strain Relationship of Sands from Self-Boring Pressuremeter Tests". Atti del Dipartimento di Ingegneria Strutturale, Politecnico di Torino, Torino.

- ROBERTSON P.K., (1982). "In-Situ Testing of Soil With Emphasis on Its Application to Liquefaction Assessment", Ph.D., Thesis, Univ. British Columbia, Vancouver.
- ROWE P.W., (1962). "The Stress-Dilatancy Relation for Static Equilibrium of An Assembly of Particles in Contact". Proc. Royal Soc.
- STROUD M.A., (1971). "Sand at Low Stress Levels in the Simple Shear Apparatus", Ph. D. Thesis, Cambridge Univ., U.K.
- STOKOE K.H. & NI F.H., (1985). "Effects of Stress State and Strain Amplitude on Shear Modulus of Dry Sand". Proc. II Symp. on Interaction of Non-Nuclear Munitions with Structures, Panama City Beach, Florida.
- VESIC A.S., (1972). "Expansion of Cavities in Infinite Soil Masses", JSMFED, ASCE, SM3.
- WINDLE D., WROTH C.P., (1977). "In-Situ Measurement of the Properties of Stiff Clays". Proc. IX ICSMFE, Tokyo, V.1
- WROTH C.P., (1982). "British Experience with the Self-Boring Pressuremeter". Proc. Symp. on the Pressuremeter and Its Marine Applications, Paris.
- WROTH C.P., RANDOLPH M.F., HOULSBY G.T. & FAHEY M., (1979). "A Review of the Engineering Properties of Soils with Particular Reference to the Shear Modulus", Cambridge Univ., CUED/D Soils TR75.

NOTATIONS

BC	= Boundary condition
L	= Length of pressuremeter membrane (490 mm)
D	= Diameter of pressuremeter (82 mm)
σ_h, σ'_h	= Horizontal stress; total and effective
σ_v, σ'_v	= Vertical stress; total and effective
D_R	= Relative density (after consolidation)
K_0	= Coefficient of earth pressure at rest
OCR	= Overconsolidation ratio
ϵ_v	= Vertical strain
M_O^t	= Tangent constrained modulus
M_O^s	= Secant constrained Modulus
ϵ_o	= Pressuremeter cavity strain
R_o	= Initial radius of cavity
ΔR	= Change in radius of cavity
P_o	= Lift-off stress
$P_o (AV)$	= Average lift-off stress (3 Arms)
p'	= Effective cavity stress
P_y	= Yield stress
p'_c	= Effective cavity stress at start of unloading cycle
ϕ^{PS}	= Friction angle under plain strain conditions
ϕ^{TX}	= Friction angle under triaxial conditions
G	= Shear modulus

- G_i = Initial shear modulus
 $G_s^{1.5}$ = Secant shear modulus at cavity strain of 1.5%
 G_{UR}, G_{RU} = Shear modulus for unload-reload and reload-unload cycle
 G_{URO}, G_{RUO} = Shear modulus from unload-reload and reload-unload cycle normalized to the stress level σ'_{ho}
 G_o = Maximum dynamic shear modulus obtained from resonant column test
 γ_d = Bulk density
 u_o = Pore pressure at center of CC
 $p'_{lim}{}^{AA}$ = Effective limit pressure using method by Al Awkati (1975)
 $p'_{lim}{}^{WW}$ = Effective limit pressure using method by Windle and Wroth (1977)
 $\Delta\gamma_{AB}$ = Shear strain increment during unload-reload or reload-unload cycle
 p'_{AV} = Calculated average effective stress around cavity
 ν = Maximum dilation angle
 β = Angle of straight line connecting p'_o and the point of peak strength $(\sigma'_r/\sigma_\theta)_{max}$
 ψ = State parameter (Been and Jefferies, 1985)

TABLE 1
SUMMARY OF INSTALLATION CONDITIONS DURING SELF-BORING

Test No.	BC	Membrane Type	Chamber Drainage	Cutter Setting cm	Advancement Rate cm/min	Cutter Speed rev/min	Water Flow l/min	Vacuum Inside Membrane t/m ²	Notes
237	B-1	Not protected	Open at top and base	2.5	3.0	50±60	11-14	5	25 cm before end of installation stopped for 3 mins
238	B-1	Not protected	Open at base	2.5	2.4	50±60	10	5	Instrument rotated 180° with respect to Test No. 237+10 cm from end of installation stopped for 3 mins. At end of installation piping in CC
239	B-1	Not protected	Open at base	2.5	2.4	50±60	9	5	10 cm from end of installation probe started to lift
240	B-1	Not protected	Open at base	2.5	3.0	50±60	10	5	Failed test due to ruptured membrane during installation
241	B-1	Protected	Open at base	2.0	3.0	50±60	10	5	
242	B-1	Not protected	Open at base	1.9	3.0	50±60	10	5	
243	B-1	Not protected	Open at base	2.5	4.2	50±60	9	5	
244	B-1	Not protected	Open at base	3.5	3.0	50±60	8.5	5	
245	B-1	Not protected	Open at base	5.4	3.0	60	8-9	5	After 22 cm of penetration installation stopped for 5 mins
246	B-3	Not protected	Open at base	4.5	3.0	60	9	5	
247	B-3	Not protected	Open at base	3.4	3.0	60	9+10	5	
250	B-4	Not protected	Open at base	3.4	3.0	60	9+10	5	
251	B-4	Not protected	Open at base	3.4	3.0	60	11	5	
252	B-4	Not protected	Open at base	3.3	3.0	60	11	5	
253	B-4	Not protected	Open at base	3.3	3.0	60	10-11	5	
254	B-1	Not protected	Open at base	3.3	3.0	60	11	5	
255	B-4	Protected	Open at base	2.4	3.0	60	11	5	
256	B-4	Protected	Open at base	2.4	3.0	60	11	5	
257	B-4	Protected	Open at base	1.9	3.0	60	11	5	
258	B-4	Protected	Open at base	1.9	3.0	60	12	5	Probably disturbed due to drilling vibrations
259	B-4	Protected	Open at base	1.9	3.0	60	11	5	Probably disturbed due to drilling vibrations
260	B-4	Protected	Open at base	1.9	3.0	60	11	5	
261	B-4	Protected	Open at base	1.9	3.0	60	11	5	

TESTS FROM 237 TO 261 SAMPLES FULLY SATURATED

SUMMARY OF GENERAL CALIBRATION CHAMBER CONDITIONS AFTER SAMPLE CONSOLIDATION

	Test No.	Sand	γ_d kN/m ³	D_{RC} %	OCR	σ'_{vo} kPa	σ'_{ho} kPa	K_o	u_o kPa	M_o MPa	Number of cycles		BC
											UR	RU	
I D E A L	201	HS	16.08	67.0	2.77	112.8	74.56	0.662	0	192.18	2	1	1
	207	HS	15.22	43.9	3.29	109.9	64.75	0.586	0	185.51	2	1	1
	208	TS-4	14.82	43.2	1.00	112.8	45.13	0.400	0	34.14	2	1	1
	209	TS-4	15.01	49.2	1.00	116.7	51.99	0.441	0	43.56	3	1	1
	210	TS-4	15.13	53.3	1.00	511.1	244.27	0.479	0	100.06	3	1	1
	211	TS-4	15.57	67.4	1.00	512.1	242.31	0.473	0	114.88	3	2	1
	212	TS-4	15.49	64.6	2.86	110.9	82.40	0.747	0	189.82	3	1	1
	213	TS-4	14.96	47.5	2.78	112.8	83.39	0.740	0	168.63	3	1	1
	214	TS-4	14.80	42.4	1.00	113.8	53.96	0.476	0	50.82	3	1	4
	215	TS-4	16.42	92.3	1.00	514.6	225.63	0.439	0	143.72	3	1	1
I N S T A L L	216	TS-4	14.92	66.3	7.57	60.8	56.90	0.927	0	156.76	3	1	1
	218	TS-4	15.51	45.4	7.66	59.8	59.84	0.980	0	169.62	3	1	1
	219	TS-4	15.52	65.9	5.46	112.9	101.04	0.902	0	207.48	3	1	1
	220	TS-4	14.95	47.2	1.00	313.3	150.09	0.481	0	80.15	3	1	1
	221	TS-4	14.87	44.6	2.88	108.9	81.42	0.751	0	167.36	3	1	1
	222	TS-4	14.92	46.2	5.50	111.8	95.16	0.850	0	199.05	3	1	1
	224	TS-4	15.81	74.6	5.38	113.8	93.20	0.816	0	222.39	3	1	1
	225	TS-4	15.81	74.6	5.46	111.8	87.31	0.775	0	218.27	3	-	1
	228	TS-4	15.89	77.0	1.00	518.0	215.82	0.417	0	120.27	3	1	1
	233	TS-4	15.98	79.6	1.00	512.1	224.65	0.439	0	121.25	3	1	1
S E L F	234	TS-4	15.93	76.1	5.34	115.8	103.99	0.904	0	216.21	3	1	1
	235	TS-4	14.99	48.5	1.00	516.0	239.36	0.465	0	80.54	3	-	1
	236	TS-4	15.83	75.2	2.72	114.8	78.48	0.686	0	190.41	3	1	1
	237	TS-4	15.79	74.6	2.90	96.1	81.42	0.850	6.87	178.35	3	1	1
	238	TS-4	15.79	74.8	2.83	101.0	83.39	0.828	5.89	171.28	3	1	1
	239	TS-4	15.79	74.8	2.84	101.0	86.33	0.856	5.89	169.32	3	1	1
	240	TS-4	16.47	94.1	2.84	101.0	90.25	0.892	5.89	195.22	3	1	1
	241	TS-4	16.38	91.8	2.76	104.0	86.33	0.829	5.89	192.37	3	1	1
	242	TS-4	14.72	40.1	1.00	103.0	49.05	0.475	6.87	32.67	3	1	1
	243	TS-4	14.79	42.7	3.10	95.2	74.56	0.785	6.87	141.46	4	-	1
B O R E D	244	TS-4	14.80	42.8	6.12	97.1	94.18	0.970	5.89	172.36	4	-	1
	245	TS-4	14.72	40.0	1.00	102.0	54.94	0.539	6.87	41.40	4	-	1
	246	TS-5	14.72	43.0	1.00	102.0	52.97	0.523	6.87	45.32	4	-	3
	247	TS-5	14.80	43.0	4.19	190.3	147.15	0.776	6.87	212.58	4	-	3
	250	TS-5	14.81	43.0	1.00	480.7	219.74	0.457	6.87	93.20	4	-	4
	251	TS-5	14.74	41.0	1.00	100.1	51.01	0.508	6.87	36.30	4	-	4
	252	TS-6	15.79	75.0	1.00	101.0	52.97	0.518	6.87	58.27	4	-	1
	253	TS-6	15.68	71.0	1.00	103.0	52.97	0.517	6.87	58.99	4	-	3
	254	TS-6	15.69	71.0	6.16	97.1	88.29	0.912	6.87	194.43	3	-	1
	255	TS-6	15.49	65.0	1.00	108.9	55.92	0.514	6.87	56.70	2	-	1
I D E A L	256	TS-7	15.46	65.0	1.73	345.3	277.62	0.690	6.87	263.69	4	-	1
	257	TS-7	16.22	87.0	1.00	130.5	77.50	0.597	6.87	69.16	4	-	1
	258	TS-7	16.18	86.0	1.00	495.4	226.61	0.458	6.87	125.47	4	-	1
	259	TS-8	16.39	92.0	4.63	138.3	139.30	1.008	6.87	215.62	4	-	1
	260	TS-8	16.29	89.0	1.00	131.5	78.48	0.595	6.87	70.53	4	-	3
	261	TS-8	16.37	91.5	3.99	199.1	157.94	0.797	6.87	261.44	4	-	1
	262	TS-9	16.28	88.7	1.00	113.8	45.10	0.398	0	73.77	4	-	1
	263	TS-9	16.29	89.1	1.00	112.8	103.00	0.913	0	229.46	4	-	1

TABLE 3
SUMMARY OF PROBE AND CC CONDITIONS DURING SELF-BORED TESTS

Test No.	BC	Membrane Type	Notes
237	B-1	Not protected	Modified arms + bushings
238	B-1	Not protected	Modified arms + bearings
239	B-1	Not protected	Arms + bushings
240	B-1	Not protected	Arms + bushings
241	B-1	Protected	Arms + bushings
242	B-1	Not protected	Arms trimmed and rounded + bushings
243	B-1	Not protected	Arms + bushings
244	B-1	Not protected	Arms + bushings
245	B-1	Not protected	Arms + bushings
246	B-3	Not protected	Arms + bushings
247	B-3	Not protected	Arms + bushings
250	B-4	Not protected	Arms+bushings. 5 lift-offs. Relaxation time=96 hrs
251	B-4	Not protected	Arms + bushings
252	B-1	Not protected	Arms+bushings. Relaxation time=71 hrs
253	B-3	Not protected	Arms+bushings. At 5 bar total pressure and 4% strain membrane ruptured
254	B-1	Not protected	Arms+bushings. At 5.5 bar total pressure membrane ruptured
255	B-1	Protected	Arms + bushings
256	B-1	Protected	Arms + bushings
257	B-1	Protected	Arms + bushings
258	B-1	Protected	Arms + bushings
259	B-1	Protected	Arms+bushings. After 1st loop manual expansion due to problems with SCU
260	B-3	Protected	Arms+bushings. After 3rd loop manual expansion due to problems with SCU
261	B-1	Protected	Arms+bushings. After 1st loop manual expansion due to problems with SCU

TABLE 4
SUMMARY OF LIFT-OFF PRESSURES OF INDIVIDUAL ARMS

	Test	σ_{ho}	ARM 1	ARM 2	ARM 3	Average (p_o)	
	No.	kPa	kPa	kPa	kPa	kPa	
I D E A L I N S T A L L A T I O N	201	74.56	82.06	84.07	71.06	76.06	O S
	207	64.75	150.53	69.05	65.05	65.05	R T
	208	45.13	28.02	34.03	34.03	28.02	I R
	209	51.99	42.03	49.04	43.03	45.04	G A
	210	244.27	87.08	61.10	136.12	81.06	I I
	211	242.31	65.02	65.02	90.03	56.04	N N
	212	82.40	108.95	114.45	104.25	104.27	A
	213	83.39	129.25	164.26	165.15	120.23	L
	214	53.96	49.23	61.19	63.25	49.21	A
	215	225.63	347.36	379.52	256.25	254.27	R
	216	56.90	139.26	97.28	80.22	73.23	M
	218	59.84	85.22	117.29	165.64	80.22	S
	219	101.04	179.27	173.29	145.24	131.28	
	220	150.09	171.32	122.29	190.35	139.28	
	221	81.42	68.26	93.26	152.30	68.26	Δ
	222	95.16	119.25	163.28	146.32	141.28	
	224	93.20	116.70	162.30	136.02	124.84	
	225	87.31	98.44	105.54	115.67	96.41	
	228	215.82	200.81	274.79	222.09	207.90	
	233	224.65	227.67	237.19	217.36	217.36	▽
	234	103.99	134.07	124.56	144.39	117.42	
	235	239.36	115.04	109.48	70.62	142.80	
	236	78.48	95.22	90.52	115.92	88.12	
S E L F B O R E D	237	88.29	88.26	148.18	86.10	86.05	M
	238	89.28	177.50	309.01	50.01	50.01	O
	239	92.22	86.78	146.42	300.68	67.15	D
	241	92.22	80.39	80.39	356.82	80.39	I
	242	55.92	30.99	30.99	27.26	30.33	F
	243	81.43	25.20	27.56	23.14	25.15	I
	244	100.07	37.27	24.71	22.07	24.58	E
	245	61.81	59.82	46.78	44.62	40.95	D
	246	59.84	70.81	18.53	97.58	19.81	
	247	154.02	26.53	18.53	78.65	18.53	S
	250	226.61	82.06	84.07	71.06	76.06	T
	251	57.88	13.15	8.49	18.33	15.09	R
	252	59.84	90.79	68.44	114.35	74.51	A
	253	59.84	12.47	13.94	29.12	10.85	I
	254	95.16	34.94	31.28	36.88	34.94	N
	255	62.79	36.47	57.51	62.38	36.47	
	256	284.49	137.17	81.83	73.14	71.83	A
	257	84.37	62.98	47.64	79.05	47.64	R
	258	233.48	122.34	122.34	53.53	50.67	M
	259	146.17	64.34	37.34	32.46	43.17	S
	260	85.35	45.00	32.65	42.90	27.40	
	261	164.81	79.79	88.16	67.02	63.65	
	262	45.10	46.93	57.12	57.81	54.54	
IDEAL	263	103.00	134.38	125.64	129.64	125.64	

IDEAL INSTALLATION: $\frac{p_o \text{ (AV)}}{\sigma_{ho}} = 1.07 \pm 0.29;$	SELF-BORED INSTALLATION: $\frac{p_o \text{ (AV)}}{\sigma_{ho}} = 0.47 \pm 0.28$
--	--

TABLE 5
SUMMARY OF LIMIT PRESSURE AND SECANT SHEAR MODULUS

Test No.	p'_o kPa	p'_{lim}^{WW} kPa	p'_{lim}^{AA} kPa	$G_s(0.5\%)$ MPa	$G_s(1\%)$ MPa	$G_s(1.5\%)$ MPa
201	76.06	1471.50	1177.20	14.81	11.83	10.10
207	65.05	882.90	784.80	13.73	10.00	8.40
208	28.02	529.74	412.02	9.71	6.66	5.44
209	45.04	686.70	637.65	9.52	7.06	5.84
210	81.06	2648.70	2158.20	30.02	22.84	19.00
211	56.04	2844.90	2158.20	58.25	39.03	32.40
212	104.27	1402.83	1226.25	15.79	12.86	10.89
213	120.23	1098.72	1079.00	17.16	12.85	10.89
214	49.21	804.42	784.80	10.40	7.83	6.67
215	254.27	3678.75	2943.00	45.42	32.67	28.05
216	73.23	725.94	588.60	16.97	11.67	9.32
218	80.22	971.19	784.80	18.25	13.44	11.09
219	131.28	1599.03	1373.40	27.57	19.82	16.49
220	139.28	1236.06	981.00	20.01	14.22	11.48
221	68.26	1059.48	833.85	20.11	13.64	11.09
222	141.28	1206.63	981.00	17.46	12.95	10.79
224	124.84	1716.75	1373.40	21.48	16.97	14.42
225	96.41	1579.41	1275.30	20.70	15.99	13.93
228	207.90	2992.05	2305.35	33.45	24.13	21.58
233	217.36	2943.00	2207.25	26.68	22.17	20.21
234	117.42	1765.80	1373.40	24.72	18.54	15.60
235	142.80	1955.13	1373.40	33.54	25.89	21.38
236	88.12	1402.83	1079.10	19.03	14.72	12.46
237	79.18	1464.63	1170.33	25.31	19.72	15.70
238	44.12	1220.36	975.11	39.34	27.37	20.99
239	61.26	1396.94	1073.21	32.57	23.54	18.93
241	74.50	1818.77	1416.56	35.81	28.84	23.25
242	23.46	454.20	336.48	4.71	4.22	3.73
243	18.28	365.91	287.43	5.59	4.71	3.92
244	18.69	680.81	455.18	8.73	7.65	6.97
245	34.08	513.06	434.58	7.11	6.07	5.60
246	12.94	689.64	532.68	12.75	9.26	7.51
247	11.66	1611.78	1170.33	9.11	8.81	8.22
250	69.19	2494.68	1906.08	53.06	32.03	24.08
251	8.22	326.67	238.38	4.28	3.58	3.12
252	67.64	1037.90	807.36	18.14	13.57	10.93
253	3.98	985.91	651.38	10.31	11.21	10.64
254	28.07	1248.81	630.78	11.60	13.33	13.30
255	29.60	1219.38	812.27	18.28	14.77	13.20
256	64.96	1629.34	1269.32	28.93	24.23	19.85
257	40.77	1098.62	822.96	21.72	17.37	14.41
258	43.80	3918.02	2667.24	38.98	33.59	30.65
259	36.30	2065.89	1269.32	37.32	31.38	26.26
260	20.93	1833.39	1254.60	22.57	17.62	15.03
261	56.78	3231.32	2262.09	42.59	37.04	32.25
262	54.54	1149.7	826.0	13.00	10.88	9.64
263	125.64	2047.3	1500.9	25.56	19.99	17.15

TABLE 6
SUMMARY OF TEST RECORDING RELOADING WAVE

Test No.	P _A sPa	P _B sPa	P _C sPa	P _A I	P _B I	P _C I	P _{AB} I	P _{AC} I	P _{BC} I	P _{ABC} I	P _{AB} I	P _{AC} I	P _{BC} I	P _{ABC} I	P _{AB} I	P _{AC} I	P _{BC} I	P _{ABC} I
201	143 20	158 46	206 83	1 118	1 141	1 227	0 246	0 189	173 8	173 8	173 8	173 8	173 8	173 8	173 8	173 8	173 8	173 8
207	175 50	210 50	254 70	1 185	1 197	1 443	0 212	0 173	146 10	146 10	146 10	146 10	146 10	146 10	146 10	146 10	146 10	146 10
208	66 45	119 10	120 51	0 190	1 146	1 138	0 212	0 448	17 56	17 56	17 56	17 56	17 56	17 56	17 56	17 56	17 56	17 56
209	87 13	135 35	143 23	0 170	0 410	1 422	0 144	0 455	55 23	55 23	55 23	55 23	55 23	55 23	55 23	55 23	55 23	55 23
210	438 13	136 17	140 53	0 440	1 123	1 473	0 130	0 516	278 17	278 17	278 17	278 17	278 17	278 17	278 17	278 17	278 17	278 17
211	401 50	405 18	503 25	0 176	0 462	0 172	0 132	0 520	200 12	200 12	200 12	200 12	200 12	200 12	200 12	200 12	200 12	200 12
212	207 50	272 48	278 60	0 190	0 148	0 410	0 118	0 403	112 17	112 17	112 17	112 17	112 17	112 17	112 17	112 17	112 17	112 17
213	132 80	262 18	268 19	0 525	1 196	1 480	0 148	0 418	112 17	112 17	112 17	112 17	112 17	112 17	112 17	112 17	112 17	112 17
214	49 18	139 48	144 21	0 446	1 124	1 477	0 136	0 484	47 12	47 12	47 12	47 12	47 12	47 12	47 12	47 12	47 12	47 12
215	472 46	144 41	172 30	0 472	1 121	1 471	0 134	0 477	47 12	47 12	47 12	47 12	47 12	47 12	47 12	47 12	47 12	47 12
216	151 43	116 12	135 42	0 155	0 410	1 42	0 146	0 400	41 42	41 42	41 42	41 42	41 42	41 42	41 42	41 42	41 42	41 42
218	147 41	157 17	203 40	0 432	1 121	1 471	0 136	0 443	47 14	47 14	47 14	47 14	47 14	47 14	47 14	47 14	47 14	47 14
219	260 24	147 17	151 20	0 118	0 418	1 44	0 144	0 146	13 13	13 13	13 13	13 13	13 13	13 13	13 13	13 13	13 13	13 13
220	263 20	129 14	119 43	1 197	1 141	1 14	0 128	0 111	173 8	173 8	173 8	173 8	173 8	173 8	173 8	173 8	173 8	173 8
221	206 12	164 45	271 10	1 137	1 140	1 233	0 128	0 408	111 46	111 46	111 46	111 46	111 46	111 46	111 46	111 46	111 46	111 46
222	247 90	114 44	121 17	0 442	1 144	1 237	0 128	0 407	130 18	130 18	130 18	130 18	130 18	130 18	130 18	130 18	130 18	130 18
224	237 80	116 40	120 44	0 526	0 509	0 606	0 130	0 391	128 45	128 45	128 45	128 45	128 45	128 45	128 45	128 45	128 45	128 45
225	228 46	118 27	125 50	0 606	0 597	0 183	0 106	0 378	123 18	123 18	123 18	123 18	123 18	123 18	123 18	123 18	123 18	123 18
226	352 67	442 16	450 17	0 506	0 573	0 483	0 134	0 520	237 17	237 17	237 17	237 17	237 17	237 17	237 17	237 17	237 17	237 17
233	335 81	433 15	443 41	0 517	0 580	0 518	0 146	0 530	230 17	230 17	230 17	230 17	230 17	230 17	230 17	230 17	230 17	230 17
234	243 77	317 28	322 15	0 130	0 509	0 507	0 140	0 420	135 44	135 44	135 44	135 44	135 44	135 44	135 44	135 44	135 44	135 44
235	327 68	414 52	422 81	0 140	0 556	1 474	0 136	0 583	244 42	244 42	244 42	244 42	244 42	244 42	244 42	244 42	244 42	244 42
236	151 24	231 81	233 48	0 451	0 522	0 517	0 142	0 436	100 12	100 12	100 12	100 12	100 12	100 12	100 12	100 12	100 12	100 12
237	252 12	305 11	314 30	0 732	0 187	0 160	0 110	0 379	116 50	116 50	116 50	116 50	116 50	116 50	116 50	116 50	116 50	116 50
238	323 13	176 10	183 57	0 320	0 476	0 364	0 116	0 334	128 13	128 13	128 13	128 13	128 13	128 13	128 13	128 13	128 13	128 13
239	302 15	362 97	360 84	0 604	0 341	0 320	0 114	0 349	128 83	128 83	128 83	128 83	128 83	128 83	128 83	128 83	128 83	128 83
241	361 01	454 20	464 80	0 977	1 342	0 880	0 130	0 302	140 20	140 20	140 20	140 20	140 20	140 20	140 20	140 20	140 20	140 20
242	84 37	107 81	100 80	1 710	1 770	1 770	0 132	0 510	50 17	50 17	50 17	50 17	50 17	50 17	50 17	50 17	50 17	50 17
243	52 87	73 50	76 52	0 808	0 782	0 745	0 144	0 791	57 40	57 40	57 40	57 40	57 40	57 40	57 40	57 40	57 40	57 40
244	60 87	87 12	80 08	0 467	0 544	0 544	0 154	0 744	73 73	73 73	73 73	73 73	73 73	73 73	73 73	73 73	73 73	73 73
245	72 30	86 63	105 75	0 478	0 537	0 779	0 162	0 540	57 13	57 13	57 13	57 13	57 13	57 13	57 13	57 13	57 13	57 13
246	87 80	120 88	132 14	0 683	0 782	1 328	0 180	0 483	63 00	63 00	63 00	63 00	63 00	63 00	63 00	63 00	63 00	63 00
247	120 60	161 77	160 54	0 855	1 334	0 801	0 150	0 710	121 10	121 10	121 10	121 10	121 10	121 10	121 10	121 10	121 10	121 10
250	401 20	507 31	601 84	0 829	1 300	1 130	0 142	0 462	270 20	270 20	270 20	270 20	270 20	270 20	270 20	270 20	270 20	270 20
251	40 10	63 50	80 00	1 044	1 135	0 821	0 162	0 672	44 82	44 82	44 82	44 82	44 82	44 82	44 82	44 82	44 82	44 82
252	162 50	237 50	242 83	0 836	0 816	1 300	0 160	0 334	81 19	81 19	81 19	81 19	81 19	81 19	81 19	81 19	81 19	81 19
253	144 62	201 30	200 71	0 905	1 379	0 750	0 160	0 306	70 30	70 30	70 30	70 30	70 30	70 30	70 30	70 30	70 30	70 30
254	161 00	222 70	229 02	0 680	0 761	0 862	0 161	0 465	100 47	100 47	100 47	100 47	100 47	100 47	100 47	100 47	100 47	100 47
255	150 70	214 54	210 33	0 784	0 872	0 862	0 170	0 300	80 62	80 62	80 62	80 62	80 62	80 62	80 62	80 62	80 62	80 62
256	250 40	342 87	351 30	0 611	0 680	0 685	0 171	0 678	237 35	237 35	237 35	237 35	237 35	237 35	237 35	237 35	237 35	237 35
257	150 60	216 80	222 83	0 463	0 552	0 544	0 170	0 435	80 00	80 00	80 00	80 00	80 00	80 00	80 00	80 00	80 00	80 00
258	362 04	403 30	400 80	0 474	0 557	0 555	0 160	0 560	220 00	220 00	220 00	220 00	220 00	220 00	220 00	220 00	220 00	220 00
259	323 44	410 80	432 50	0 620	0 774	0 774	0 163	0 617	100 40	100 40	100 40	100 40	100 40	100 40	100 40	100 40	100 40	100 40
260	100 84	234 47	261 80	0 771	0 881	0 867	0 170	0 400	100 70	100 70	100 70	100 70	100 70	100 70	100 70	100 70	100 70	100 70
261	332 18	434 70	430 70	0 447	0 520	0 530	0 163	0 444	100 80	100 80	100 80	100 80	100 80	100 80	100 80	100 80	100 80	100 80
262	103 80	100 10	171 00	0 400	0 500	0 371	0 170	0 371	83 40	83 40	83 40	83 40	83 40	83 40	83 40	83 40	83 40	83 40
263	229 16	340 80	343 84	0 402	0 500	0 505	0 174	0 301	134 30	134 30	134 30	134 30	134 30	134 30	134 30	134 30	134 30	134 30

G_{me} = measured unload-reload modulus

G_{me} = unload-reload modulus corrected for stress level (σ_{me})

G_d = maximum dynamic shear modulus from resonant column tests

TABLE 7
SCHEDULE OF THE RELOADING RELOADING CYCLE

[illegible]

E_{me} = measured mixed-reel modulus

E_{res} = residual modulus corrected for stress level (%)

G_0 = maximum dynamic shear modulus from resonant column tests

TABLE 8
SUMMARY OF 3RD UNLOADING RELOADING CYCLE

Test No	P _A kPa	P _B kPa	P _C kPa	ε _A %	ε _B %	ε _C %	Δγ _{AB} %	ε	P _{AV} kPa	Δγ _{AV} %	G _R MPa	G _{UR} MPa	G _{UR0} MPa
201													15.114
207													2.441
209													16.442
209	158 48	223 58	225 63	2 550	2 613	2 600	0 138	3 343	13 34	3 42	41 417	34 147	13 147
210	559 36	761 30	779 30	2 332	2 338	1 973	0 132	3 421	12 43	3 449	79 143	69 143	12 43
211	705 25	810 42	827 36	2 582	2 949	2 815	0 134	3 472	332 58	0 163	81 521	71 521	332 58
212	433 54	313 46	493 44	3 124	3 138	3 177	0 148	3 385	143 53	0 147	52 247	41 247	143 53
213	339 54	406 48	421 33	2 303	2 471	2 829	0 116	3 314	134 34	0 161	51 474	41 474	134 34
214	179 18	234 15	244 27	2 474	2 442	2 426	0 176	3 342	43 41	0 171	36 450	26 450	43 41
215	145 51	393 45	311 35	1 428	1 394	1 594	0 174	3 347	124 21	0 171	34 477	24 477	124 21
216	251 22	303 46	314 42	2 523	2 539	2 467	0 132	3 371	34 45	0 174	41 474	31 474	34 45
217	319 44	367 19	378 47	2 365	2 424	2 417	0 124	3 374	44 45	0 171	47 474	37 474	44 45
219	433 43	536 45	554 27	2 147	2 258	2 107	0 162	3 311	146 43	0 171	53 474	43 474	146 43
220	85 21	455 13	474 47	3 354	3 431	3 164	0 134	3 424	211 12	0 161	54 141	44 141	211 12
221	312 47	371 59	389 46	1 253	3 121	3 293	0 124	3 311	124 43	0 176	44 474	34 474	124 43
222	433 25	468 14	487 16	3 254	3 129	3 117	0 130	3 316	114 14	0 179	41 431	31 431	114 14
224	157 36	499 21	423 39	2 340	2 154	2 219	0 228	3 337	142 52	0 133	48 564	38 564	142 52
225	427 17	498 42	513 36	2 569	2 637	2 638	0 136	3 297	147 45	0 161	54 249	43 249	147 45
228	537 44	629 58	655 31	1 309	1 307	1 281	0 122	3 427	243 10	0 155	77 133	69 133	243 10
233	546 16	653 40	676 39	1 373	1 442	1 363	0 138	3 429	240 16	0 162	75 676	65 676	240 16
234	578 41	661 43	684 74	3 546	3 611	3 587	0 130	3 267	143 14	0 159	67 100	52 100	143 14
235	709 56	907 58	947 58	3 735	3 865	3 459	0 143	3 387	134 47	0 163	72 140	62 140	134 47
236	435 98	515 58	535 63	3 564	3 552	3 623	0 136	3 251	139 33	0 188	64 550	50 550	139 33
237	453 22	536 41	554 27	2 377	3 161	3 331	0 168	3 242	145 18	0 175	51 356	40 356	145 18
238	448 32	545 44	579 77	3 250	3 350	3 276	0 250	3 259	149 11	0 190	50 420	39 420	149 11
239	437 17	603 32	629 40	3 672	3 730	3 737	0 236	3 252	157 47	0 186	46 734	36 734	157 47
241	569 04	778 31	813 25	3 862	3 956	3 891	0 188	3 211	171 39	0 145	61 607	45 607	171 39
242	133 42	173 64	186 39	5 805	5 322	5 881	0 234	3 340	70 39	0 105	18 443	15 742	57 716
243	118 70	145 19	154 02	4 394	4 477	4 404	0 166	3 536	82 54	0 175	16 775	16 157	70 229
244	198 18	237 40	249 17	3 398	3 483	3 452	0 168	3 469	116 35	0 176	24 231	22 276	77 428
245	149 31	204 83	224 18	2 398	2 561	2 558	0 330	3 359	90 21	0 149	17 285	14 549	50 600
246	170 90	224 16	245 94	4 390	4 214	4 151	0 248	3 316	92 56	0 112	22 279	19 159	59 656
247	384 84	432 91	450 28	4 134	4 226	4 162	0 184	3 433	135 07	0 193	38 799	34 369	94 291
250	825 22	928 28	979 45	4 432	4 518	4 468	0 168	3 446	139 31	0 176	63 128	52 340	112 291
251	87 61	123 31	129 33	5 125	5 209	5 218	0 168	3 460	51 35	0 178	16 079	14 740	58 369
252	358 07	413 20	436 94	3 951	4 029	3 963	0 158	3 231	130 89	0 170	36 719	27 834	74 303
253	333 64	396 72	416 92	3 473	3 562	3 550	0 178	3 238	98 32	0 180	36 650	27 373	73 229
254													91 489
255	339 23	403 39	421 22	3 888	3 952	3 924	0 188	3 245	133 35	0 178	39 652	30 447	72 210
256	536 31	633 04	657 06	3 358	3 443	3 357	0 174	3 434	124 36	0 178	57 428	53 711	142 340
257	300 50	471 96	483 23	4 081	4 171	4 152	0 180	3 272	134 32	0 181	42 408	33 478	95 696
258	708 93	831 95	858 75	2 114	2 201	2 203	0 174	3 351	137 00	0 178	78 029	65 798	150 685
259	638 86	739 97	754 21	2 837	2 932	2 908	0 198	3 301	127 23	0 184	58 958	47 771	126 988
260	482 98	481 08	503 57	3 184	3 278	3 243	0 188	3 271	136 35	0 185	42 840	33 782	97 450
261	883 87	982 88	1012 51	2 867	2 752	2 747	0 170	3 271	274 84	0 177	71 956	56 734	133 554
262	354 43	437 62	458 87	3 613	3 723	3 680	0 216	3 202	91 11	0 197	39 890	23 250	80 523
263	536 31	677 48	682 97	2 656	2 771	2 764	0 230	3 282	101 35	0 193	62 970	40 482	113 808

G_{UR} = measured unload-reload modulus

G_{UR0} = unload-reload modulus corrected for stress level (σ'_{ho})

G_o = maximum dynamic shear modulus from resonant column tests

TABLE 9
SUMMARY OF 4TH UNLOADING-RELOADING CYCLE

Test No	P _A kPa	P _B kPa	P _C kPa	ε _A %	ε _B %	ε _C %	Δε _{AB} %	ε	P _{AV} kPa	Δε _{AV} %	G _{UR} MPa	G _{URo} MPa	G _o MPa
243	144.13	178.54	191.30	7.878	7.975	7.779	0.194	0.477	91.22	0.087	17.462	16.011	70.229
244	284.87	304.11	319.81	6.825	6.709	6.847	0.168	0.427	130.14	0.076	25.114	21.853	77.828
245	188.65	252.51	270.07	5.798	5.997	5.953	0.198	0.323	86.47	0.179	17.320	14.304	60.600
246	244.07	288.32	303.91	7.317	7.411	7.256	0.188	0.294	89.39	0.085	25.437	20.312	59.556
247	489.62	489.62	592.03	6.476	6.573	6.496	0.194	0.368	218.08	0.087	42.615	35.383	94.291
250	1013.08	1112.65	1163.56	6.988	7.069	6.900	0.190	0.310	361.26	0.072	66.286	53.536	112.291
251	121.84	150.30	154.82	7.907	7.995	7.999	0.178	0.433	67.11	0.079	17.432	15.493	58.969
252	445.47	504.33	529.79	6.541	6.626	6.508	0.170	0.203	107.51	0.077	16.575	27.199	74.903
253	-	-	-	-	-	-	-	-	-	-	-	-	73.299
254	-	-	-	-	-	-	-	-	-	-	-	-	91.483
255	437.33	500.90	525.49	6.128	6.205	6.150	0.154	0.212	111.29	0.069	43.732	32.573	72.210
256	674.34	774.01	845.43	5.612	5.702	6.213	0.140	0.430	163.11	0.081	64.418	52.145	142.340
257	501.39	570.35	598.92	5.985	7.076	7.320	0.142	0.241	144.14	0.082	40.525	31.235	35.496
258	1052.81	1192.60	1240.01	3.421	3.504	3.489	0.158	0.101	372.65	0.075	87.054	70.291	150.685
259	786.76	987.91	923.61	4.344	4.434	4.424	0.140	0.256	245.26	0.081	58.546	45.304	126.988
260	520.71	600.47	625.91	4.784	4.854	4.807	0.130	0.236	147.54	0.041	46.401	35.370	97.450
261	1132.96	1246.75	1336.83	4.437	4.517	4.755	0.160	0.227	303.41	0.072	74.252	56.078	133.554
262	498.64	586.63	584.68	6.531	6.618	6.543	0.174	0.173	99.13	0.078	41.460	24.297	80.523
263	716.03	842.88	857.98	4.206	4.311	4.313	0.210	0.228	195.81	0.035	62.910	49.049	113.878

G_{UR} = measured unload-reload modulus

G_{URo} = unload-reload modulus corrected for stress level (σ_{ho})

G_o = maximum dynamic shear modulus from resonant column tests

TABLE 10
SUMMARY OF 1ST RELOADING UNLOADING CYCLE

Test No	P _A kPa	P _B kPa	P _C kPa	E _A E	E _B E	E _C E	E _{AB} E	E _{AC} E	E _{BC} E	P _{AV} kPa	ΔT _{AV} E	G _{RU} MPa	G _{RUo} MPa	G _o MPa
201	446.36	582.71	575.85	13.604	13.731	13.731	0.254	0.241	0.39.03	0.114	61.313	4.4	4.1	4.1
207	206.01	306.07	306.07	9.376	9.502	9.502	0.252	0.333	101.78	0.113	43.844	3.6	3.4	3.4
208	77.50	127.53	127.53	9.238	9.340	9.340	0.254	0.451	57.46	0.122	27.471	2.6	2.4	2.4
209	104.97	152.06	152.06	9.232	9.299	9.299	0.134	0.440	56.97	0.140	8.133	3.6	3.4	3.4
210	605.28	671.00	671.00	9.177	9.218	9.218	0.192	0.459	337.89	0.137	54.055	4.1	3.9	3.9
211*	1164.45	1287.37	1287.07	9.638	9.705	9.705	0.134	0.508	336.24	0.140	109.24	5.1	4.8	4.8
211**	554.27	658.25	658.25	9.089	9.155	9.155	0.192	0.458	331.17	0.139	54.026	4.1	3.9	3.9
212	577.81	652.37	652.37	9.626	9.696	9.696	0.140	0.216	114.39	0.163	58.42	4.4	4.1	4.1
213	464.99	556.23	553.28	9.555	9.641	9.641	0.175	0.267	147.18	0.179	54.06	4.4	4.1	4.1
214	312.34	380.63	380.63	9.310	9.388	9.388	0.146	0.247	37.77	0.171	43.074	3.6	3.4	3.4
215	1422.45	1579.41	1580.39	9.643	9.713	9.713	0.141	0.247	475.41	0.141	111.074	5.1	4.8	4.8
216	336.48	401.23	401.23	9.515	9.591	9.591	0.142	0.247	113.6	0.171	43.074	3.6	3.4	3.4
218	441.45	507.19	509.24	10.095	10.161	10.161	0.142	0.246	115.25	0.171	43.074	3.6	3.4	3.4
219	507.18	619.99	618.99	9.433	9.495	9.495	0.124	0.290	213.43	0.174	54.072	4.4	4.1	4.1
220	368.86	439.43	439.43	9.398	10.042	10.042	0.114	0.443	194.43	0.174	43.072	3.6	3.4	3.4
221	273.70	335.50	335.50	9.311	9.379	9.379	0.146	0.262	121.47	0.191	43.072	3.6	3.4	3.4
222	460.09	534.55	534.65	10.028	10.095	10.095	0.134	0.298	159.39	0.161	54.06	4.4	4.1	4.1
224	658.25	752.43	750.47	10.315	10.382	10.382	0.134	0.235	176.16	0.160	54.061	4.4	4.1	4.1
225	-	-	-	-	-	-	-	-	-	-	-	-	-	-
228	1186.03	1320.43	1320.43	10.405	10.474	10.474	0.138	0.281	370.72	0.162	116.127	5.1	4.8	4.8
233	1189.95	1319.45	1319.45	8.619	8.684	8.684	0.130	0.288	379.98	0.149	119.443	4.8	4.5	4.5
234	552.30	663.17	663.16	8.221	8.126	8.126	0.170	0.213	142.32	0.171	54.071	4.4	4.1	4.1
235	-	-	-	-	-	-	-	-	-	-	-	-	-	-
236	470.88	573.39	571.92	7.110	7.176	7.176	0.142	0.250	143.24	0.149	44.066	3.6	3.4	3.4
237	526.80	596.45	594.49	7.655	7.719	7.719	0.126	0.250	148.74	0.148	43.064	3.6	3.4	3.4
238	470.88	527.78	526.90	7.544	7.624	7.624	0.123	0.275	144.62	0.174	43.071	3.6	3.4	3.4
239	475.79	589.58	587.62	8.101	8.217	8.217	0.232	0.262	153.93	0.134	53.170	4.1	3.9	3.9
240	-	-	-	-	-	-	-	-	-	-	-	-	-	-
241	771.07	863.28	863.28	9.201	9.272	9.272	0.142	0.203	175.37	0.064	71.221	4.2	4.1	4.1
242	137.34	174.62	174.62	9.810	9.892	9.892	0.164	0.385	69.04	0.076	24.721	2.1	1.62	1.62

* 1st Reloading-Unloading Cycle;

** 2nd Reloading Unloading Cycle

G_{RU} = measured reload-unload modulus

G_{RUo} = reload-unload modulus corrected for stress level (σ_{ho})

G_o = maximum dynamic shear modulus from resonant column tests

TABLE 11
SUMMARY OF CALCULATED ANGLES OF FRICTION AND DILATANCY
($\phi_{cv} = 34^\circ$)

	Test No	S	PS P(1)	PS P(2)	PS P(3)	$\nu(1)$	$\nu(2)$	$\nu(3)$	β	ν	ϕ_p
I D E A L	201	0.45	41.3	49.1		12.4	19.3			0.209	48.3
	207	0.46	41.2	44.0		11.1	13.0			0.148	48.3
	208	0.43	39.1	42.2	14.6	11.9				0.106	48.3
	209	0.46	41.2	43.8	2.2	13.0	10.7			0.126	48.3
	210	0.43	39.1	42.2	14.6	10.3	8.1			0.126	48.3
	211	0.44	41.0	41.4	12.2	12.8	18.1			0.111	48.3
	212	0.44	41.0	44.9	12.2	12.4	12.4			0.111	48.3
	213	0.43	34.8	39.1	15.1	11.3	12.4			0.111	48.3
	214	0.48	42.0	46.3	11.1	14.2	11.6			0.101	48.3
	215	0.47	41.9	46.3	11.1	13.5	13.1			0.142	48.3
S E L F	216	0.32	31.1	36.3	31.3	3.3	3.9			0.122	48.3
	218	0.38	35.6	39.5	37.6	2.3	4.4			0.188	48.3
	219	0.41	37.7	41.0	34.4	4.6	6.1			0.176	48.3
	220	0.40	37.0	40.3	34.1	3.8	5.1			0.095	48.3
	221	0.42	38.4	41.6	34.1	5.1	10.2			0.105	48.3
	222	0.39	36.3	40.0	36.1	3.8	8.0			0.109	48.3
	224	0.46	41.2	43.8	42.4	13.0	10.7			0.208	48.3
	225	0.47	41.9	44.3	42.6	10.9	10.9			0.209	48.3
	228	0.47	41.9	44.3	43.9	10.0	13.5			0.188	48.3
	233	0.49	43.3	45.5	42.0	11.8	14.8			0.198	48.3
B O R E	234	0.45	40.5	43.3	42.9	8.2	12.0			0.219	48.3
	235	0.42	38.4	41.5	39.3	3.7	9.5			0.088	48.3
	236	0.48	42.6	45.0	44.8	10.9	14.2			0.212	48.3
	237	0.45	40.5	43.1	43.4	8.2	11.9			0.210	48.3
	238	0.34	32.6	37.6	32.7	1.7	4.8			0.209	48.3
	239	0.38	35.6	39.4	36.0	1.9	7.1			0.208	48.3
	241	0.40	37.0	40.5	40.9	3.7	8.4			0.268	48.3
	242	0.40	37.1	40.5	43.8	3.7	8.4			0.095	48.3
	243	0.37	34.8	38.9	33.2	1.0	6.5			0.098	48.3
	244	0.40	37.0	40.5	38.1	3.7	8.4			0.095	48.3
I D E A L	245	0.52	45.3	47.4		14.6	16.6			0.093	48.3
	246	0.39	36.3	39.9		2.8	7.8			0.094	48.3
	247	0.67	55.3	55.3	48.6	29.0				0.082	48.3
	250	0.43	39.1	42.0	43.0	6.4	10.5			0.068	48.3
	251	0.47	41.9	44.3	42.0	10.0	13.5			0.097	48.3
	252	0.42	38.4	41.6	39.0	5.5	10.2			0.215	48.3
	253	0.59	50.0	51.8	44.7	21.2	21.9			0.203	48.3
	254	0.56	48.0	49.8	51.3	18.3	19.3			0.197	48.3
	255	0.47	41.9	44.3	47.0	10.0	13.5			0.181	48.3
	256	0.42	38.4	41.6	38.4	5.5	10.2			0.167	48.3
I D E A L	257	0.48	42.6	44.3	36.9	10.9	14.2			0.251	48.3
	258	0.76	61.4	61.4	52.7	38.7				0.218	48.3
	259	0.48	42.6	44.3	44.2	10.9	14.2			0.259	48.3
	260	0.46	41.2	44.0	53.0	9.1	13.0			0.262	48.3
	261	0.51	44.6	46.7	43.8	13.7	16.0			0.252	48.3
	262	0.53	46.0	48.1	49.4	15.5	17.2			0.271	48.3
	263	0.55	47.3	49.1	46.8	17.4	19.0			0.256	48.3
	IDEAL										

Methods: 1: Hughes et al (1977)
2: Robertson (1982)
3: Manassero (1987)

FIG 1 SCHEMATIC CROSS-SECTION OF ENEL CRIS CALIBRATION CHAMBER

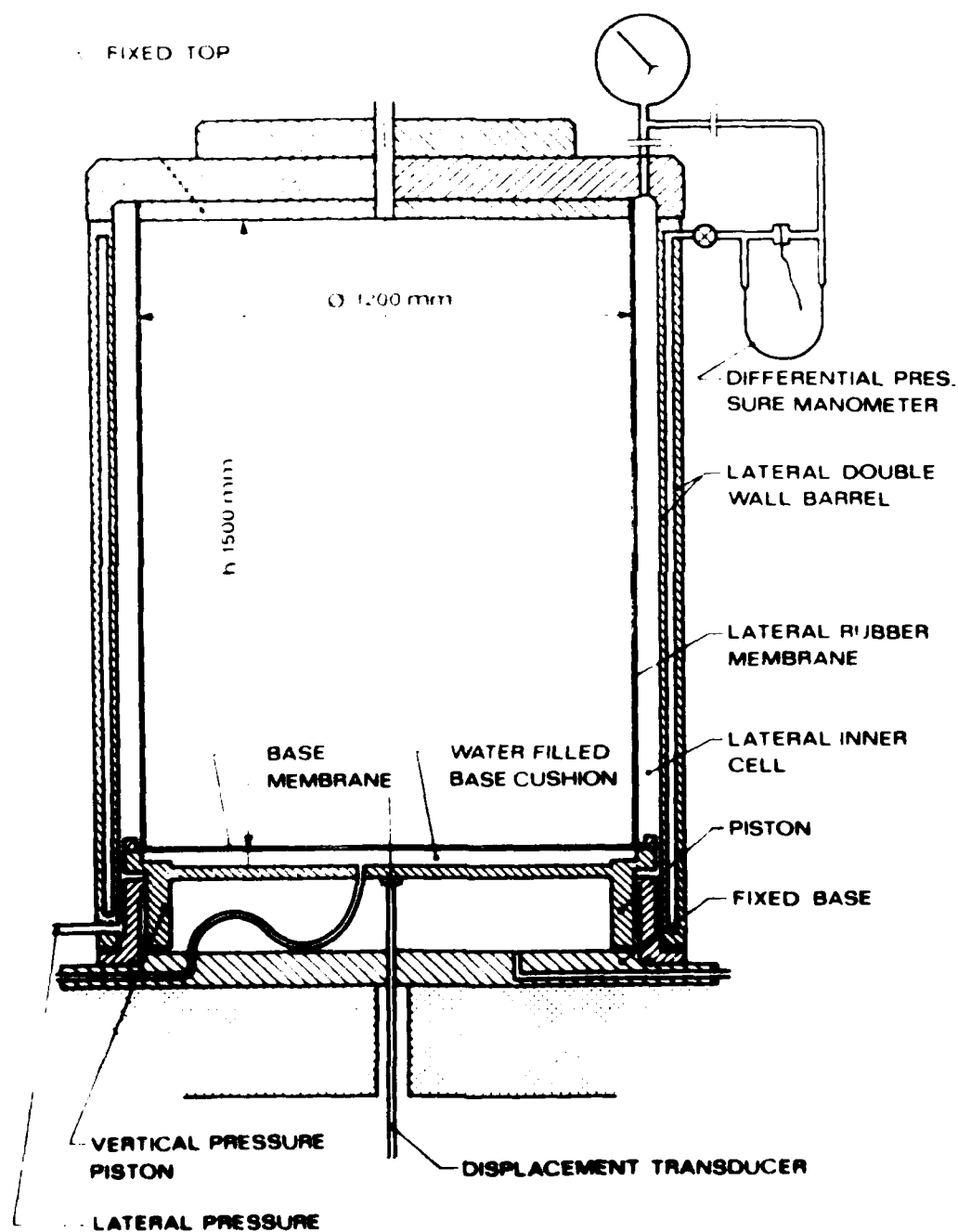
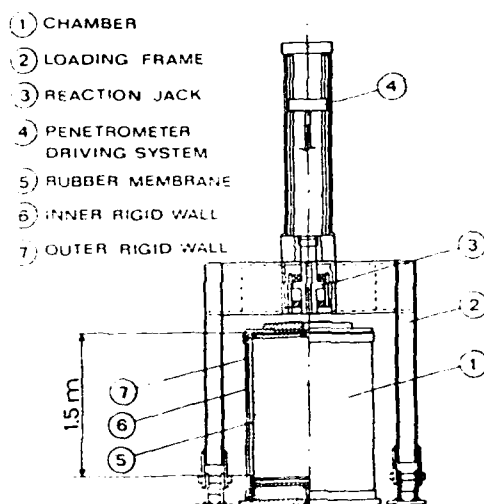


FIG. 2: SCHEMATIC OUTLINE OF CC LOADING SYSTEM AND OF
DATA ACQUISITION SYSTEM FOR SBPT IN SAND

CC LOADING SYSTEM



DATA ACQUISITION SYSTEM

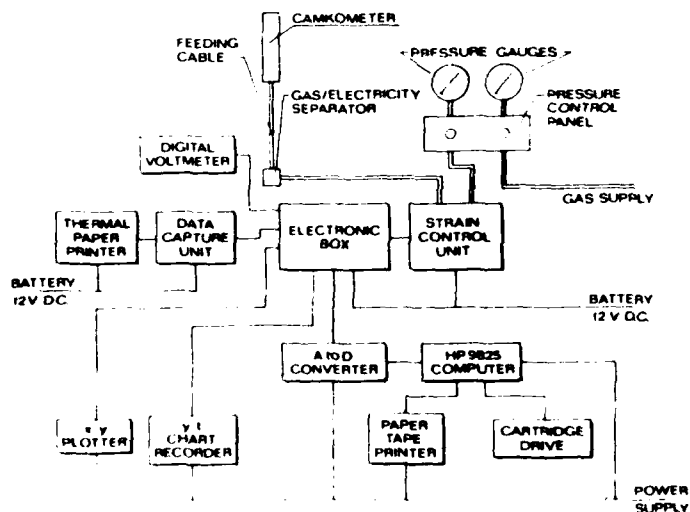
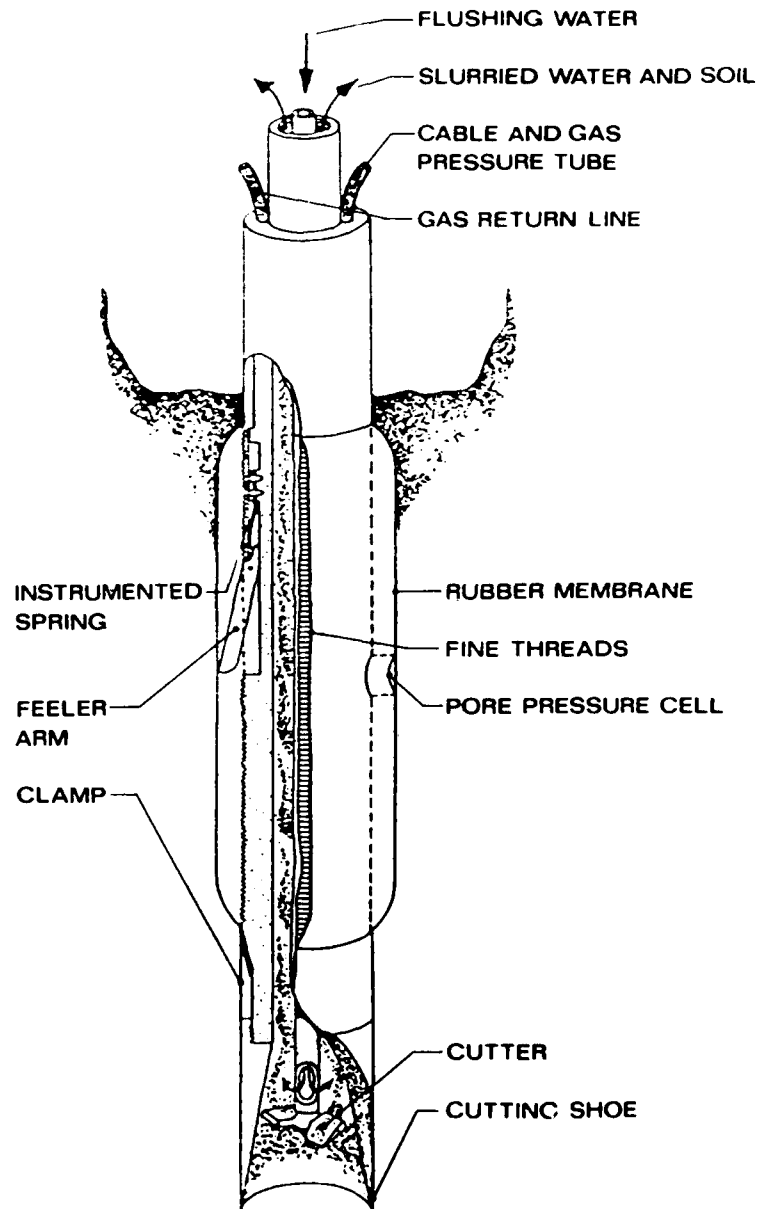


FIG.3: SCHEMATIC OUTLINE OF SELF BORING
PRESSUREMETER PROBE - CAMKOMETER
MARK VIII



SAND	1- TICINO	2-HOKKSUND
DOMINANT MINERAL	QUARTZ (30%)	QUARTZ (35%)
ANGULARITY (LEES' CHART)	8 + 9	6 + 8
MICA	~5%	~10%
ρ_{\max} (t/m ³)	1700	1.759
ρ_{\min} (t/m ³)	1391	1.438

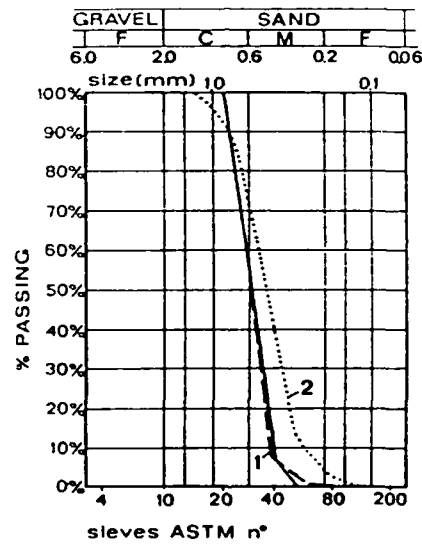


FIG.4 : CHARACTERISTICS OF THE TESTED SANDS

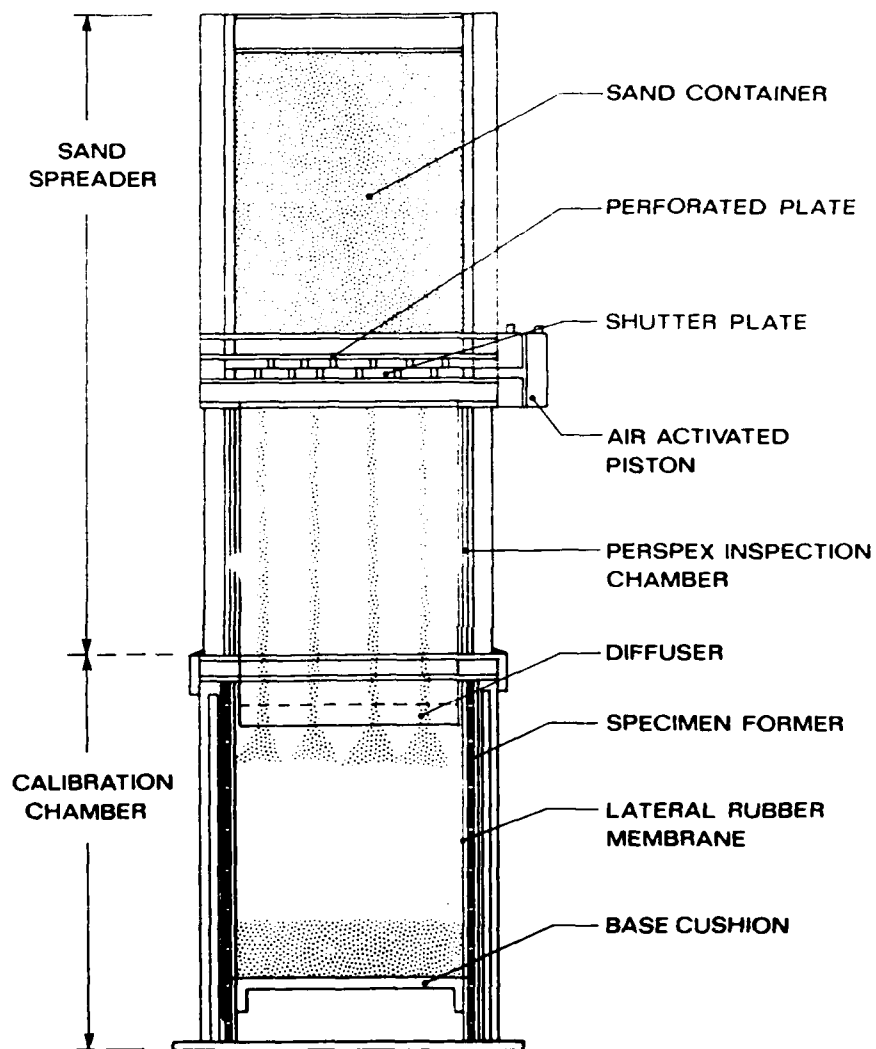
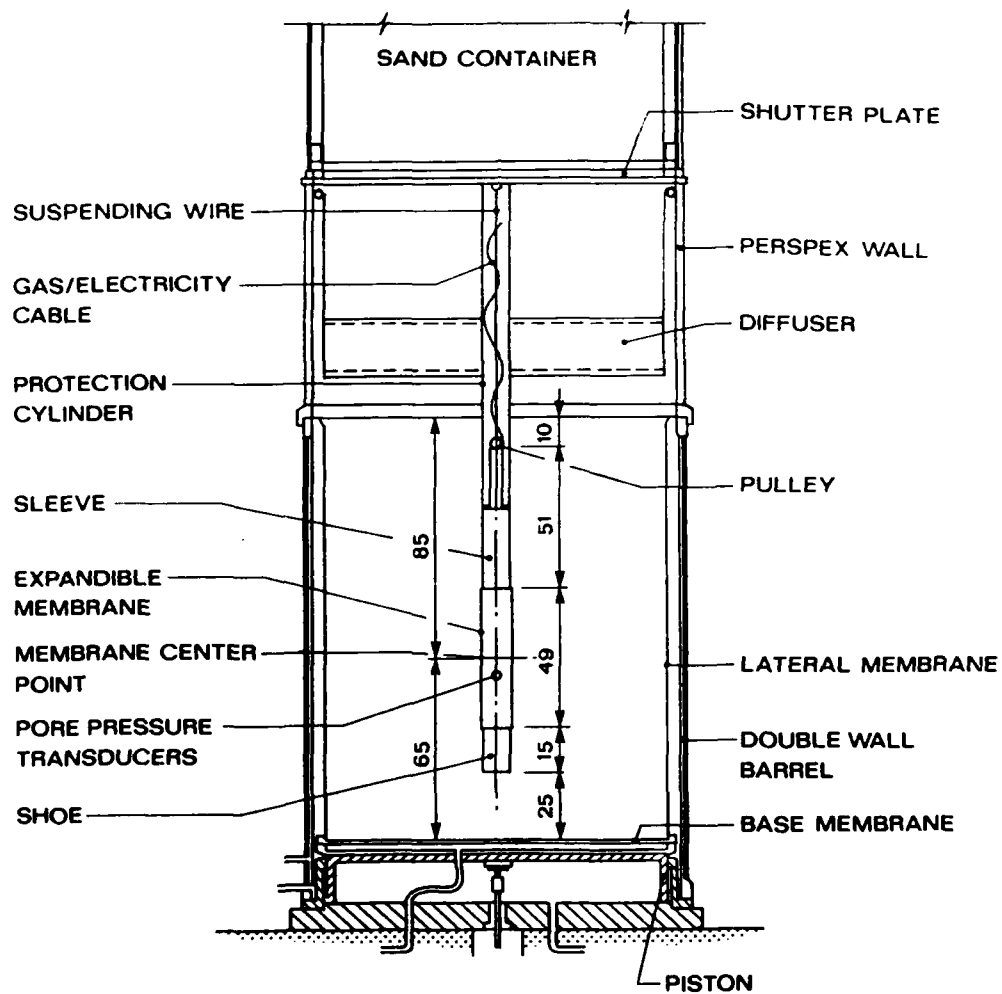


FIG.5 : SCHEMATIC OUTLINE OF SAND SPREADER

FIG. 6: SCHEMATIC OUTLINE OF IDEAL INSTALLATION IN CC



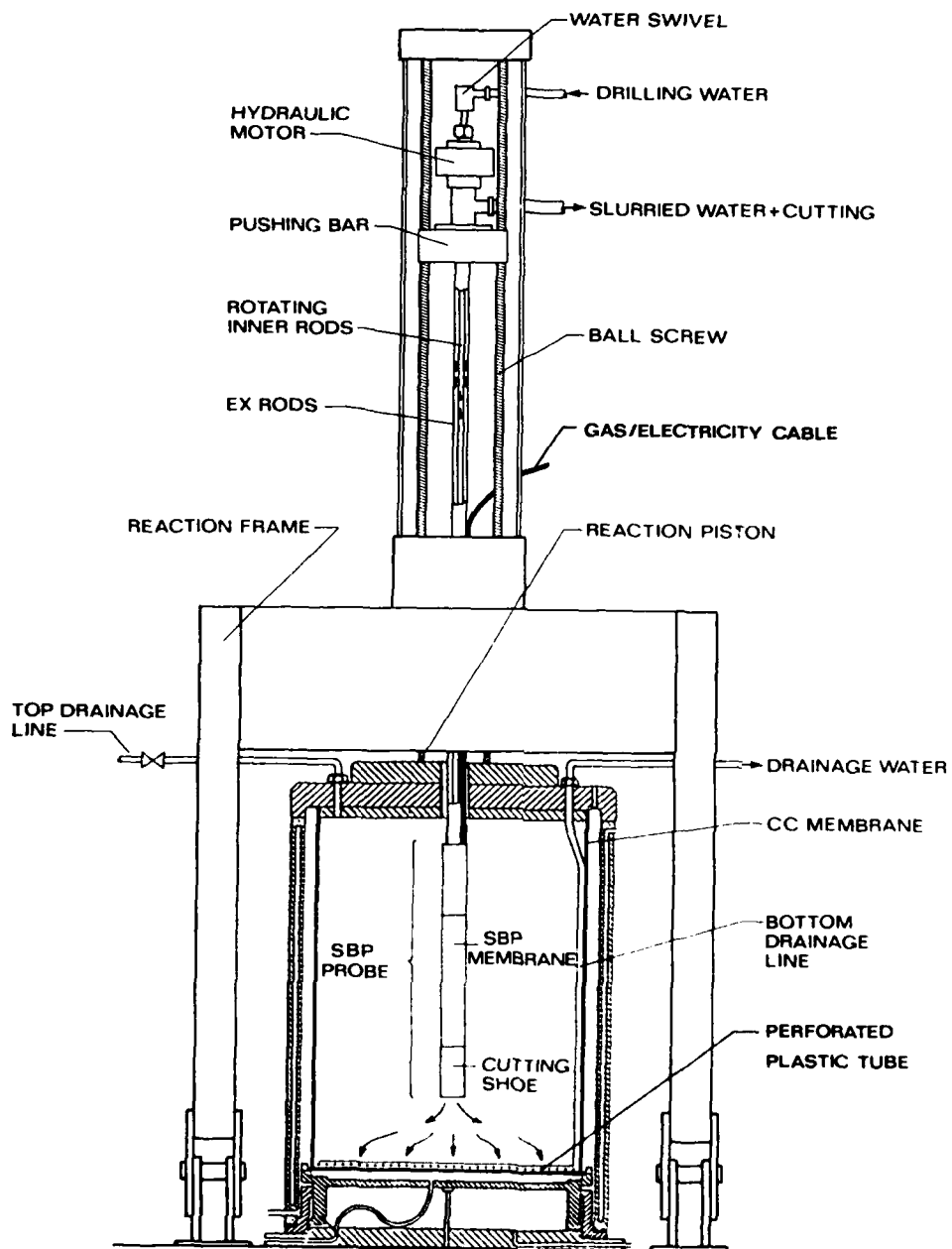


FIG. 7: SCHEMATIC OUTLINE OF SELF-BORING INSTALLATION
PROCEDURE IN CC

FIG.8: EXAMPLE OF SAMPLE CONSOLIDATION

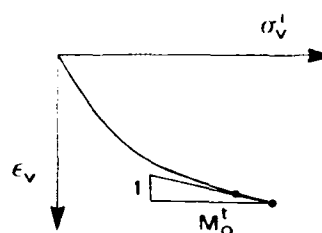
GC TEST 234 - SBP

TICINO SAND TS-4; $D_R = 76.1\%$; $OCR = 5.34$

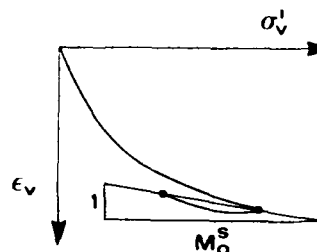
CONSOLIDATION PHASE, BC3

Vertical Stress	Radial Stress	K_o	Tangent Constrained Modulus
σ'_v	σ'_h		M_o^t
[kg/cm ²]	[kg/cm ²]	[-]	[kg/cm ²]
0.12	0.08	0.613	346.7
0.34	0.15	0.445	524.8
0.68	0.30	0.441	676.1
1.19	0.52	0.433	794.3
1.71	0.75	0.433	891.3
2.20	0.97	0.439	912.0
2.71	1.19	0.440	1047.1
3.19	1.40	0.439	1122.0
3.70	1.62	0.439	1202.3
4.21	1.82	0.439	1225.9
4.73	2.08	0.439	1318.3
5.24	2.30	0.439	1349.0
5.76	2.53	0.439	1412.5
6.28	2.76	0.439	

PRIMARY LOADING



UNLOADING



Vertical Stress	Radial Stress	K_o	Secant Constrained Modulus
σ'_v	σ'_h		M_o^s
[kg/cm ²]	[kg/cm ²]	[-]	[kg/cm ²]
6.05	2.71	0.448	2884.0
5.84	2.66	0.456	3890.5
5.63	2.61	0.464	3890.5
5.43	2.56	0.473	3630.8
5.22	2.52	0.482	3388.4
4.72	2.39	0.507	3162.3
4.18	2.25	0.538	2818.4
3.69	2.11	0.572	2630.3
3.18	1.95	0.611	2290.9
2.70	1.78	0.657	2089.3
2.16	1.56	0.722	1862.1
1.60	1.30	0.812	1513.6
1.18	1.06	0.904	1174.9

1. Stresses at mid-height of sample (75 cm)

2. No lateral strain $\Delta\epsilon_h = 0$

FIG. 9 : AVAILABLE BOUNDARY CONDITIONS IN CC

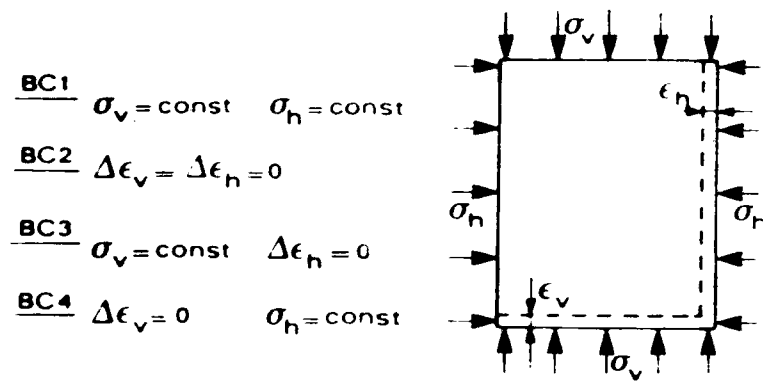
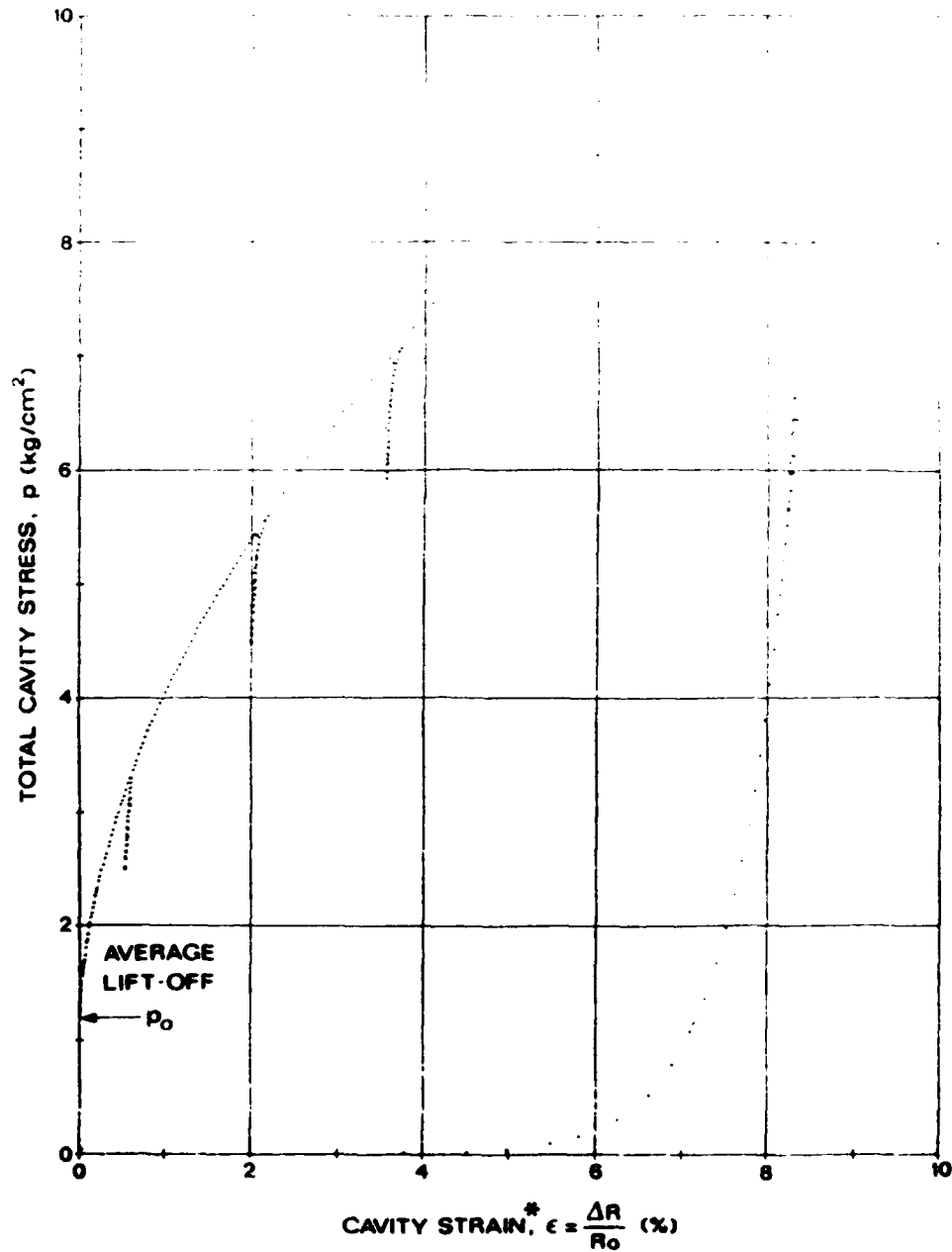


FIG 10 TYPICAL TEST RESULT FROM SBPT IN CC

CC TEST N° 234 SBP
TICINO SAND TS 4, $D_R = 76.1\%$, $OCR = 5.34$
PRESSUREMETER TEST, BC1

*All data referred to the average strain of the three strain
arms, corrected for membrane stiffness



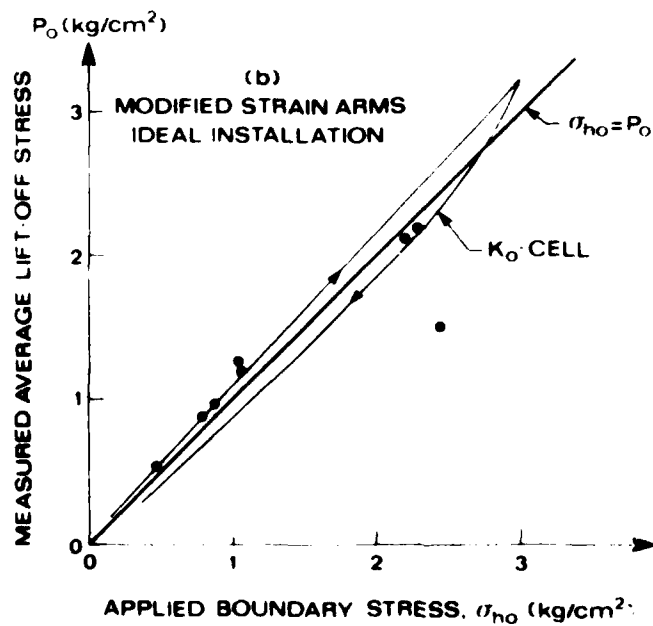
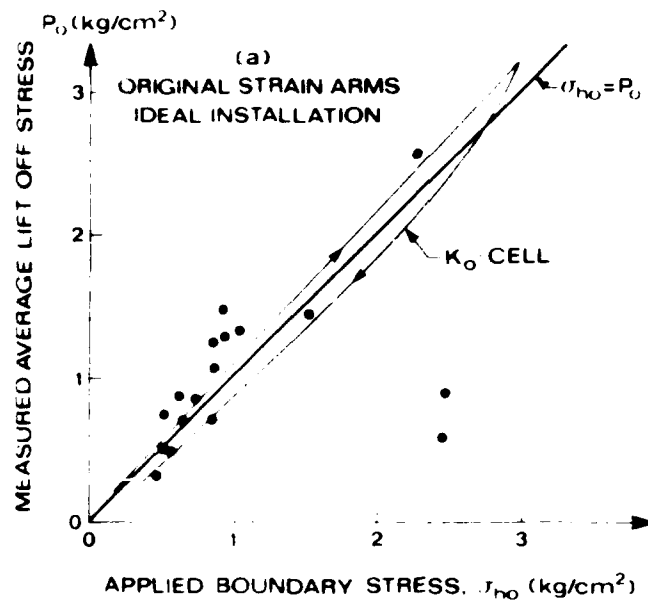
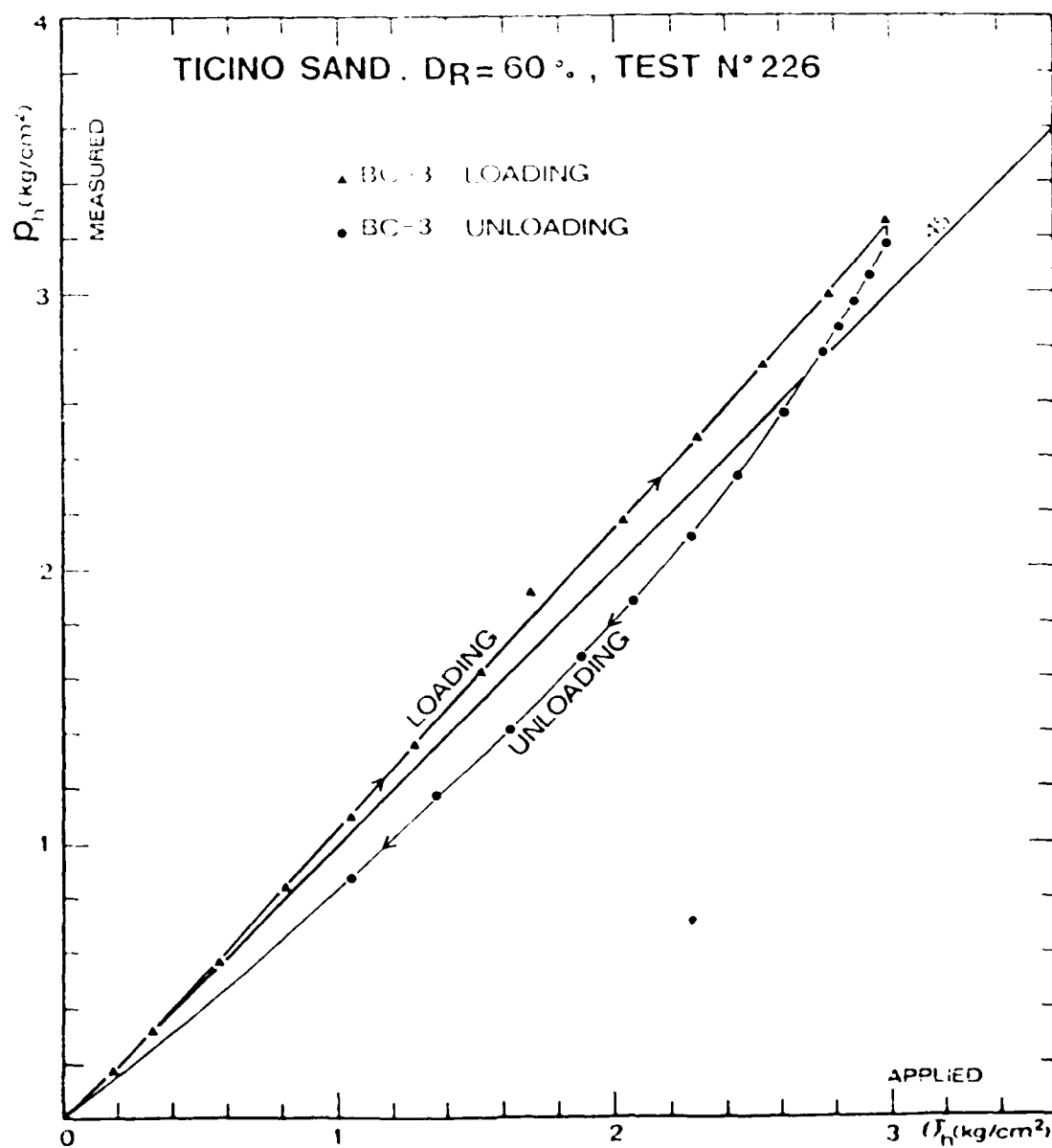


FIG. 11: COMPARISON OF MEASURED LIFT-OFF STRESS AND
APPLIED HORIZONTAL STRESS FOR IDEAL INSTALLATION
IN CC

FIG. 12

1-D STRESSING OF THE CAMBRIDGE K_0 -CELL IN CC



FEELER ARM COMPLIANCE
DURING COMPRESSION PHASE
IDEAL INSTALLATION TEST N 213

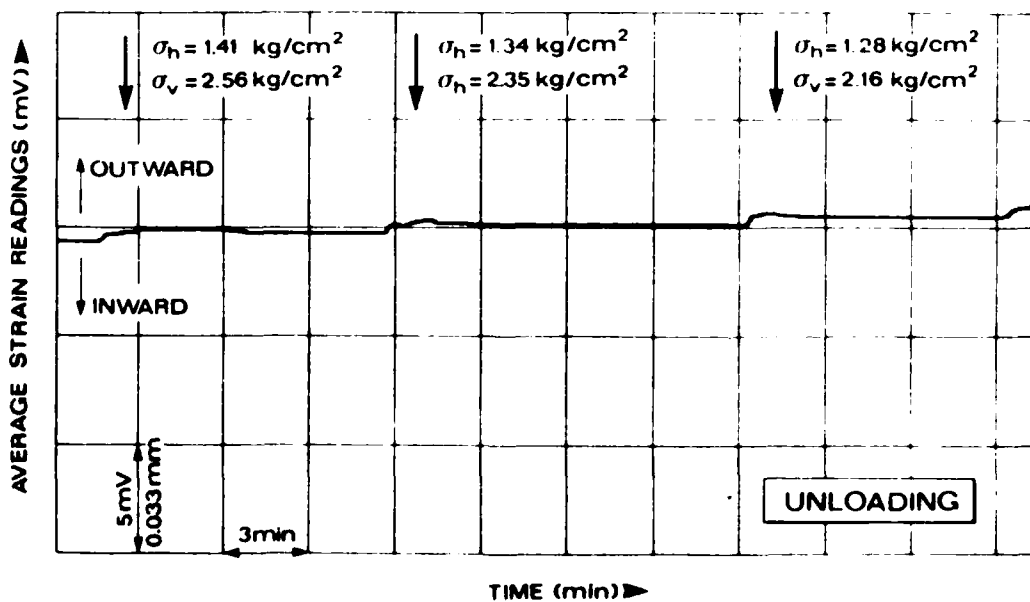
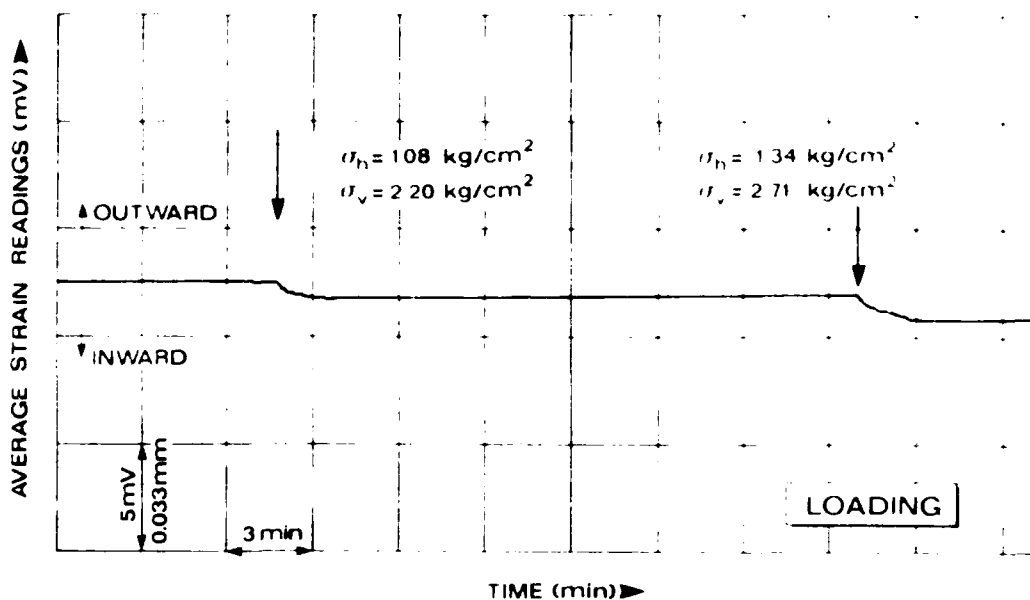
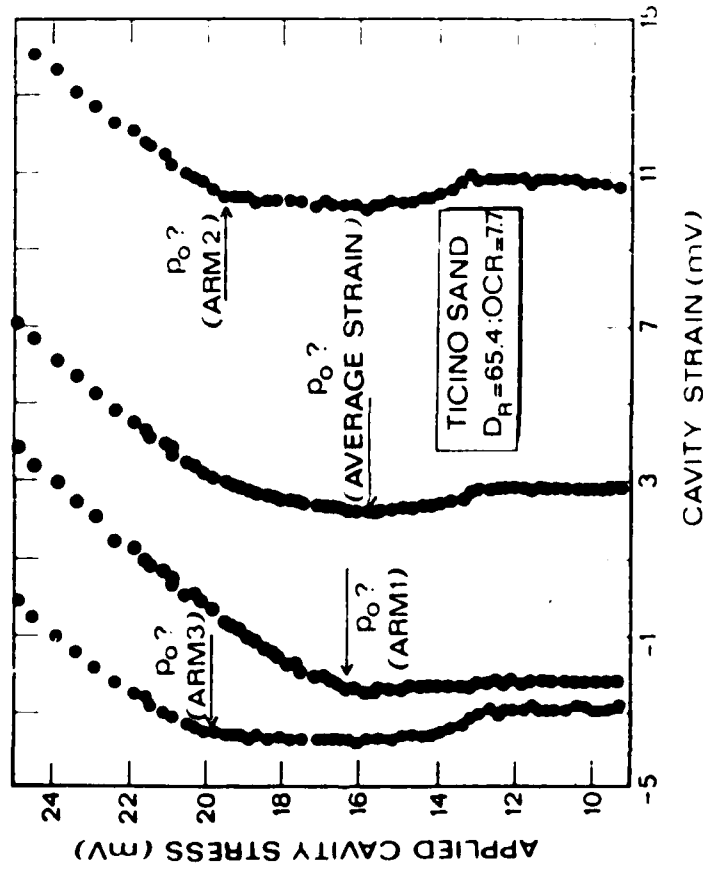


FIG. 13

FIG.14: EXAMPLE OF PRONOUNCED MECHANICAL COMPLIANCE DURING EXPANSION

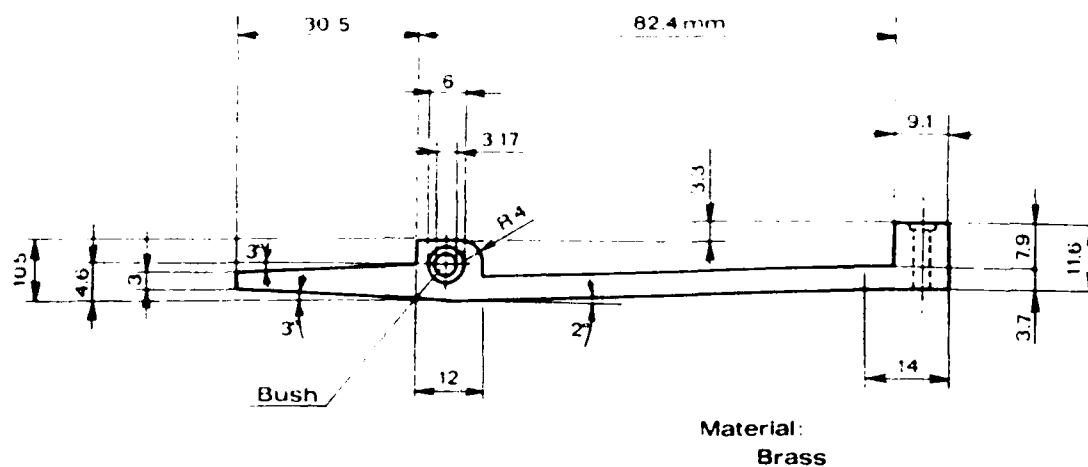


STRAIN OF "LIFT OFF" p_o (kPa)	
TOTAL	80.3
ARM 1	85.3
ARM 2	11.5
ARM 3	120.9
APPLIED LATERAL BOUNDARY STRESS	
$\sigma'_h = 67.3$ kPa	

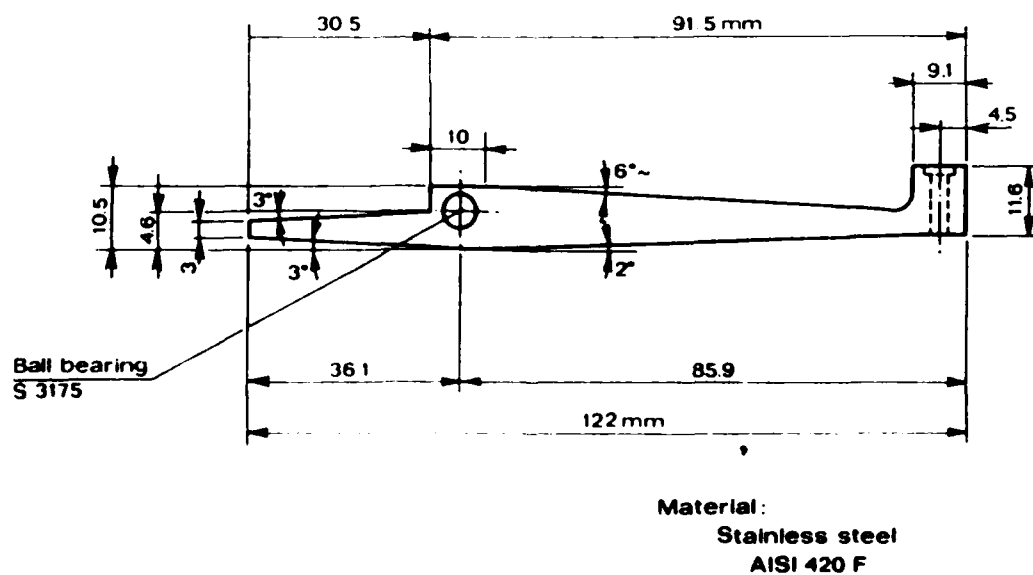
AVERAGE STRAIN: $10\mu V = 6.9 \cdot 10^{-3}$
 SINGLE ARM : $10\mu V = 2.1 \cdot 10^{-2}$
 CAVITY STRESS : $10\mu V = 10.02$ kPa

FIG 15: DETAILS OF ORIGINAL AND MODIFIED SBP
STRAIN ARMS

ORIGINAL DESIGN



MODIFIED DESIGN



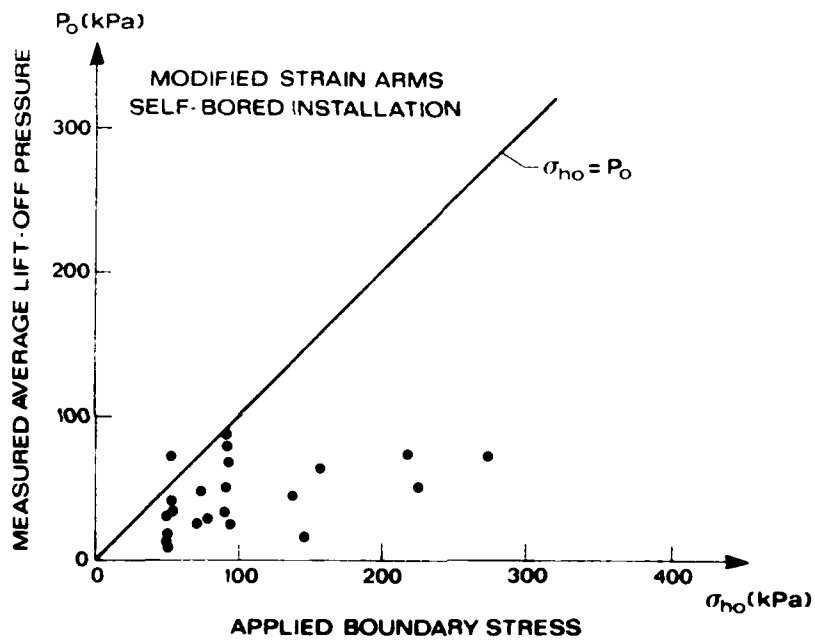


FIG.16: COMPARISON BETWEEN MEASURED AVERAGE LIFT-OFF PRESSURES AND APPLIED STRESSES FOR SELF-BORED INSTALLATION

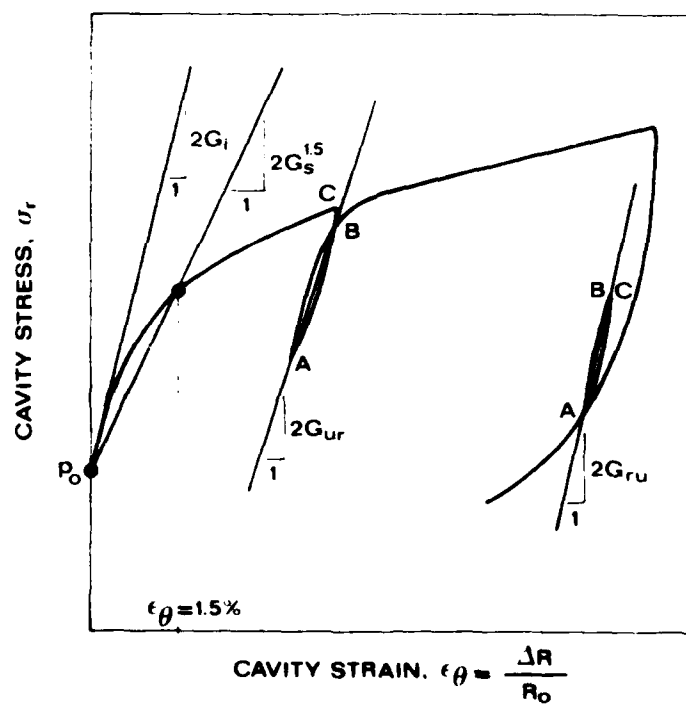
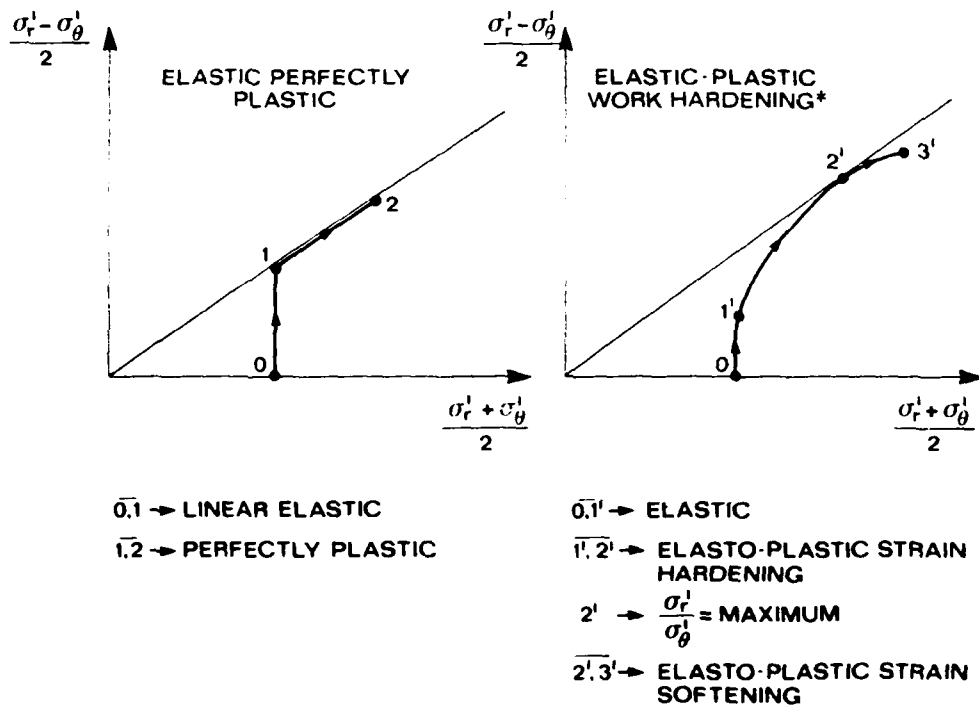


FIG.17: SCHEMATIC OF SHEAR MODULI FROM SBP TESTS



(*) ACCORDING MANASSERO (1987)

FIG. 18: SCHEMATIC OF EFFECTIVE STRESS PATH
OF SOIL ELEMENT ADJACENT TO AN
EXPANDING PRESSUREMETER

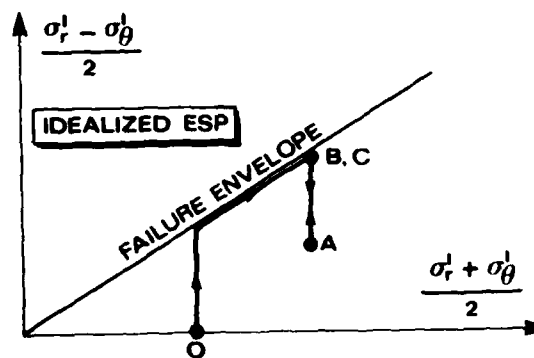
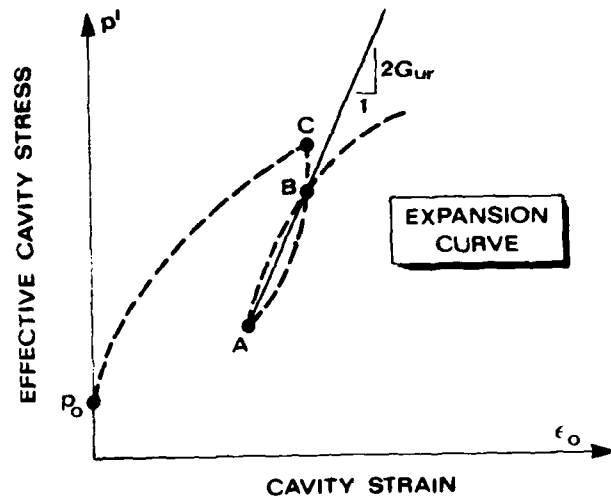
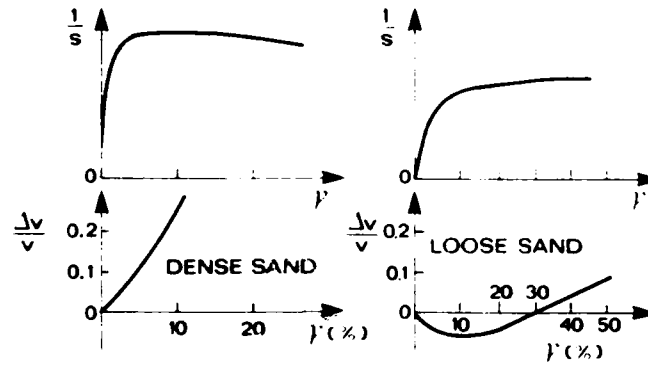
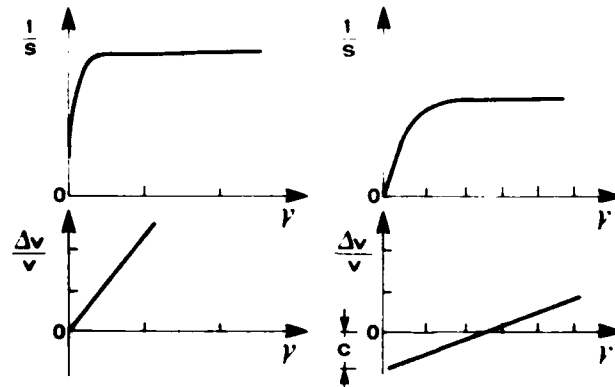


FIG.19: SCHEMATIC OF UNLOADING-RELOADING CYCLE DURING SBPT IN SAND



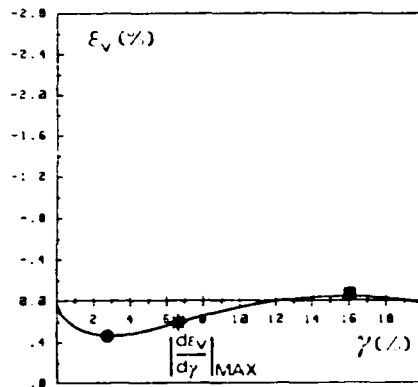
a) RESULTS OF SIMPLE SHEAR TEST (AFTER STROUD 1971)



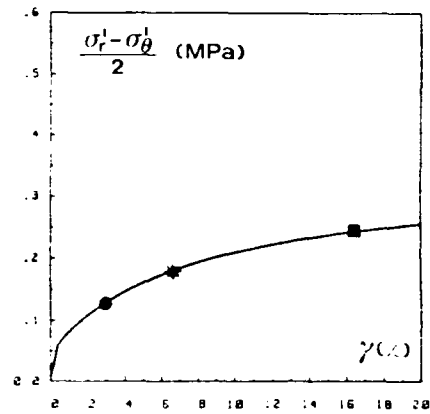
b) SIMPLIFIED MODEL ASSUMED BY HUGES ET AL (1977)

FIG 20 : STRESS-STRAIN AND VOLUMETRIC STRAIN-SHEAR STRAIN CURVES FOR a) SIMPLE SHEAR TEST RESULTS (STROUD, 1971), b) IDEALIZED BY HUGES ET AL (1977)

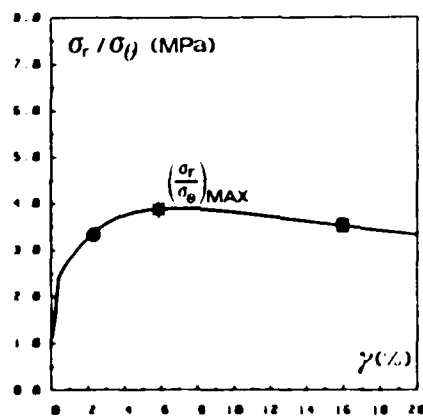
FIG.21: Stress / strain relationships from test N 222 ($D_R = 46.2\%$)
MANASSERO (1987)



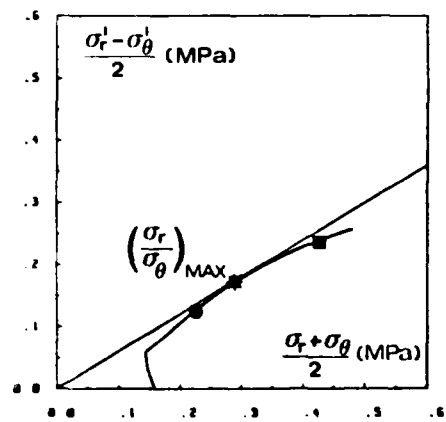
a) Volumetric strain vs shear strain



b) Shear stress vs shear strain

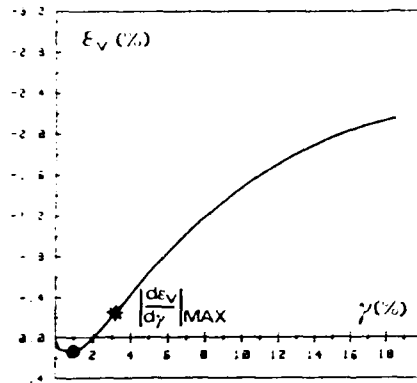


c) Stress ratio vs shear strain

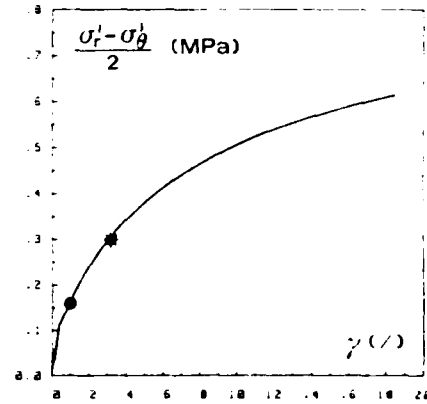


d) Shear stress vs mean normal stress

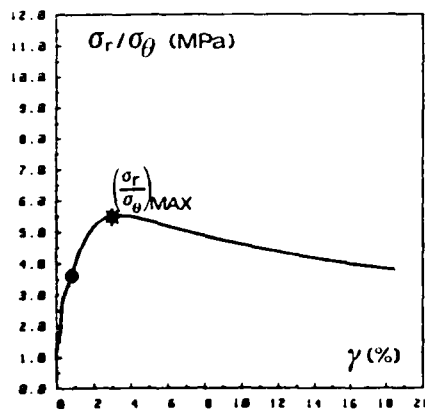
FIG.22 Stress / strain relationships from test N.228 ($D_R = 77.0\%$)
MANASSERO (1987)



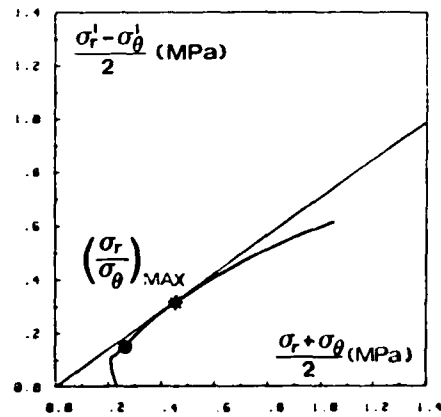
a) Volumetric strain vs shear strain



b) Shear stress vs shear strain



c) Stress ratio vs shear strain



d) Shear stress vs mean normal stress

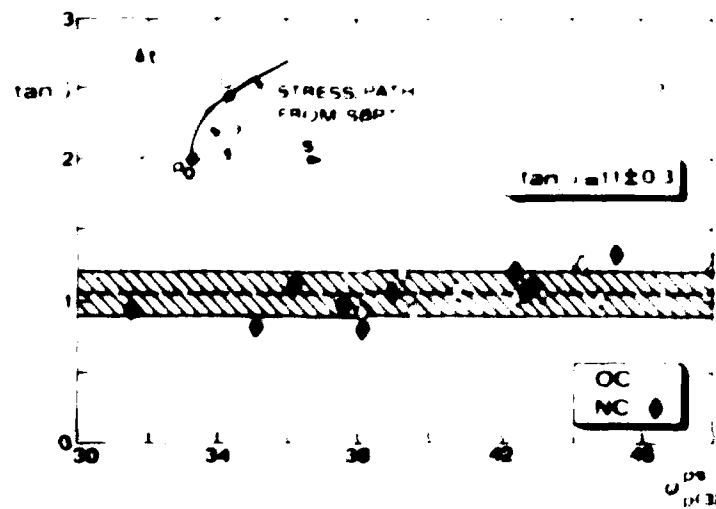
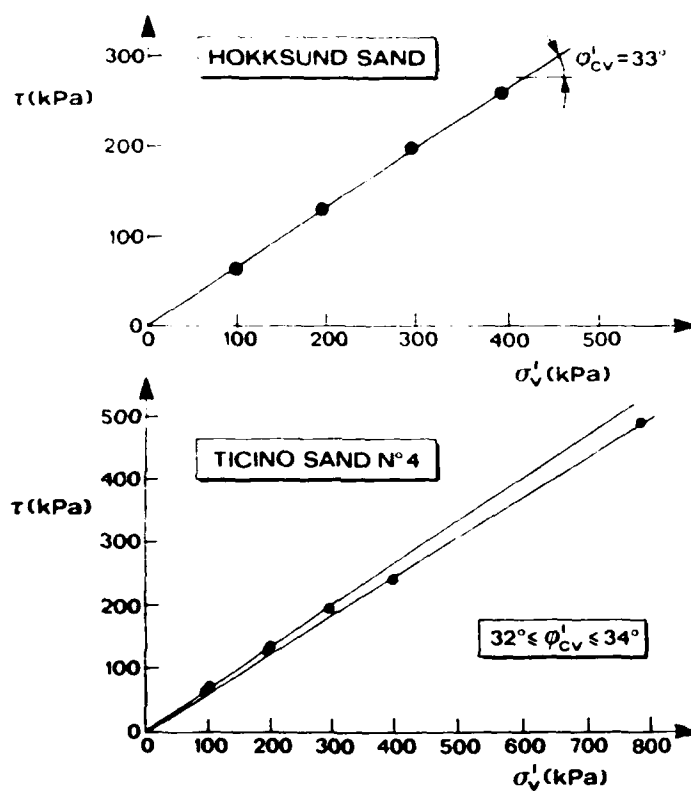


FIG. 23. ANGLE β . DEVIATION OF THE ESP FROM ISOTROPIC ELASTIC BEHAVIOUR (FOR WHICH $\beta = 90^\circ$)
MANASSERO (1967)

FIG. 24: ϕ_{cv} OF SANDS USED IN CC TEST



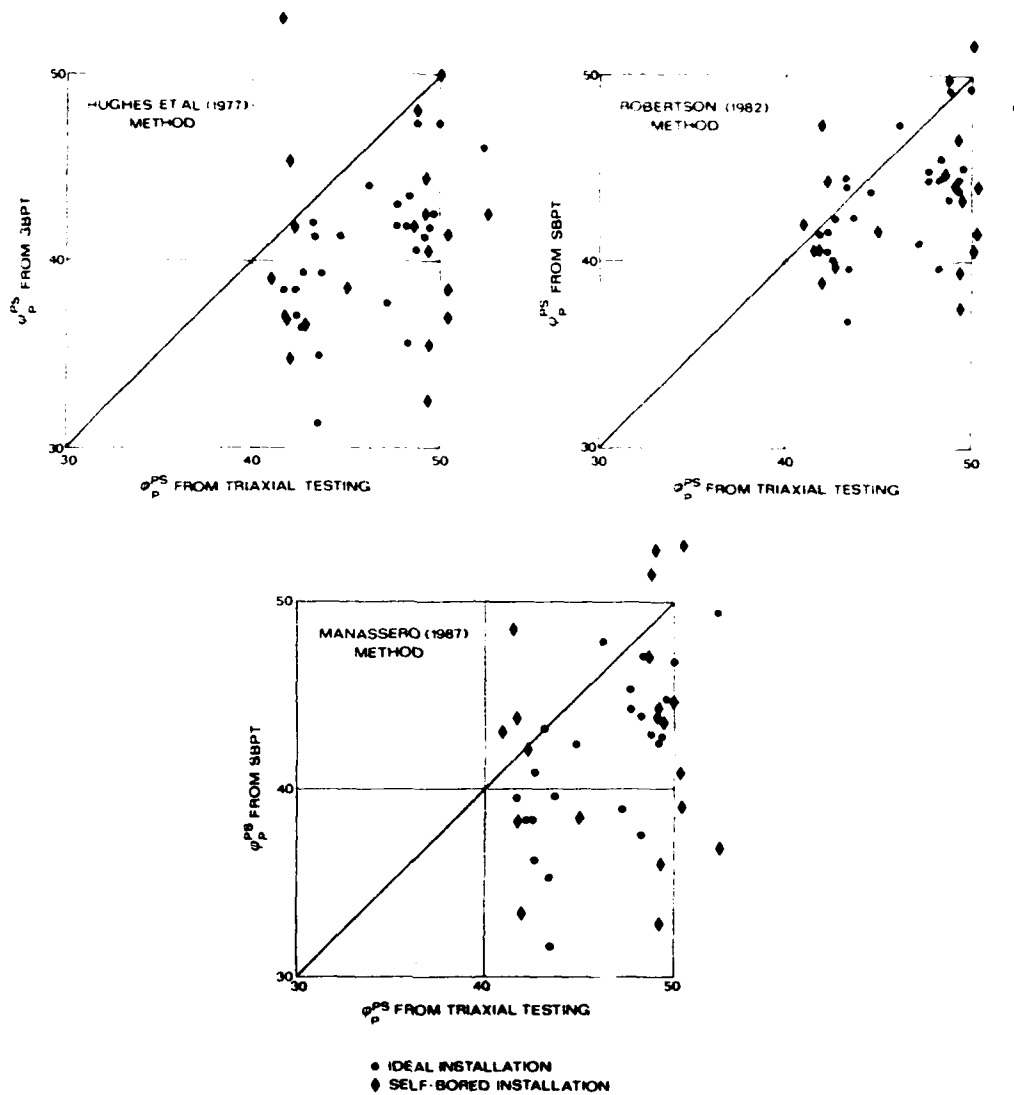


FIG. 25: COMPARISON OF CALCULATED ϕ_p^{PS} FROM SBPT AND EQUIVALENT ϕ_p^{PS} FROM TRIAXIAL TESTS

APPENDIX I
EXAMPLE OF COMPUTER GENERATED PLOTS
FOR TYPICAL SBPT RESULT

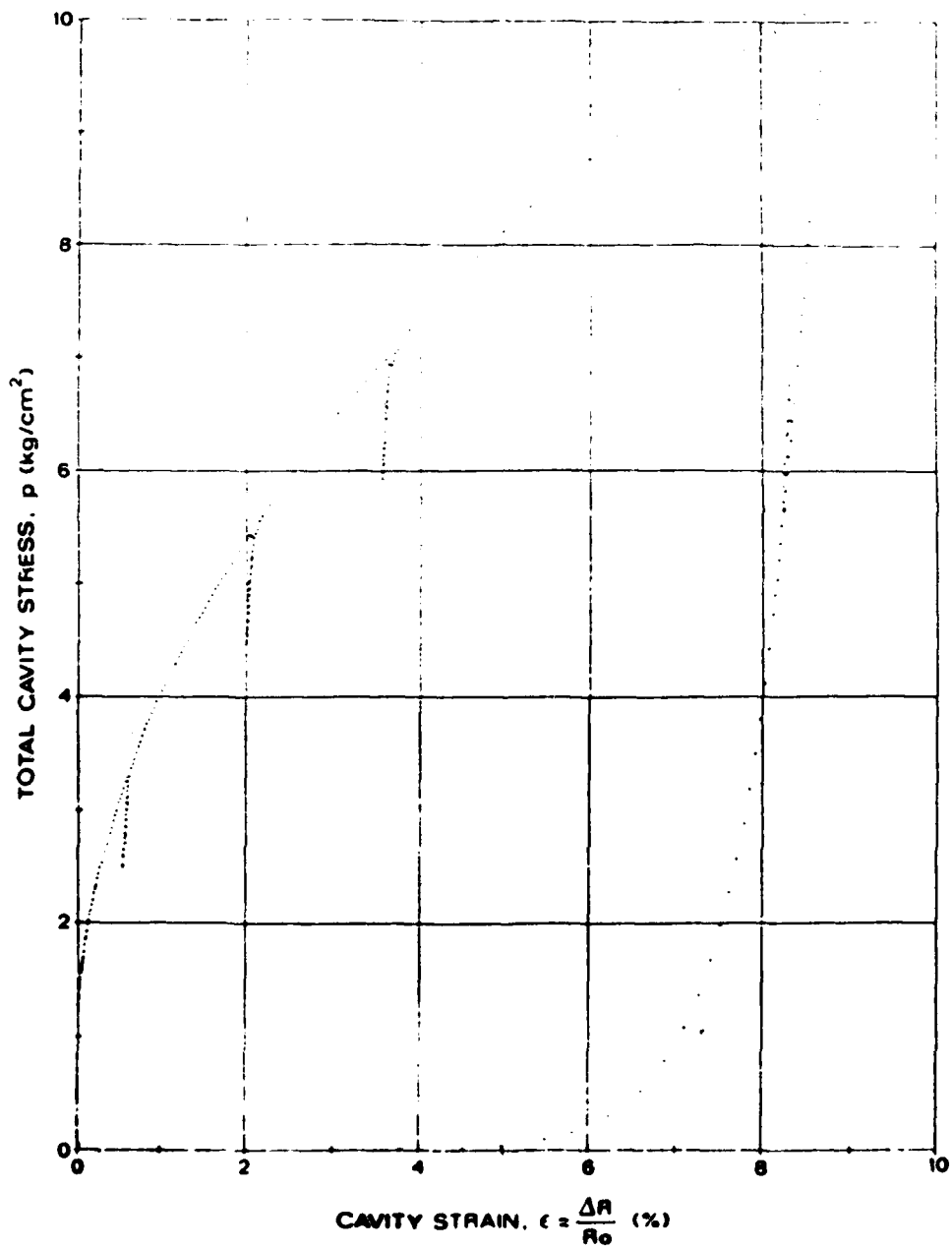
ENEL-CRIS OF MILAN AND TECHNICAL UNIVERSITY OF TURIN

CC TEST N 234 - SBP

TICINO SAND TS-4; $D_r=76.1\%$; $OCR=5.34$

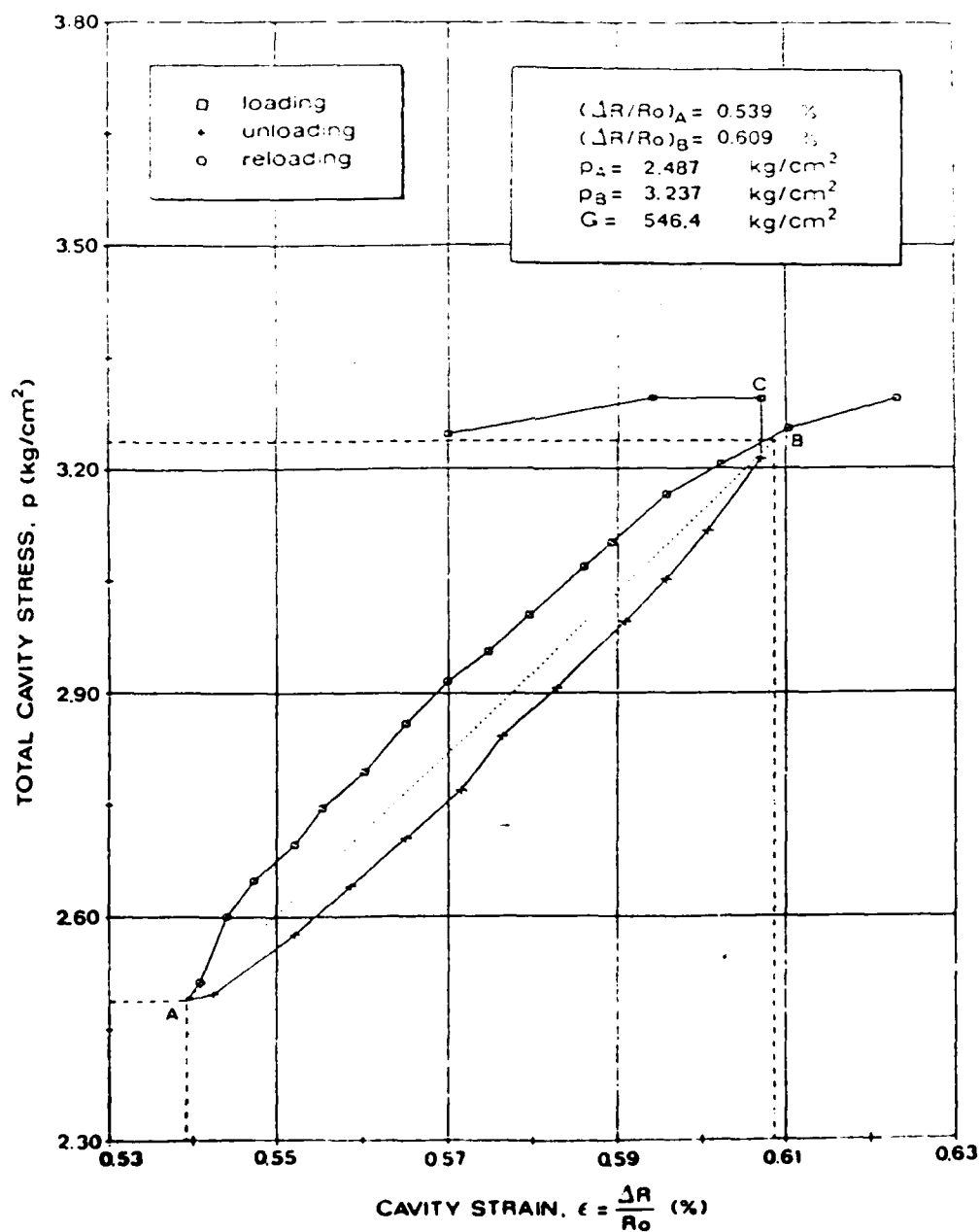
PRESSUREMETER TEST, BCI

(All data referred to the average strain of the three strain arms)



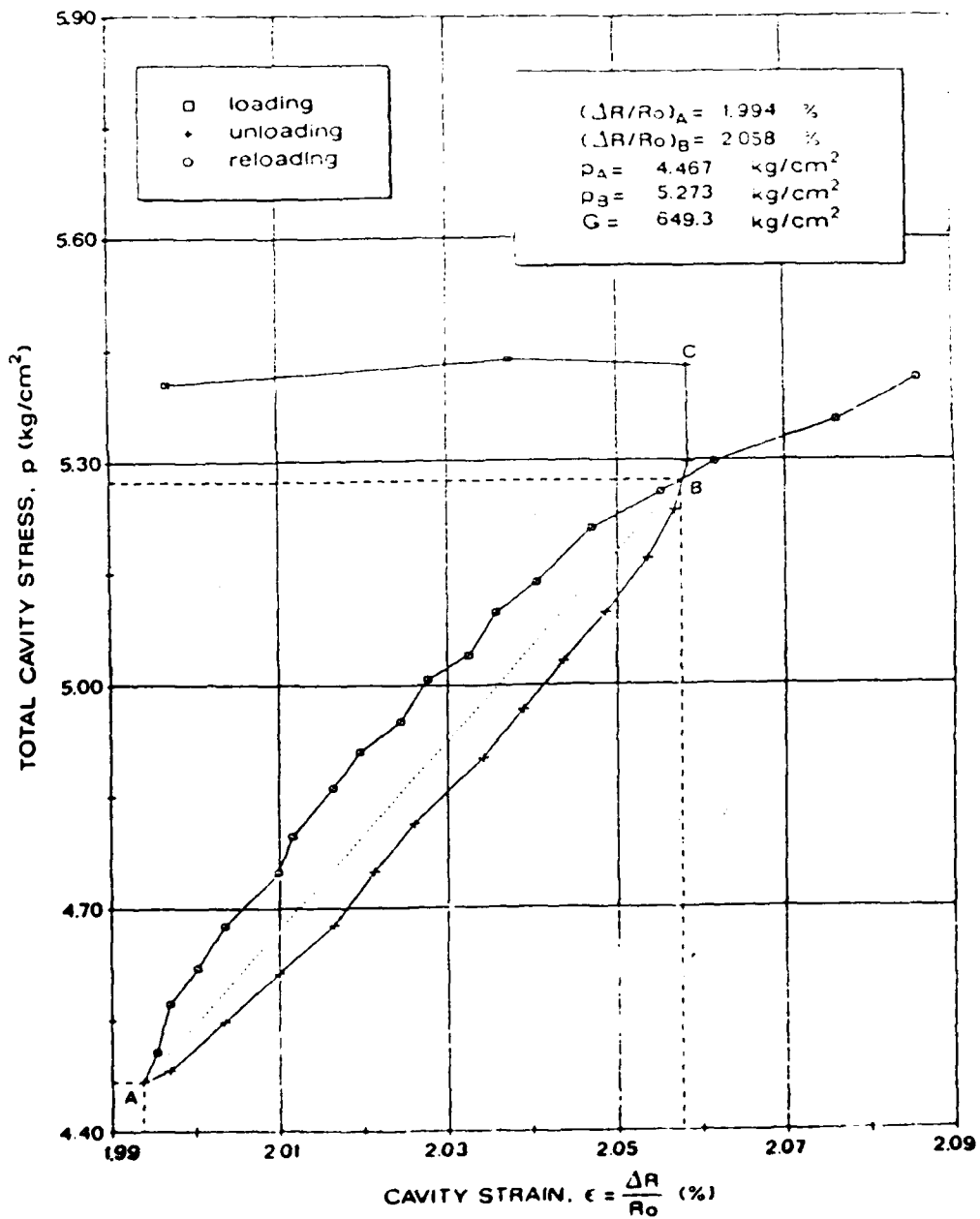
ENELCRIS OF MILAN AND TECHNICAL UNIVERSITY OF TURIN
 CC TEST N. 234 - SEP
 TIDING SAND TS-4; Dr=76.14; DCR=5.34
 PRESSUREMETER TEST, B01
 (All data referred to the average strain of the three strain arms)

LOOP N°1 CR



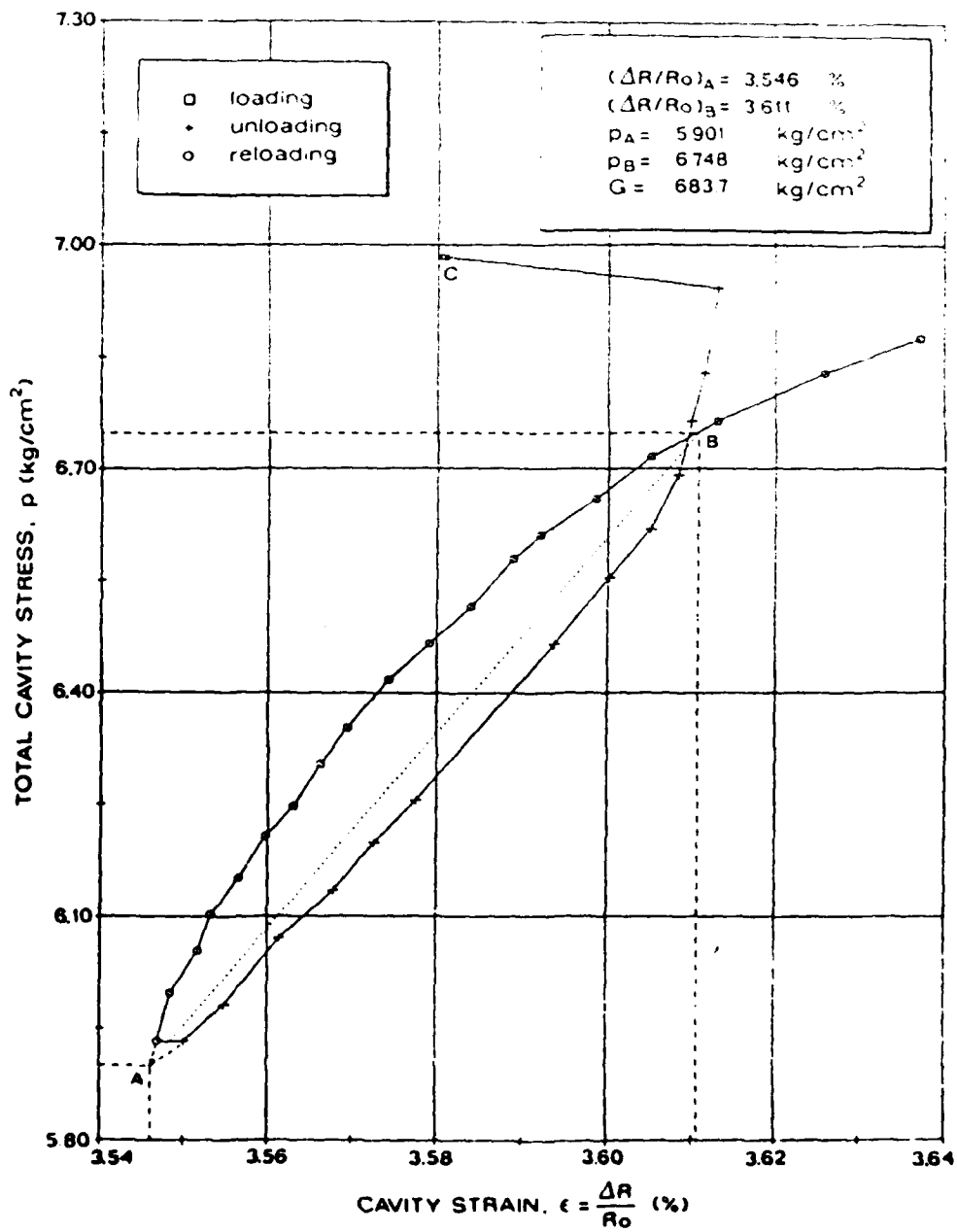
ENEL ERIS F MILAN AND TECHNICAL UNIVERSITY OF TURIN
 CC TEST N 234 - SBP
 TICINO SAND TS-4; $D_r=76\%$; $OCR=5.34$
 PRESSUREMETER TEST, BC1
 (All data referred to the average strain of the three strain arms)

LOOP N°2 UR



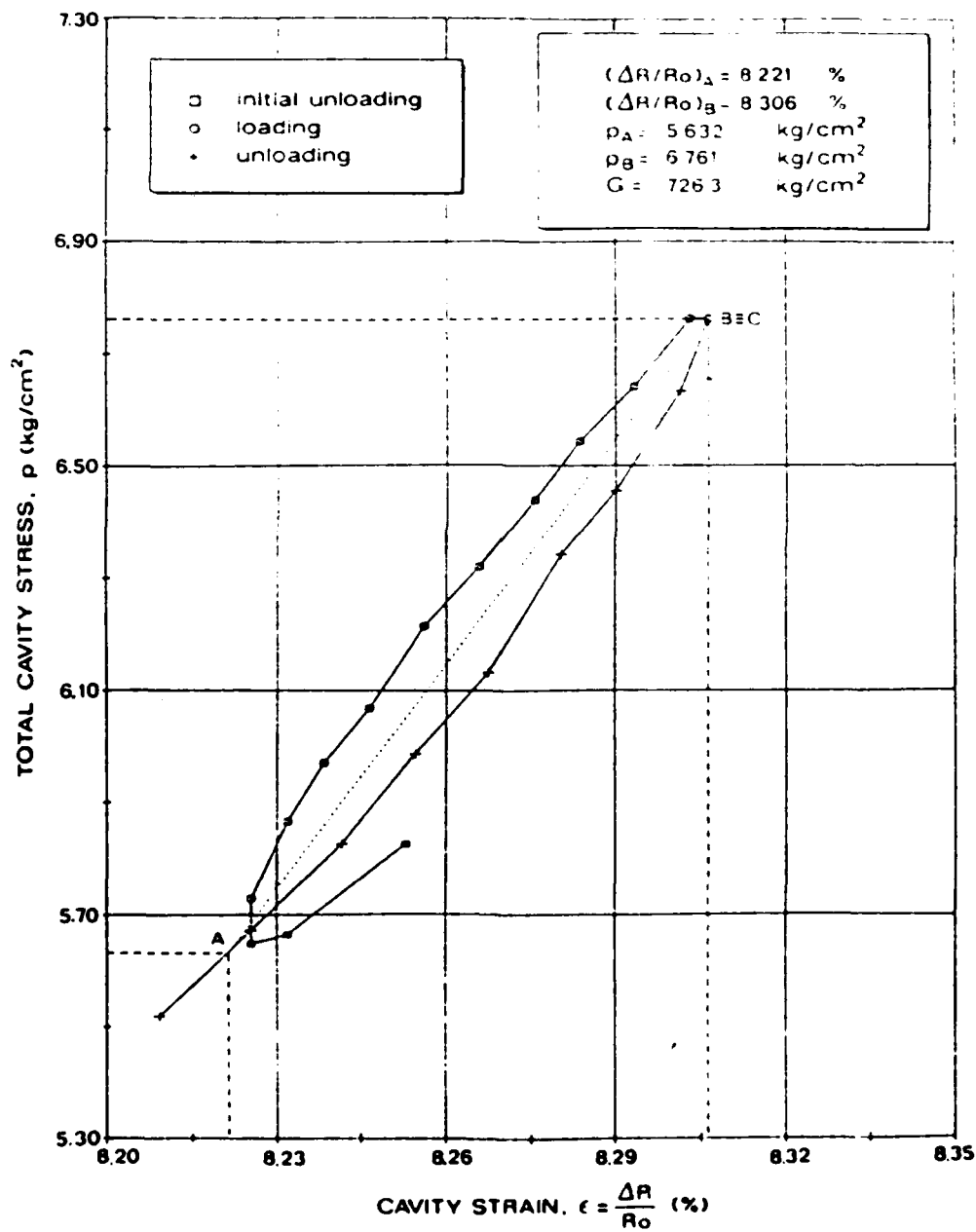
ENEL CRIS OF MILAN AND TECHNICAL UNIVERSITY OF TURIN
 CC TEST N° 234 - SBP
 TICINO SAND TS-4, $Dr=75\%$, $OCR=5\%$
 PRESSUREMETER TEST, BC1
 All data referred to the average strain of the three strain arms

LOOP N°3 UR

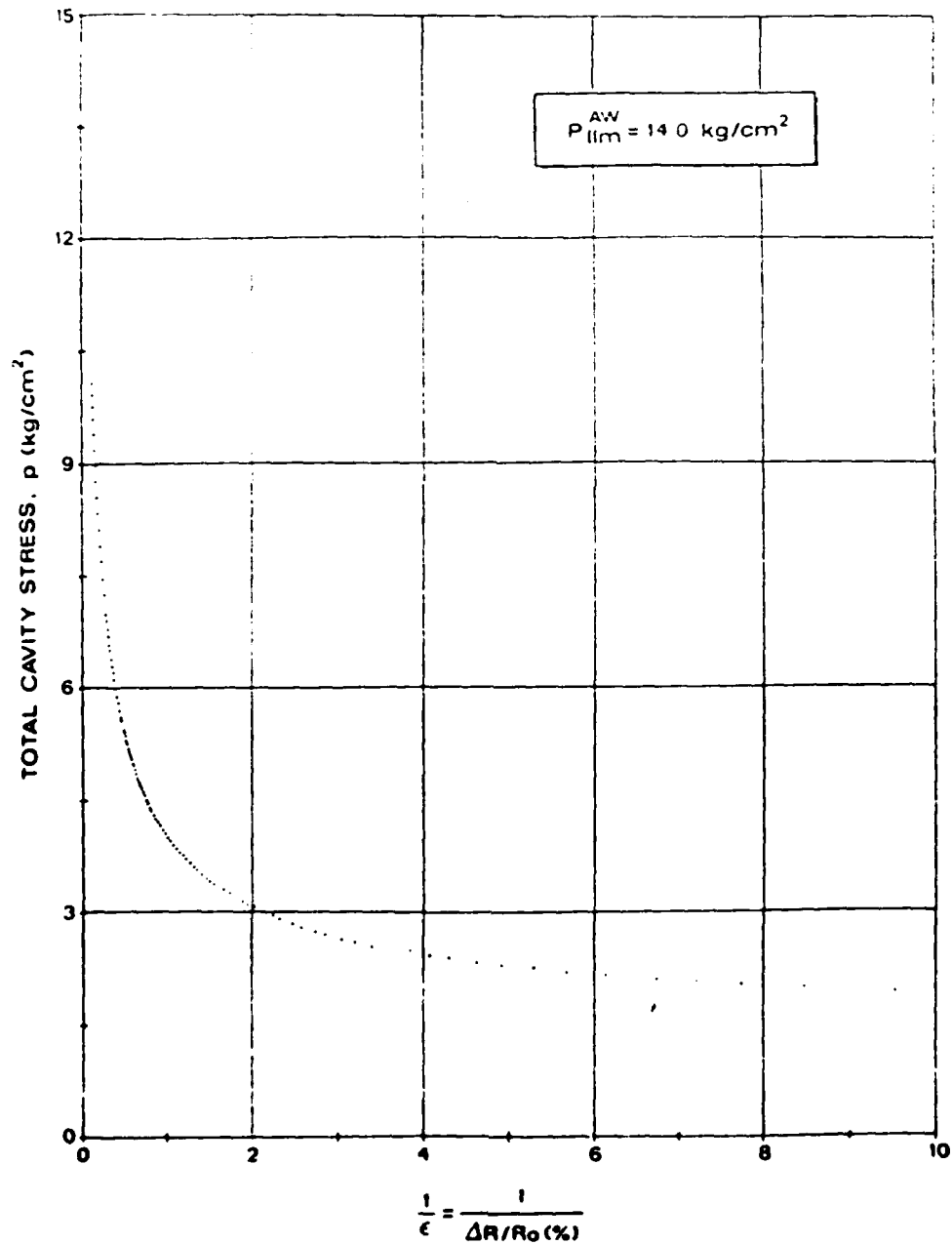


ENEL ERIS OF MILAN AND TECHNICAL UNIVERSITY OF TURIN
 CC TEST N° 21, GBP
 TIRINO SAND TS 4, $D_r = 76.1\%$, $G/P = 5.1\%$
 PRESSUREMETER TEST, BCI
 (All data referred to the average strain of the three strain arms)

LOOP N° 4 RU



ENELTIRIS OF MILAN AND TECHNICAL UNIVERSITY OF TURIN
 CC TEST N. 234 - SBP
 TICINO SAND TS-4; Dr=76.1%; OCR=5.34
 PRESSUREMETER TEST, B01
 (All data referred to the average strain of the three strain arms)



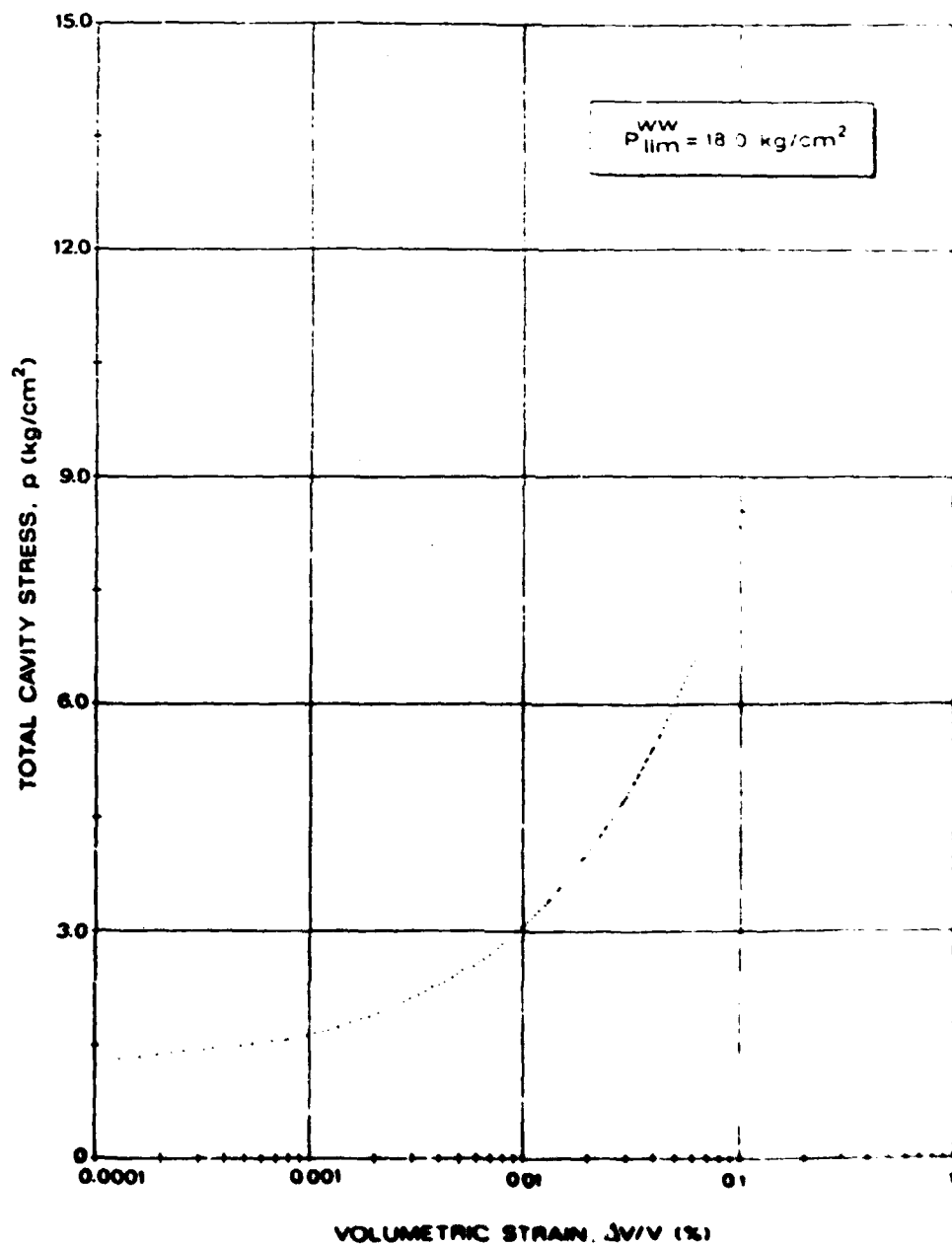
ENEL-CRIS OF MILAN AND TECHNICAL UNIVERSITY OF TURIN

CC TEST N. 234 - SBP

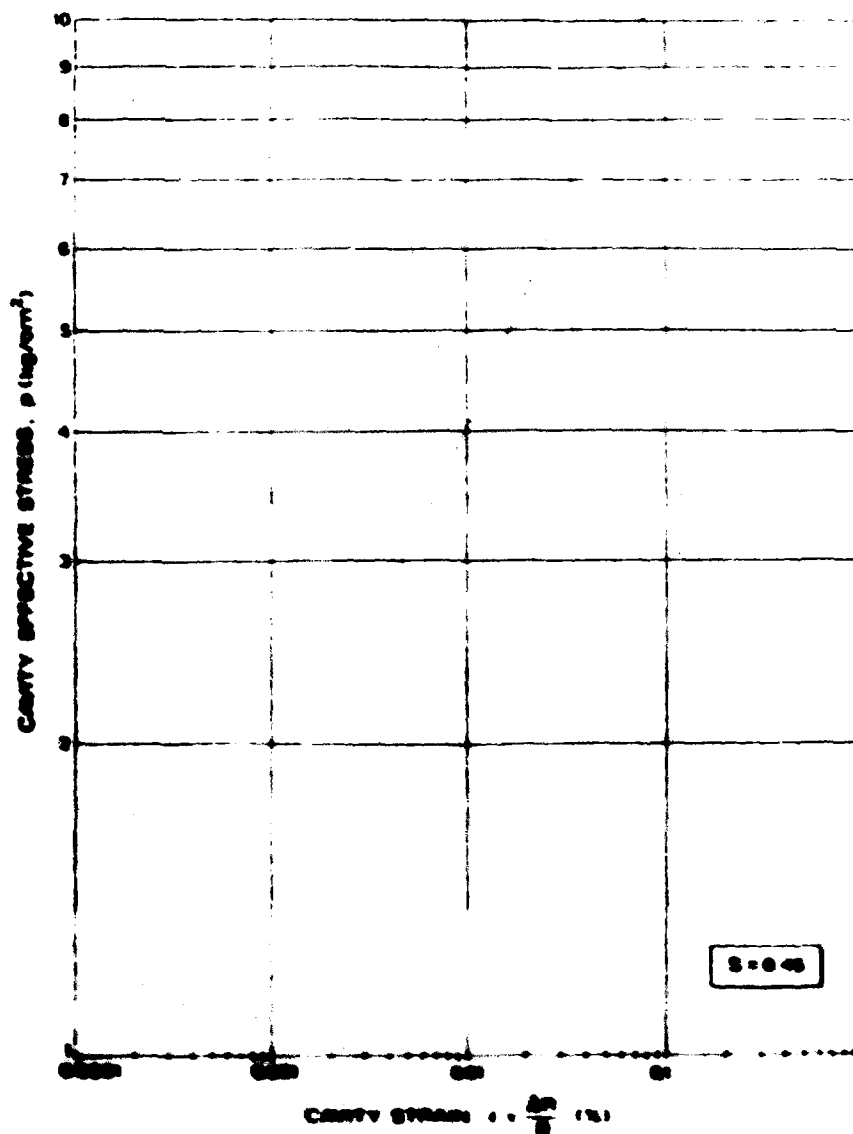
TICINO SAND TS-4; $D_r=76.1\%$, $OCR=5.3\%$

PRESSUREMETER TEST, BCI

(All data referred to the average strain of the three strain arms)



ENEL CRIS OF MILAN AND TECHNICAL UNIVERSITY OF TURIN
 CC TEST N 234 SBP
 TICINO SAND TS-4, Dr=76.10, OCR=5.14
 PRESSUREMETER TEST, BCI
 (All data referred to the average strain of the three strain arms)



APPENDIX II
COMPLETE LISTING FOR EACH
SBPT RESULTS

APPENDIX III
CALCULATION OF AVERAGE STRESS ON
HORIZONTAL PLANE IN PLASTIC ZONE
AROUND EXPANDING CAVITY

AVERAGE STRESS ON HORIZONTAL PLANE IN PLASTIC ZONE

$$s = \frac{\sigma'_r + \sigma'_\theta}{2} = \frac{p'_c}{1 + \sin \phi'_{PS}} \left(\frac{R}{r} \right)^{1-K_a} \quad \dots (1)$$

where:

σ'_r = radial effective stress at a generic radial distance

$r \leq R_p$

σ'_θ = circumferential effective stress at a generic radial distance $r \leq R_p$

p'_c = effective cavity stress at which unloading-reloading loop starts

r = radial distance

R_p = radius of plastic zone

R = current cavity radius

$$K_a = \frac{1 - \sin \phi'_{PS}}{1 + \sin \phi'_{PS}}$$

$$p'_{AV} = \frac{\int_{R_p}^{R_p} s \, dr}{\int_{R_p}^{R_p} dr} \quad \dots (2a)$$

or:

$$p'_{AV} = \frac{\int_{R_p}^{R_p} s \cdot 2\pi r \cdot dr}{\int_{R_p}^{R_p} 2\pi r \cdot dr} \quad \dots (2b)$$

Due to the tentative and preliminary nature of the proposed approach, the more simple solution ... (2a) integrating s along the radius r is the only method considered here.

Introducing the value of s from equation ... (1) into equation ... (2a) one obtains:

$$p'_{AV} = \frac{p'_c}{1 + \sin \phi'_{PS}} \left(\frac{R}{R_p} \right)^{1-K_a} \frac{\int_{R_p}^{R_p} \left(\frac{R}{r} \right)^{K_a-1} dr}{R_p - R}$$

$$p'_{AV} = \frac{p'_c}{1 + \sin \phi'_{PS}} \cdot \frac{\left(\frac{R_p}{R} \right)^{K_a} - 1}{\frac{R_p}{R} - 1} \quad \dots (3)$$

$$\text{Also: } \frac{R_p}{R} = \left[\frac{\frac{p'_c}{\sigma'_{ho}}}{1 + \sin \phi'_{ps}} \right]^{\frac{1}{1-K_a}} \quad \dots (4)$$

Introducing the ratio $\frac{R_p}{R}$ from equation ... (4) into equation ... (3) one obtains:

$$\frac{p'_{Av}}{\sigma'_{ho}} = \frac{p'_c}{\sigma'_{ho} (1 - \sin \phi'_{ps})} \left[\frac{\frac{p'_c}{\sigma'_{ho} (1 + \sin \phi'_{ps})}}{\frac{p'_c}{\sigma'_{ho} (1 + \sin \phi'_{ps})}} \right]^{\omega_1 - 1} \quad \dots (5)$$

where:

$$\omega_1 = \frac{K_a}{1-K_a} = \frac{1 - \sin \phi'_{ps}}{2 \sin \phi'_{ps}}$$

$$\omega_2 = \frac{1}{1-K_a} = \frac{2 \sin \phi'_{ps}}{1 + \sin \phi'_{ps}}$$

From equation ... (5) the following two formulae allows the evaluation of p'_{Av} in the plastic zone around the expanding cavity

$$p'_{Av} = \sigma'_{ho} + \alpha (p'_c - \sigma'_{ho}) \quad \dots (6a)$$

or:

$$p'_{Av} = x p'_c \quad \dots (6b)$$

where:

$$x = \frac{1}{(1 - \sin \phi'_{ps})} \cdot \frac{\left[\frac{p'_c}{\sigma'_{ho} (1 + \sin \phi'_{ps})} \right]^{\omega_1 - 1}}{\left[\frac{p'_c}{\sigma'_{ho} (1 + \sin \phi'_{ps})} \right]^{\omega_2 - 1}} \quad \dots (7)$$

$$\alpha = \frac{\frac{p'_c}{\sigma'_{ho} (1 - \sin \phi'_{ps})} \cdot \left[\frac{\frac{p'_c}{\sigma'_{ho} (1 + \sin \phi'_{ps})}}{\frac{p'_c}{\sigma'_{ho} (1 + \sin \phi'_{ps})}} \right]^{\omega_1 - 1}}{\left[\frac{\frac{p'_c}{\sigma'_{ho} (1 + \sin \phi'_{ps})}}{\frac{p'_c}{\sigma'_{ho} (1 + \sin \phi'_{ps})}} \right]^{\omega_2 - 1}} \quad \dots (8)$$

$$\alpha = \frac{\frac{p'_c}{\sigma'_{ho}} - 1}{\frac{p'_c}{\sigma'_{ho}} - 1}$$

III.3

Equations (6a) and (6b) are valid only if a plastic zone exists which means:

$$p'_c > \sigma'_{ho} (1 + \sin \phi'_{ps}) \quad \dots (9)$$

Otherwise one has to assume $p'_{AV} = \sigma'_{ho} = p'_o$

APPENDIX IV

DETAILS ON MANASSERO (1987) METHOD

FOR DETERMINATION OF ϕ FROM SBPT IN SAND

STRESS-STRAIN RELATIONSHIPS
FROM DRAINED SELF BORING PRESSUREMETER TESTS IN SAND

by

MARIO MANASSEPO

DIPARTIMENTO DI INGEGNERIA STRUTTURALE DEL POLITECNICO DI TORINO

ATTO N° 6678910

ABSTRACT

A numerical method is presented in order to obtain the complete stresses and strains path during a self boring pressuremeter test (SBPT) in sand.

Plane strain conditions and a material behaviour according to Rowe's /23/24/ dilatancy theory are assumed.

The obtained results have been checked using a large number of SBPT in sand performed in a calibration chamber (CC).

RIASSUNTO

Viene illustrato un procedimento di calcolo numerico che permette di ottenere gli andamenti completi delle componenti di tensione e deformazione durante una prova di espansione eseguita con il pressiometro autoperforante (SBPT) in sabbia.

Si ipotizzano condizioni di deformazione piane ed un comportamento del materiale in accordo con la teoria della dilatanza di Rowe /23/24/.

I risultati ottenuti sono stati controllati usando numerosi SBPT in sabbia, eseguiti in camera di calibrazione (CC).

1. INTRODUCTION

The first closed form solution of an expanding cavity problem has been obtained considering a linear elastic material and small deformations (Lamé /18/).

By using this solution it is possible to find the elastic shear modulus G both from the first part of the SBPT and from an unload-reload cycle.

Solutions for a linear elastic-perfectly plastic material have been presented later by Bishop et al. /6/ for a pure cohesive soil, and by Hill /17/, Menard /19/ /20/, Cassan /8/, Salençon /25/ and Vesic /26/ for a frictional and cohesive soil.

On the basis of the above mentioned solutions, Gibson et al. /10/, Ladanyi /13/14/15/16/, Palmer /21/, Baguelin et al. /11/, Wroth et al. /27/, Hughes et al. /12/ and Robertson /22/ have presented procedures for the interpretation of pressuremeter tests, allowing the derivation of the stress-strain relationships of a soil element at the inner boundary of the expanding cavity.

The interpretation method for a pure frictional material presented in this paper is closely related to Wroth's et al. /27/ and Hughes's et al. /12/ analyses and it is based on Rowe's /23/24/ dilatancy theory.

2. BASIC ASSUMPTION

The basic assumptions, used in the here presented approach, are briefly summarized in the following points

- a) The particulate material surrounding the infinitely long expanding cavity deforms in plane strain conditions, i.e. the vertical strain $\epsilon_z = 0$.

IV.3

- b) The principal stresses $\sigma_1, \sigma_2, \sigma_3$ are coincident with radial, vertical, hoop stresses around the cavity, $\sigma_r, \sigma_z, \sigma_\theta$, the same applies to the strains $\epsilon_1, \epsilon_2, \epsilon_3$ and $\epsilon_r, \epsilon_z, \epsilon_\theta$. In the following either subscript notations can be used.
- c) Stresses and strains are positive in compression.
- d) All stresses and strength parameters are in terms of effective stress.
- e) The strains are considered to be completely plastic. Elastic strains are not considered.
- f) Only frictional forces act at the contact points of particles (sand grains).
- g) Strains due to particle crushing or plastic yield at contact points are supposed not affecting the soil behaviour in the case of the contemplated sand.
- h) The hypothesis of small strains is adopted.

3. CONSTITUTIVE RELATIONSHIP

According to Rowe's /23/24/ theory, the behaviour of a particulate medium may be described by the following equation:

$$\frac{\sigma_1 d\epsilon_1}{(\sigma_2 d\epsilon_2 + \sigma_3 d\epsilon_3)} = - K_p^{cv} \quad (1)$$

where:

$$K_p^{cv} = \frac{1 + \sin \phi_{cv}}{1 - \sin \phi_{cv}} \quad ; \text{ constant volume principal stress ratio coefficient;}$$

$$\phi_{cv} = \text{constant volume friction angle}$$

Taking into account for plain strain conditions

($d\epsilon_2 = 0$) the eq. (1) reduces to:

$$\frac{\sigma_1}{\sigma_3} = -K_p^{cv} \frac{d\epsilon_3}{d\epsilon_1} \quad (2)$$

Shear (γ) and volumetric (ϵ_v) strains are defined by the following:

$$\gamma = \epsilon_1 - \epsilon_3 \quad (3)$$

$$\epsilon_v = \epsilon_1 + \epsilon_3 \quad (4)$$

Using this last set of equations the stress ratio (σ_1/σ_3) can be expressed also as follows

$$\frac{\sigma_1}{\sigma_3} = K_p^{cv} \frac{1 - \frac{d\epsilon_v}{d\epsilon_1}}{1 + \frac{d\epsilon_v}{d\epsilon_1}} \quad (5)$$

The introduced relationships of the adopted constitutive model are qualitatively shown in Fig. 1.

4. CAVITY EXPANSION RELATIONSHIPS

The equations of equilibrium and compatibility of strains all around the cavity are: (see also Fig.2)

$$\frac{d\sigma_r}{dr} = \frac{\sigma_\theta - \sigma_r}{r} \quad (6)$$

$$\frac{d\epsilon_r}{dr} = \frac{\epsilon_r - \epsilon_\theta}{r} \quad (7)$$

where:

σ_r, σ_θ : principal stresses (MAX and min) around the cavity (corresponding to σ_1 and σ_3)

$\epsilon_r, \epsilon_\theta$: principal strains around the cavity (corresponding to ϵ_1 and ϵ_3)

r : radial distance.

IV.5

This last set of equations with eq. (2) described in chapter 2 allows to obtain the solution of the expanding cylindrical cavity problem (See 5th Sect.).

5. PROPOSED METHOD

Expressing the equations (6) and (7) as function of $\frac{r}{dr}$ and referring them to a generic radius r around the expanding cavity, one can write:

$$\frac{\sigma_{\theta} - \sigma_r}{d\epsilon_r} = \frac{\epsilon_r - \epsilon_0}{d\epsilon_0} \quad (8)$$

Introducing into eq. (8):

$$\sigma_{\theta} = - \frac{\sigma_r}{K_p^{cv}} \frac{d\epsilon_r}{d\epsilon_0}$$

given by eq. (2) and rearranging it, one gets

$$\frac{d\sigma_r}{d\epsilon_0} = - \frac{\sigma_r (1 + K_a^{cv} \frac{d\epsilon_r}{d\epsilon_0})}{\epsilon_r - \epsilon_0} \quad (9)$$

$$\text{being : } K_a^{cv} = \frac{1}{K_p^{cv}}$$

This equation of general validity can be solved for a soil element at the cavity wall where the $\sigma_r = p$ and $\epsilon_0 = \epsilon$ are measured. To do this analytically, a relationship $\epsilon_r = f(\epsilon_0)$ is required (see Hughes et al. /12/), nevertheless knowing $p = F(\epsilon)$ one can solve eq. (9) using numerical techniques, like finite difference.

6. NUMERICAL ANALYSIS

With the aim to assess the ϵ_r at the cavity wall through a numerical procedure, the following equations at the points (i) and (i-1) can be setup (see also Fig. 3).

$$\frac{dp}{d\epsilon} = \frac{p(i) - p(i-1)}{\epsilon(i) - \epsilon(i-1)} \quad (10)$$

$$\frac{d\epsilon_r}{d\epsilon} = \frac{\epsilon_r(i) - \epsilon_r(i-1)}{\epsilon(i) - \epsilon(i-1)} \quad (11)$$

Introducing eqs. (10) and (11) into eq. (9), using average criteria between forward and backwards interpolations techniques and making appropriate arrangements it is obtained:

$$\begin{aligned} \epsilon_r(i) = & \frac{p(i) [\epsilon(i-1) + K_a^{cv} \epsilon_r(i-1)] - p(i-1) \epsilon(i)}{2 [p(i) (1 + K_a^{cv}) - p(i-1)]} + \\ & + \frac{p(i) [\epsilon(i-1) - \epsilon_r(i-1)] + p(i-1) [\epsilon_r(i-1) (1 + K_a^{cv}) - \epsilon(i)]}{2 K_a^{cv} p(i-1)} \end{aligned} \quad (12)$$

Moreover knowing that $\epsilon_r(0) = 0$, equation (12) allows to compute step by step the unknown values $\epsilon_r(i)$ from $i = 1$ to $i = n$.

Once $\epsilon_r(i)$, $\epsilon(i)$, $p(i)$ and $\sigma_y(0) = p(0)$ are known, one can compute from eqs. (3) and (4) the deformation components $\gamma(i)$, $\epsilon_v(i)$ and solving equation (2) or (5), once more with finite difference technique, the complete stress-strain curve and stress-path for the soil element at the cavity wall can be assessed.

ACKNOWLEDGEMENTS

The author wishes to acknowledge Dr. P. Bertacchi and Dr. L. Bellotti of ENEL-CRIS - Milan, who made available the results of the SBPT's performed in the CC, used to validate the interpretation method exposed in the paper.

REFERENCES

- /1/ BAGUELIN, F., JÉLÉQUEL, J.F., LEMES, R., "Expansion of Cylindrical Probes in Cohesive Soils", Journal of the Soil Mechanics and Foundations Division, American Society of Civil Engineers, Vol. 98, No. 4, Proc. Paper 9377, (1972) November, pp. 1139-1143.
- /2/ BAGUELIN, F., JÉLÉQUEL, J.F. and SHIELD, D.H., "The pressuremeter and foundation engineering", Series on Soil and Rock Mechanics, Vol. 2, No. 4, Trans Tech Publications, (1978).
- /3/ BALIGH, M.M., "Cavity Expansion in Sand with Curved Envelopes", Journ. Geot. Eng. Div. ASCE, GT. 11, (1976).
- /4/ BALDI ET AL., "Laboratory Validation of in-Situ Tests", Published by A.G.I. on the occasion of the ISSMFE Golden Jubilee, (1985a).
- /5/ BELLOTTI, R., BRUZZI G. and GHIONNA V., "Design, Construction and Use of a Calibration Chamber", Proc. ESOP 11, Amsterdam, Vol. 2, (1982), pp. 439-446.
- /6/ BISHOP, R.F., HILL, R., and MOTT, N.F., "Theory of indentation and hardness tests", Proc. Phys. Soc. 57, 147, (1945).
- /7/ CARTER, J.P., BOOKER, J. and YEUNG, S.K., "Cavity expansion in cohesive frictional soils", Geotechnique 36, No. 3, (1986), pp. 349-358.

- 14 LADANYI, B., "Evaluation of Pressuremeter Tests in Granular Soils", Proceedings of the Second Pan American Conference on Soil Mechanics and Foundation Engineering, Brazil, Vol. 1, (1963), pp. 9-20.
- 15 LADANYI, B., "Expansion of a Cavity in a saturated Clay Medium", Journal of the Soil Mechanics and Foundation Division, Proceedings of the American Society of Civil Engineers, Vol. 90, No SM4, Proc. Paper 3577, (1963), July, pp. 127-161.
- /16/ LADANYI, B., "In Situ Determination of Undrained Stress-Strain Behavior of Sensitive Clays with the Pressuremeter", Canadian Geotechnical Journal, Vol. 9, (1972).
- /17/ LADE, P.V. and LEE, K.L. "Engineering Properties of Soils", Report, UCLA-ENG-7652, (1976), pp. 145.
- /18/ LAMÉ, G., "Leçons sur la théorie mathématique de l'élasticité des corps solides", Bachelier, Paris, France, (1852).
- /19/ MÉNARD, L., "Mesure in situ des propriétés physiques des sols", Annales des Ponts et Chaussées, Paris, No. 14, (1957), Mai-Juin, pp. 357-377.
- /20/ MÉNARD, L., "An Apparatus for Measuring the Strength of Soils in Place", Thesis, University of Illinois, (1957).

IV.9

- /21/ PALMER, A.C., "Undrained plane-strain expansion of a cylindrical cavity in clay: a simple interpretation of the pressuremeter test", *Géotechnique* 22, No. 3, (1972), pp. 451-457.
- /22/ ROBERTSON, P.K., "In Situ Testing of Soil with emphasis on its application to liquefaction assessment", PhD Thesis Department of Civil Engineering, Vancouver (Canada), (1982).
- /23/ ROWE, P.W., "The stress-dilatancy relation for static equilibrium of an assembly of particles in contact", *Proc. Royal Soc.*, Vol. 269, (1962), pp. 500-527.
- /24/ ROWE, P.W., "Stress-Strain Relationship for Particulate Materials at equilibrium", *Proc. of the specialty Conference on Performance of Earth and Earth-supported Structures*, Purdue University, Lafayette (Indiana). Published by ASCE, (1972).
- /25/ SALENÇON, J., "Expansion quasi-statique d'une cavité à symétrie sphérique ou cylindrique dans un milieu élasto plastique", *Annales des Ponts et Chaussées*, Paris, Vol. III, (1966), pp. 175-187.
- /26/ VESIC, A.S., "Expansion of cavities in infinite soil mass.", *J. Soil Mech. Fdns Div. Am.Soc. Civ. Engrs* 98, SM3, (1972), pp. 265-290.
- /27/ WROTH, C.P. and WINDLE, D., "Analysis of the pressuremeter test allowing for volume change", *Technical Note, Geotechnique* 25, (1975), pp. 598-610.

AD-A188 792

SELF-BORING PRESSUREMETER IN PLUVIALLY DEPOSITED SANDS
(U) CENTRO DI RICERCA IDRAULICA E STRUTTURALE MILAN
(ITALY) R BELLOTTI ET AL. JUN 87 DAJ445-84-C-0034

2/2

UNCLASSIFIED

F/G 14/2

NL

END
DATE
PAGE
84

11
12
13
14
15
16
17
18
19
20
21
22
23
24
25
26
27
28
29
30
31
32
33
34
35
36
37
38
39
40
41
42
43
44
45
46
47
48
49
50
51
52
53
54
55
56
57
58
59
60
61
62
63
64
65
66
67
68
69
70
71
72
73
74
75
76
77
78
79
80
81
82
83
84
85
86
87
88
89
90
91
92
93
94
95
96
97
98
99
100

TAB. 1 - TESTED SAND SHEAR STRENGTH

TICINO SAND			
D_R (%)	ϕ_o^{TX} (°)	α (°)	R^2 (-)
45	38.2	4.2	0.67
65	40.2	6.5	0.78
85	42.9	8.1	0.89
ϕ_o^{TX} parameters describing the curved α strength envelopes (Baligh/3/)(*) R^2 = correlation coefficient D_R = average relative density of the tested specimens, at the end of consolidation			

$$(*) \operatorname{tg} \phi_p^{TX} = \frac{\tau_{ff}}{\sigma_{ff}} = \left[\operatorname{tg} \phi_o^{TX} + \operatorname{tg} \alpha \left(\frac{1}{2.3} - \log_{10} \frac{\sigma_{ff}}{\sigma_o} \right) \right]$$

where:

ϕ_p^{TX} : secant peak friction angle from laboratory triaxial compression test

τ_{ff} = shear stress on the failure surface at failure

σ_{ff} = effective normal stress on the failure surface at failure

σ_o = reference stress, assumed equal to 1 Kg/cm²
= 98.2 KPa

ϕ_o^{TX} = secant friction angle from laboratory triaxial compression test at $\sigma_{ff} = 2.72 \sigma_o$

α = angle which describes the curvature of the failure envelope.

TAB. 2 : Experimental readings from Test N. 228

R _d N.	-ε [%]	p [MPa]	R _d N.	-ε [%]	p [MPa]	R _d N.	-ε [%]	p [MPa]
1	2.22200	.2080	40	.34545	.4124	73	2.11714	.8243
2	.20350	.2131	41	.36219	.4164	82	2.24836	.8462
3	.20700	.2181	42	.37734	.4202	81	2.38134	.9572
4	.21225	.2232	43	.39134	.4266	82	2.51781	.8891
5	.31575	.2282	44	.42534	.4312	83	2.65953	.9118
6	.22100	.2343	45	.42168	.4349	84	2.80826	.9337
7	.22625	.2383	46	.43323	.4395	85	2.88174	.9446
8	.22974	.2444	47	.45143	.4462	86	3.03221	.9674
9	.23849	.2524	48	.45993	.4506	87	3.19143	.9901
10	.24199	.2555	49	.48117	.4543	88	3.35055	1.0129
11	.24724	.2606	50	.54591	.4709	89	3.51336	1.0319
12	.25424	.2656	51	.55991	.4755	92	3.67958	1.0558
13	.26124	.2716	52	.57216	.4801	91	3.84929	1.0777
14	.26649	.2757	53	.58366	.4847	92	4.02950	1.0996
15	.27174	.2807	54	.62130	.4893	93	4.21146	1.1216
16	.28049	.2877	55	.62115	.4948	94	4.39517	1.1444
17	.29099	.2927	56	.53690	.4994	95	4.58588	1.1664
18	.29798	.2969	57	.65440	.5050	96	4.78184	1.1883
19	.12673	.3019	58	.67189	.5096	97	4.98129	1.2111
20	.11548	.3079	59	.68939	.5133	98	5.18425	1.2339
21	.12598	.3139	60	.71039	.5206	99	5.39595	1.2558
22	.13473	.3179	61	.72613	.5234	100	5.61289	1.2795
23	.14348	.3229	62	.76463	.5335	101	5.83684	1.3032
24	.15398	.3280	63	.80312	.5437	102	6.05904	1.3241
25	.16622	.3351	64	.84511	.5556	103	6.28823	1.3468
26	.17672	.3390	65	.95884	.5804	104	6.52617	1.3686
27	.18722	.3451	66	1.02084	.5905	105	6.76586	1.3923
28	.19597	.3491	67	1.04108	.6006	106	7.01430	1.4142
29	.20997	.3562	68	1.08132	.6108	107	7.27498	1.4377
30	.22047	.3602	69	1.12507	.6209	108	7.53216	1.4584
31	.23096	.3652	70	1.16881	.6310	109	7.80334	1.4821
32	.24321	.3713	71	1.21255	.6411	110	8.07802	1.5056
33	.25546	.3763	72	1.25824	.6502	111	8.36144	1.5282
34	.26596	.3803	73	1.43301	.6888	112	8.65186	1.5499
35	.27996	.3884	74	1.53299	.7127	113	8.95103	1.5715
36	.29395	.3924	75	1.63773	.7337	114	9.26594	1.5950
37	.30795	.3984	76	1.74971	.7566	115	9.58785	1.6156
38	.32020	.4034	77	1.86593	.7795	116	9.91325	1.6391
39	.33420	.4084	78	1.98765	.8015	117	10.25265	1.6595

R_d : number of the experimental reading

ε : hoop strain at the cavity wall

p : radial stress at the cavity wall

FIG.1: Stress - strain relationships for plane strain conditions

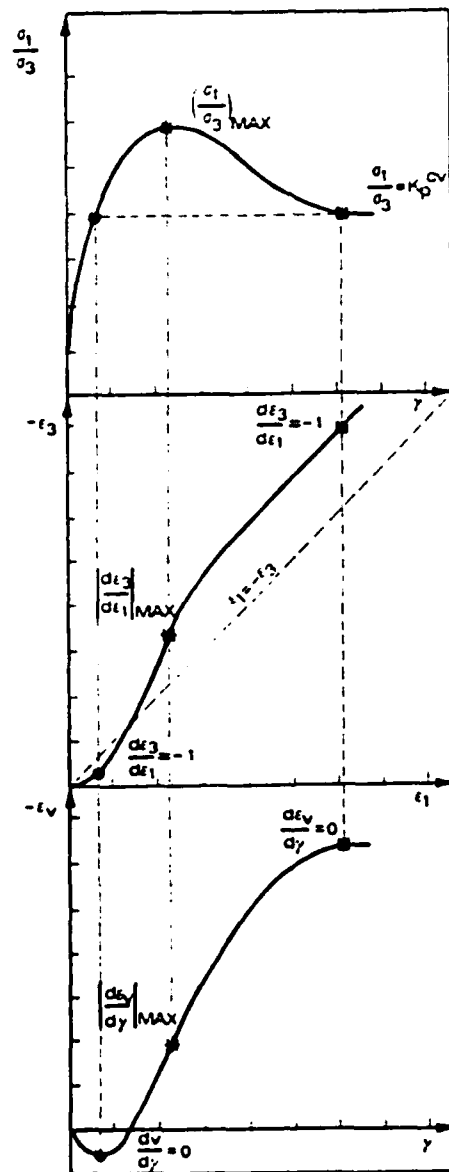
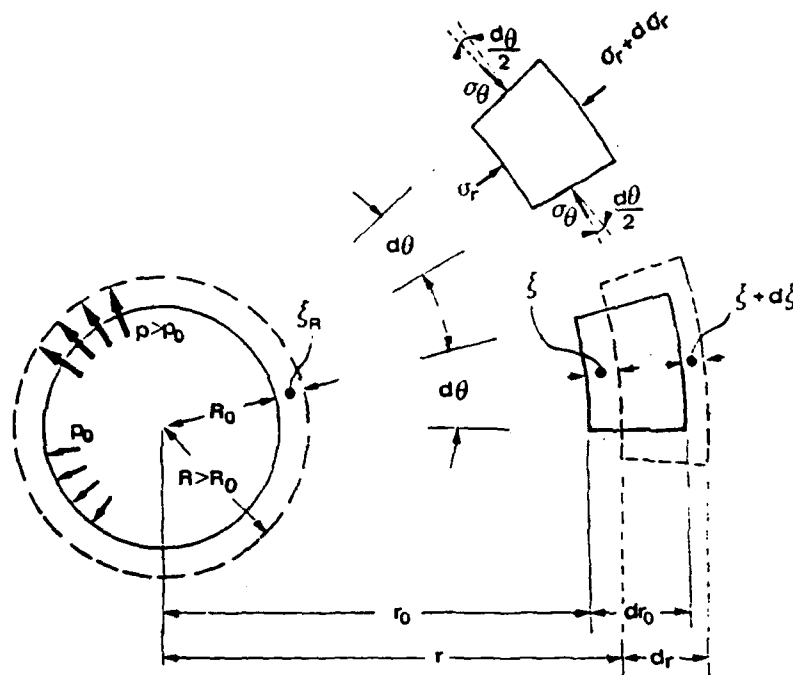


FIG.2 : Stresses and strains around the expanding cavity



Compatibility equations

$$\left\{ \begin{array}{l} \epsilon_r \quad (\text{radial strain}) = -d\xi/dr \\ \epsilon_\theta \quad (\text{hoop strain}) = -\xi/r \end{array} \right.$$

At the cavity wall

$$\epsilon \quad (\text{"cavity strain"}) = -\xi_R/R_0$$

Equilibrium equation

$$\frac{d\sigma_r}{dr} = \frac{\sigma_\theta - \sigma_r}{r}$$

FIG. 3: Use of pressuremeter curve for numerical analysis

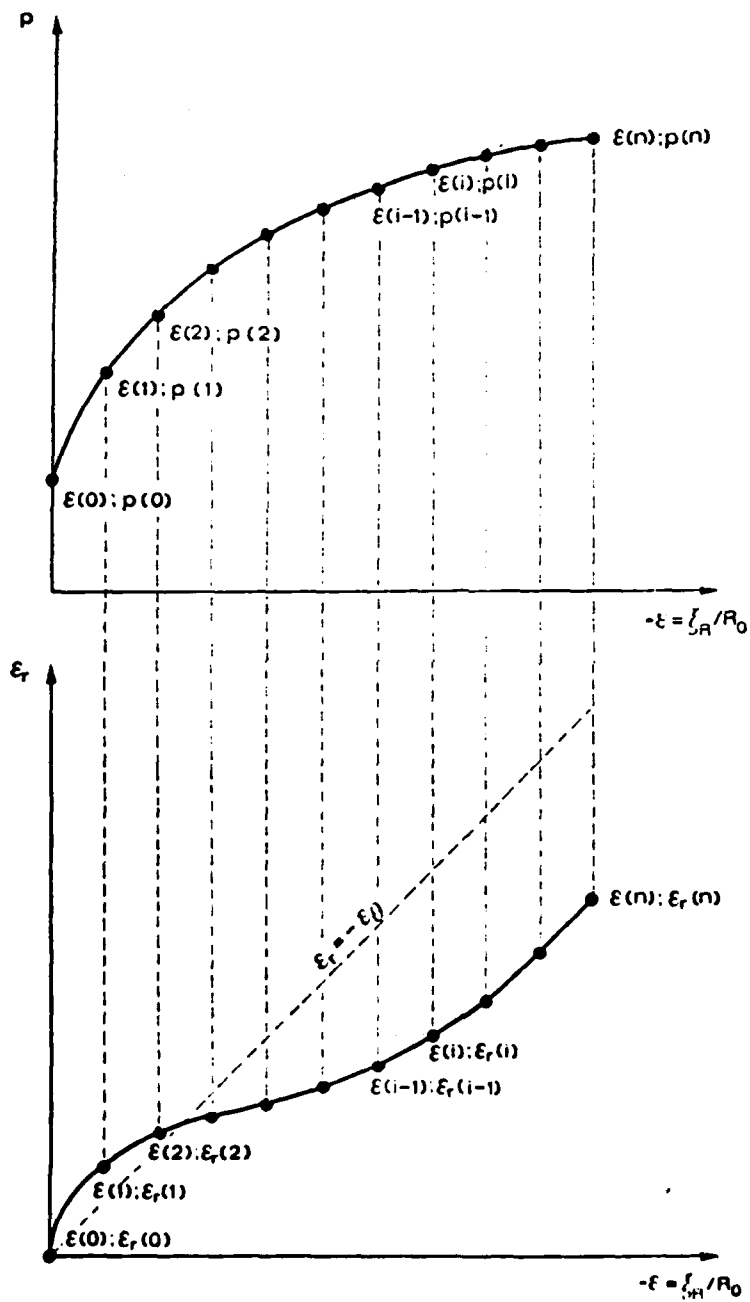


FIG. 4: Characteristics of the tested sand

SAND	1,2-TICINO
DOMINANT MINERAL	QUARTZ (30%)
ANGULARITY (LEE'S CHART)	8-9
MICA	~5%
γ_{\max} (t/m ³)	1) 1.705 2) 1.700
γ_{\min} (t/m ³)	1) 1.398 2) 1.391

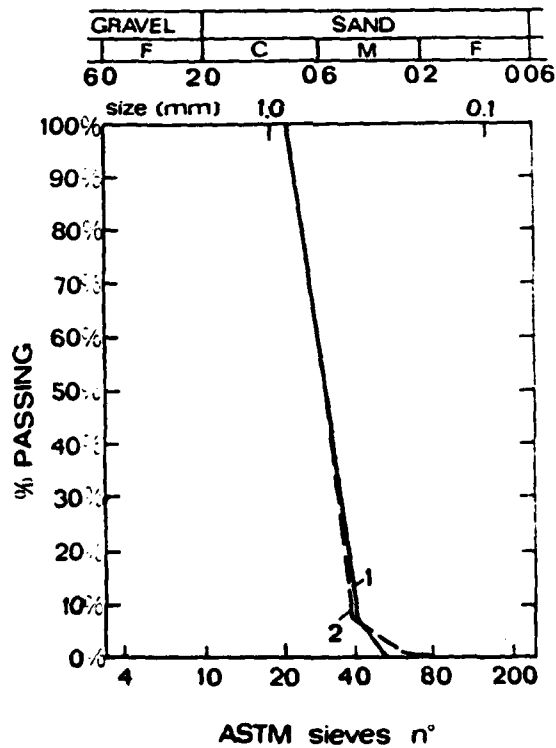
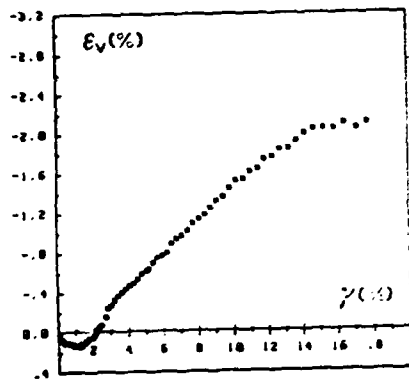
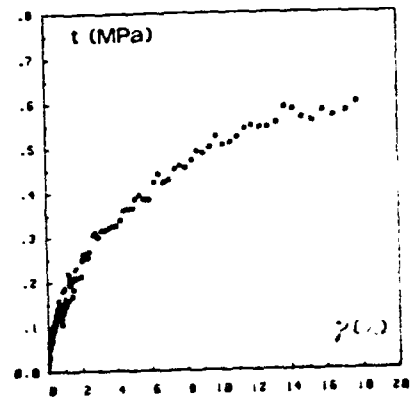


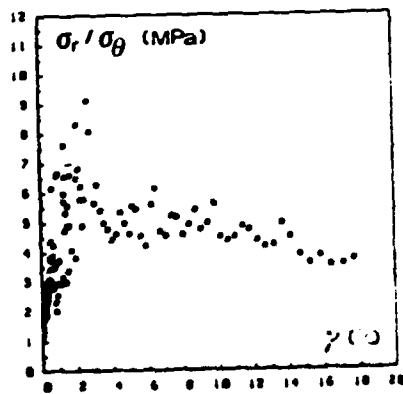
FIG.5: Stress/strain relationships using the experimental readings from test N: 228 ($D_R=77.0\%$)



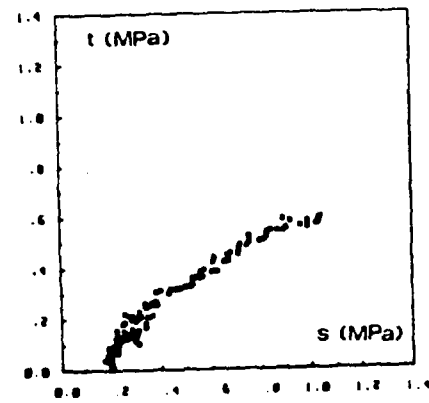
a) Volumetric strain vs shear strain



b) Shear stress vs shear strain

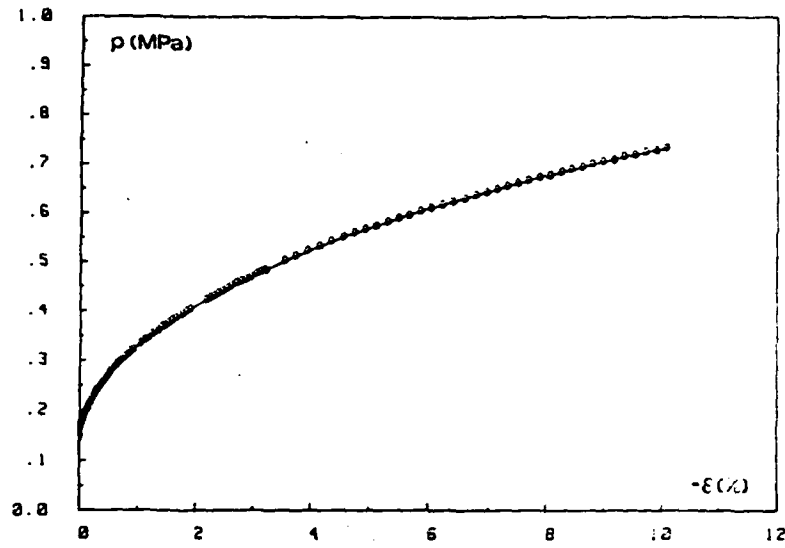


c) Stress ratio vs shear strain

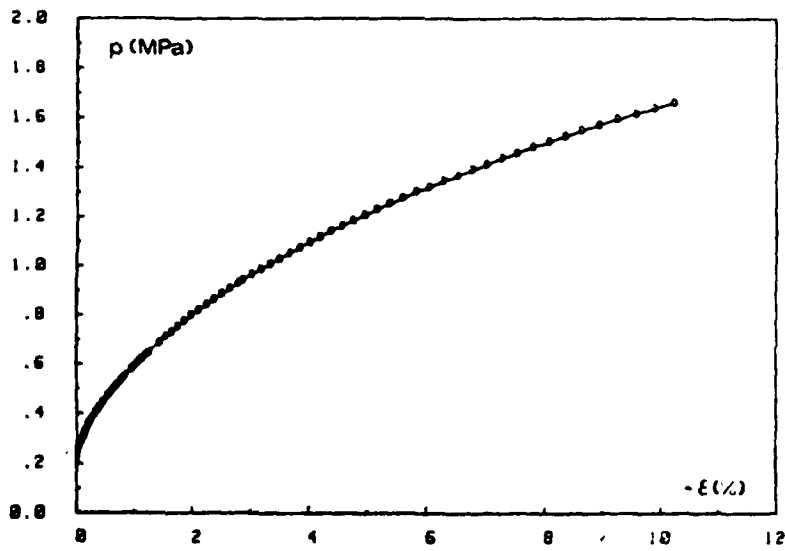


d) Shear stress vs mean normal stress

FIG.6 : Curve fitting results with 7th polynomial degree in original p vs ϵ plot



a) Test No. 222



b) Test No. 228

FIG.7 : Stress ratio - strain curve for 5th, 7th and 9th degree polynomials (Test N. 228)

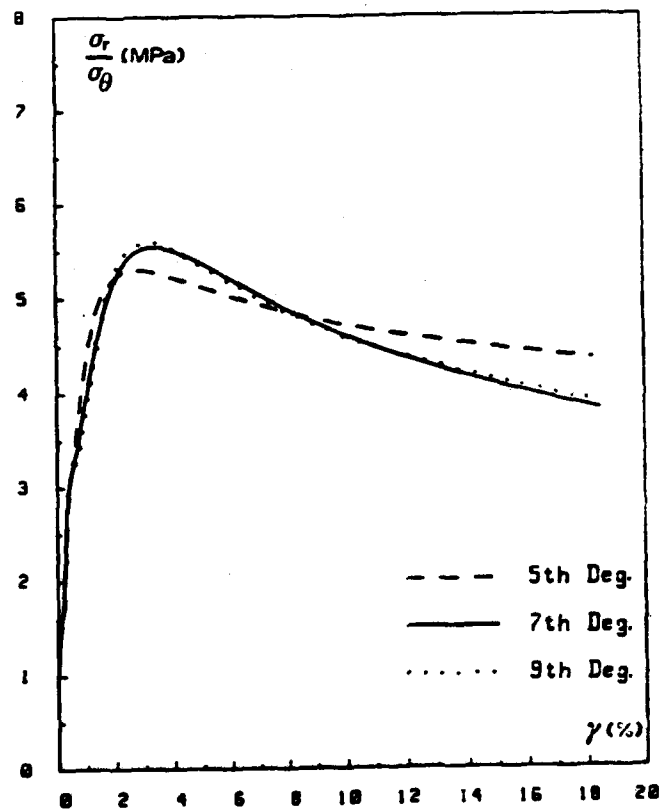
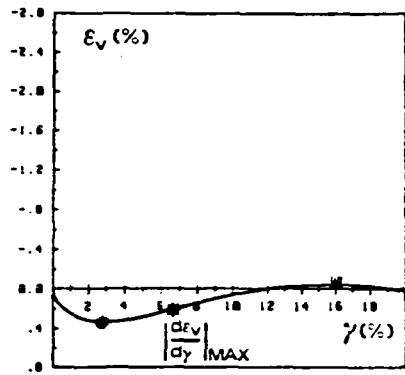
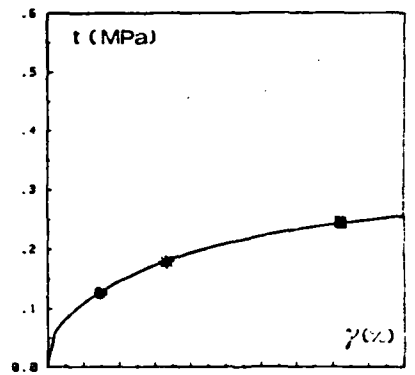


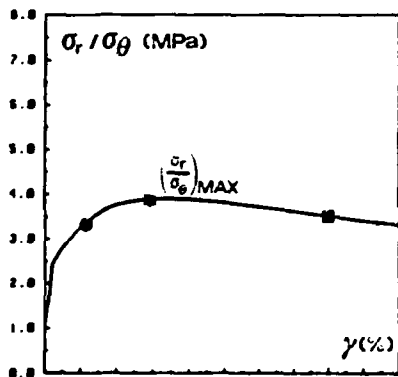
FIG.8 : Stress / strain relationships from test N.222 ($D_R = 46.2\%$)



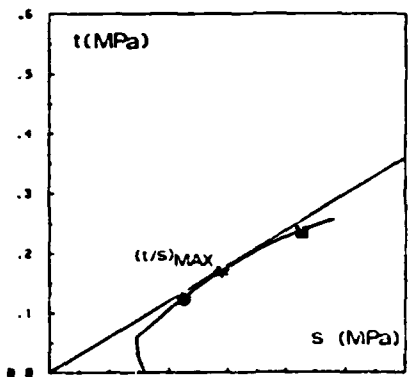
a) Volumetric strain vs shear strain



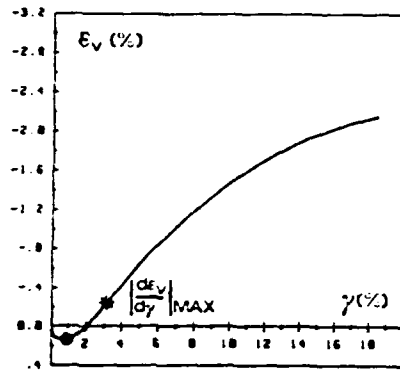
b) Shear stress vs shear strain



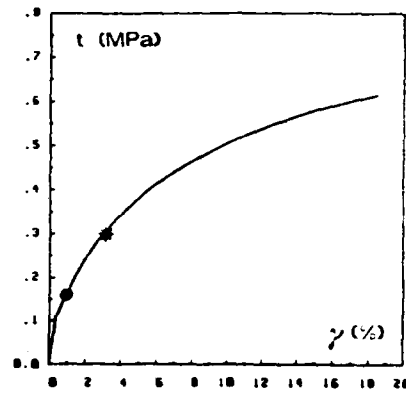
c) Stress ratio vs shear strain



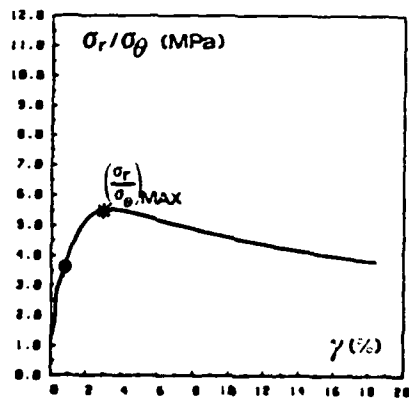
d) Shear stress vs mean normal stress

FIG.9: Stress / strain relationships from test N.228 ($D_R=77.0\%$)

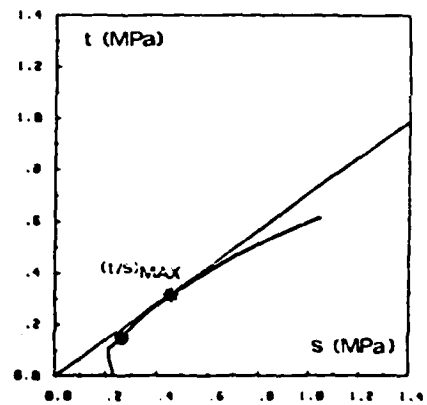
a) Volumetric strain vs shear strain



b) Shear stress vs shear strain



c) Stress ratio vs shear strain



d) Shear stress vs mean normal stress

END

DATE
FILMED

3 88